

博士論文

THE IMPACT OF INTERACTION BETWEEN SEDIMENT SIZE AND
CHANNEL ASPECT RATIO ON RIVER PLANFORM DYNAMICS

(河床材料の粒度と川幅水深比の相互作用が
河道の平面形状の動態に及ぼす影響)

HENDRA RAMDHANI

ヘンドラ ラムダニ

The Impact of Interaction Between Sediment Size and Channel Aspect Ratio on River Planform Dynamics

by
Hendra Ramdhani

Thesis submitted
for the degree of
Doctor in Engineering

Department of Civil Engineering
School of Engineering
The University of Tokyo
Tokyo, Japan



2021

The Impact of Interaction Between Sediment Size and Channel Aspect Ratio on River Planform Dynamics

by
Hendra Ramdhani

Dissertation Committee:

Associate Professor Takeyoshi CHIBANA (Supervisor)

Professor Norio TANAKA

Professor Yoshimitsu TAJIMA

Associate Professor Kenji WATANABE

Associate Professor Takenori SHIMOZONO

Department of Civil Engineering

School of Engineering

The University of Tokyo

Tokyo, Japan



2021

Author's Declaration

I hereby declare that the thesis has been composed by myself and my own, except where work which has formed part of jointly-authored publication has been included. My contribution and those of the other authors to this work is indicated below.

"Meandering Characteristics of Cimanuk River Focusing on Aspect Ratio Variations and Geological Condition" in a conference paper by Hendra Ramdhani, Takeyoshi Chibana and Agus Santoso. This study was conceived by all of the authors.

I authorize the University of Tokyo to lend this thesis to other institutions or individuals for the purpose of scholarly research.

(Hendra Ramdhani)

I further authorize the University of Tokyo to reproduce this thesis by photocopying or by other means, in total or in part, at the request of other institutions or individuals for the purpose of scholarly research.

(Hendra Ramdhani)

Acknowledgement

I would like to convey my gratitude to Allah SWT for His blessing during my study, which allow me to complete this research.

*K*indness and continuous motivation were given by my academic advisor Prof. Takeyoshi Chibana, I was able to understand many things about river morphology and enjoying my study life in Japan. Thank you Sensei, for many good memories for the past 10 years.

*I*mprovement of doctoral thesis content was carried out by comprehensive and objective comment from co-advisors. I am deeply grateful to Professor Norio Tanaka, Professor Yoshimitsu Tajima, Professor Kenji Watanabe and Professor Takenori Shimozono.

*M*y sincere gratitude also to Professor Koji Ikeuchi, Professor Akiyuki Kawasaki, Professor Yohei Sawada, Professor Satoshi Watanabe, Professor Masashi Minamide and all REEL member for comments, suggestion and discussions during labhour.

*O*f course, I have to say many thanks to Chibana group member which giving me a lot of fun, especially during field survey. Muto-san, Ori-kun, Kanba, Itsumi, Yu-san, other group member (and OBOG as well), thank you for make me happy during our daily conversation.

*N*ew knowledge of numerical simulation was given by Harada-san, thank you for giving the internship chance in ICHARM. I am learning so many things during that time.

*O*bjectives of this study was inspired by past studies from Agus-san, which was told me for the first time about stable channel. This inspiration bring me to new level of understanding about river.

*G*reat chance of doctoral course study was given by UEDA MEMORIAL FOUNDATION, thank you very much for support and understanding my difficulties during study period.

*A*oyama-san, Tonegawa-san, Nagamatsu-san, Arai-san, FSO, and OIS, thank you for your kindness and tireless help to support me.

*K*ind help and support also from Wakhidatik Nurfaida during my first year of doctoral course and thank you for helping me to conduct the test for soil samples.

*A*lvin, Zamzam, Aat and all member of PPI Todai, thanks a lot for great discussions and chance to join PPI Todai FC in Kanto Cup.

*R*iver survey for additional data was conducted by Dodo, Aa Ridho, Mas Tatang, Pak Jono, Mas Ook, thank you for spared the time and help me. Thank you also to BBWS Cimanuk Cisanggarung, BBWS Serayu Opak, BBWS Ciliwung Cisadane, for providing river data.

*I*n most of my time, I always thinking about my family, Dian Anggraeni, Kamila Annikaputri, Alby Kamil Ardhani, my father Haji Burhan, and my brother Hendri Mardiansyah, thank you for always pray for me, understanding my situation, endless love and support.

Abstract

Flood disaster often causes serious problems for cities which located around a meandering river. Maintaining stability of meandering rivers remains as the most challenging task for river management. Some studies propose various approaches to understand meandering characteristics. One of the most common approaches is the classification of meandering pattern. Based on the past studies, there are three types of meandering channel by focusing on sediment characteristics, aspect ratio and sinuosity. These parameters can represent the characteristics of meandering rivers well, but the mechanism of meandering river is diverse and complex. Detailed investigation on each parameter can contribute to better understandings of such mechanism. In this study, the relationship of bank and bed materials and their impacts on meandering characteristics are examined especially focusing on aspect ratio of river channel. Besides, bank erosion process is also one of important factors which determine the characteristics of channel migration on small scale (reach scale) and channel planform change on large scale (segment scale). Some target rivers in Indonesia, Japan and Cambodia are introduced to evaluate those parameters through field measurement and numerical simulation.

The bed material of the target rivers could be classified into 3 types, based on the grain size distribution: coarse sand (0.5-2mm) with occasional gravel (2mm-), fine sand (0.075-0.5mm), and silt and clay (mainly <0.075mm cohesive material). It was clarified that the difference of the bed material is caused by basin geology. On the other hand, the grain size distribution of sand is almost same in all river banks, while the ratio of cohesive material is different especially between Japan and South Asia. Hence, the bank material could be classified into 2 types: cohesive and non-cohesive materials. In terms of aspect ratio and sinuosity, aspect ratio of 12 and 25 as well as sinuosity of 1.5 were found to be important criteria to classify target rivers based on meandering characteristics. By using these parameters, previous classification with three meandering types were modified because the meandering rivers with low-moderate (12-25) aspect ratio (Type 2) shows diverse sinuosity. Then Type 2 was divided into Type 2a which has lower sinuosity than 1.5 and Type 2b that has higher sinuosity than 1.5. Other meander parameters such as meander wavelength and radius of curvature also showed individual characteristics in each type similar to the results of aspect ratio and sinuosity. Especially there is clear relationship between aspect ratio and meander wavelength or radius of curvature in Type2 and it was implied that scroll bar formation affect the meander process. This study also investigated how the weighted mean of silt-clay percentage (M value) affect the channel migration and channel planform as well as aspect ratio. Basically, M value more than 20 is considered to be cohesive

The relationship of sediment size and aspect ratio was investigated by several approaches and it was found that sediment size has important role to maintain channel stability. While active sediment movement is considered to be active in rivers with high sinuosity, low aspect ratio and cohesive sediment (Type 1), the extent of bank erosion is governed by high silt-clay percentage (that means M value is more than 20). In Type 1 which has cohesive bed and bank, bed deformation was found to be active but channel migration was quite limited because of high silt-clay percentage in the bank. In Type 3 which has low sinuosity, high aspect ratio and erodible bank with fine sand materials, both bed and bank are not so stable. Usually, braided channel is created on the river bed. Type 2 is the intermediate condition between Type 1 and 3, but both sinuosity and M value are quite diverse. Therefore, there are no clear relationship between M value and aspect ratio or sinuosity. However, the bed and bank material have some unique characteristics. Some of Type 2 rivers have similar material with Type 1, but some rivers have coarser material than that of Type 3 and others have lower silt-clay percentage in the bank than that of Type 1. As these results show, it was clarified that the bed and bank material of Type 2 tends to be different. Moreover, analysis of old maps clarified that some of Type 2a rivers with lower silt-clay percentage on the bank used to be Type 2b before straightening.

In order to understand the mechanism to make difference between Type 2a and Type 2b, numerical simulation (ICHARM Bank Erosion Model) was carried out in addition to the analysis of field data. By comparing the results of several cases in the simulation, forming mechanism of Type 2a and 2b could be clarified. The target river is the Cimanuk River where steeper channel is Type 2b and milder channel is Type 2a. Several parameters were set based on actual condition of the Cimanuk River, but bank or bed material was changed in order to understand the effect of sediment size on river channel. Through the simulation following pattern were clarified. In the milder channel, Type 1 may become Type 2a when the cohesive material on the riverbed is less and it cannot form the bank. Bank cohesion is also essential factor because riverbed material is supplied from less cohesive bank and it is transported well. Then wider and shallower channel is formed because the bank is usually stabilized by the cohesion in milder river. That means lower silt-clay percentage of on bank or bed may change Type 1 channel to Type 2 channel, but still high-silt clay percentage stabilizes the channel and Type 2a is formed. However, the high silt-clay percentage of the Sangkae River is as high as other Type 1 rivers. It is the future task to clarify the mechanism. In the steeper channel, Type 3 may become Type 2b by increasing depth when coarser material is contained in riverbed. It might be caused by coarser material at bank-toe stabilizes the riverbank and suspended sand forms bank. Moreover, if the silt-clay percentage of the bank of type 3 is increased, scroll bar is formed in narrow channel and type 2b is formed. In both cases, such a narrow and deep channel with high stream power has higher sinuosity.

Proposed meandering characteristics is important to understand meandering river characteristics. Parameters of this classification could distinguish the type of meandering rivers. Detailed investigation of each parameters gives comprehensive perspectives about

each meandering type. Each type needs different approaches to maintain stable cross-sectional shape in terms of river management. Type 1 and Type 2a have relatively stable river shapes, and thus a river manager may spend less effort to maintain the river compared to the other types. Of course, some parts might have small scale characteristics such as local bank erosion due to human activities or impact of river crossing structures that still need to be considered. For Type 3, river managers need to understand bar formation mechanism and give more attention to check the bar in every flood events. Rivers in type 2b tend to be unstable and are typically located in upper part of lower reach. Active erosion and deposition must be monitored through periodic and frequent cross-sectional surveys. One important message is that the sediment size change causes the change of channel dynamics as well as cross-sectional shape. A river manager needs to identify several active zones, at which stability of the cross-sectional shape needs to be maintained. Therefore, suitable river works plans to maintain the stability of cross-sectional shape could be selected to carry out based on design and budget optimization.

Contents

AUTHOR'S DECLARATION	VII
ACKNOWLEDGEMENT.....	IX
ABSTRACT.....	X
CONTENTS	XIII
LIST OF FIGURES	XV
LIST OF TABLES	XX
LIST OF SYMBOL	XXI
CHAPTER 1 INTRODUCTION.....	1
1.1 BACKGROUND	1
1.2 OBJECTIVE	4
1.3 METHODOLOGY.....	4
1.4 THESIS OUTLINE	5
CHAPTER 2 LITERATURE REVIEW	6
2.1 RIVER CLASSIFICATION	6
2.2 REGIME THEORY	14
2.3 STREAM POWER AND CHANNEL PATTERN	15
2.4 SILT-CLAY PERCENTAGES IN BANK AND BED MATERIAL	19
2.5 BANKFULL SHEAR STRESS, EXCESS SHEAR STRESS, SILT-CLAY PERCENTAGE AND EROSION RATE	21
CHAPTER 3 FIELD OBSERVATION AND DATA COLLECTION	25
3.1 TARGET RIVERS.....	25
3.2 TARGET RIVERS IN SOUTHEAST ASIA	27
3.3 TARGET RIVERS IN JAPAN.....	34
3.4 DATA COLLECTION	41
CHAPTER 4 RESULTS AND DISCUSSION	50
4.1 SEDIMENT SIZE VARIATION	50
4.2 SEDIMENT MOBILITY AND TRANSPORT TYPE.....	54
4.3 ASPECT RATIO VARIATION	55
4.4 SINUOSITY, MEANDER WAVELENGTH, RADIUS OF CURVATURE AND ASPECT RATIO VARIATION	57

4.5 SILT-CLAY PERCENTAGE, ASPECT RATIO AND SINUOSITY	59
4.6 APPLICABILITY OF REGIME THEORY	61
4.7 CLASSIFICATION OF CHANNEL PATTERN BY USING STREAM POWER	63
4.8 BANK EROSION RATE AND SILT—CLAY PERCENTAGE	66
4.9 PROPOSED CLASSIFICATION OF MEANDERING RIVER	68
4.10 SUMMARY OF RESULTS AND DISCUSSION.....	75
CHAPTER 5 DISCUSSION ON FORMING PROCESS OF ASPECT RATIOS.....	76
5.1 NUMERICAL SIMULATION OF CIMANUK RIVER (ICHARM BANK EROSION MODEL)	76
5.2 RESULTS OF NUMERICAL SIMULATION.....	85
5.3 BANK SHIFTING, CENTERLINE MOVEMENT AND ASPECT RATIO	91
CHAPTER 6 SUMMARY, LIMITATION, AND CONCLUSIONS.....	98
6.1 SUMMARY	98
6.2 LIMITATION	99
6.3 CONCLUSIONS	99
REFERENCES	101

List of Figures

Figure 1.1 Disaster Events in Indonesia from 2003 – 2017 (BNPB Database).....	2
Figure 1.2 (a) Flood Events Trend in Indonesia (b) Annual DGWR Budget	2
Figure 1.3 Cities with Meandering Rivers in Indonesia	3
Figure 2.1. River channel types according to the longitudinal profiles.....	6
Figure 2.2. Longitudinal river profile from upstream to downstream and the different component characteristics. (modified from Maryono (2005)).....	7
Figure 2.3. Fluvial geomorphology from mountain to the sea.....	7
Figure 2.4. Categorization of Meandering Rivers (a) Channel Type (Schumm, 1963,1977) (b) Character of Sinuosity (Brice, 1975) (c) Geomorphic Characterization (Rosgen, 1994) (d) Morphological Description (Rosgen, 1994)	9
Figure 2.5. Classification of meandering river (based on Soar & Thorne, 2001).	10
Figure 2.6. Cumulative frequency of 499 measurements of bankfull aspect ratios of natural channels (Church & Rood, 1983).....	11
Figure 2.7. Kuroki-kishi Diagram (Kuroki & Kishi, 1984) and Aspect Ratio Interpretation (after Santoso, 2017)	12
Figure 2.8. (a) Sinuosity (Rosgen, 1996). (b) Meandering Rivers Cross-Sectional Shapes (Soar & Thorne, 2001).....	13
Figure 2.9. Dimensionless water surface width and water depth to dimensionless channel-forming discharge (Fukuoka, 2010)	15
Figure 2.10. Unit Stream Power of Bankfull Flow versus Valley Slope (van den Berg, 1995)	16
Figure 2.11. Patterns of equilibrium alluvial rivers plotted with the potential specific streampower related to valley gradient and predicted width. A. Data subdivided by bar pattern and B. Data subdivided by sinuosity (Kleinhans & van den Berg, 2011)	17
Figure 2.12. River Channel Pattern Prediction From Self-constraining Leading to a Tortuous Channel Pattern, and Freely Eroding Banks Leading to a Normal Meandering Channel Pattern (Candel et al., 2021).....	18
Figure 2.13 Relationship Sinuosity and Width-Depth Ratio (left) and Relationship Sinuosity and Silt-Clay Index (right) (Schumm, 1963).....	19

Figure 2.14 Schematic Cross-Section Under Bankfull Condition (Modified from (Dunne, 2020)).....	22
Figure 2.15 Bankfull shear stress τ_{bf} against median grain size D50 for gravel-bedded ($D > 1$ cm) and fine-grained ($D < 1$ cm) rivers (Dunne, 2020)	22
Figure 3.1 Cimanuk River Basin (Ministry of Public Works and Housing, 2017)	27
Figure 3.2 Target Area of The Cimanuk River (Ramdhani et al., 2020)	27
Figure 3.3 Pictures of the Cimanuk River	28
Figure 3.4 Geological Map of Cimanuk River.....	29
Figure 3.5 The Ciliwung River Basin (Ramdhani & Setiawan, 2015).....	30
Figure 3.6 Pictures of the Ciliwung River	30
Figure 3.7 Geological Map of The Ciliwung River	31
Figure 3.8 The Serayu River Basin (Ministry of Public Works and Housing, 2016)	32
Figure 3.9 Geological Map of The Serayu River	32
Figure 3.10 The Sangkae River Basin (Diepart, 2015).....	33
Figure 3.11 Pictures of The Sangkae River Condition.....	34
Figure 3.12 Kano River Basin (MLIT, 2012).....	35
Figure 3.13 Pictures of The Kano River.....	35
Figure 3.14 The Ara River Basin (MLIT, 2012).....	36
Figure 3.15 Picture of The Old Ara River	36
Figure 3.16 Pictures of The Iruma River	37
Figure 3.17 Pictures of The Oppe River	37
Figure 3.18 The Watarase River Basin (MLIT, 2012).....	38
Figure 3.19 Pictures of The Watarase River	38
Figure 3.20 The Naka River Basin (MLIT, 2012).....	39
Figure 3.21 Picture of The Naka River (Santoso, 2017).....	39
Figure 3.22 The Kuji River Basin (MLIT, 2012)	40
Figure 3.23 Picture of Kuji River (Santoso, 2017)	40
Figure 3.24. Field Measurement Using Total Station and Depth Measurement Device .	42
Figure 3.25 Cross-Sectional Dimension (D. Rosgen, 1996).....	42
Figure 3.26 Samples Cross-Sectional Shapes for Each Rivers (AR is Aspect Ratio)	43
Figure 3.27 Bankfull and Mean Annual Maximum Discharge	44

Figure 3.28 Schematic Condition of Bed-Bank Material.....	44
Figure 3.29 Ekman Berge Sampler and Scoop	45
Figure 3.30. Sample collection on riverbed by using Ekman Berge (left) and Scoop (right)	45
Figure 3.31. Sample collection on riverbank	46
Figure 3.32. River Centerline and Sinuosity Analysis.....	46
Figure 3.33. Historical Map - 1899 Historic Agriculture Environment	49
Figure 3.34. Time Series Topographic Map Website Interface	49
Figure 4.1. Grain Size Distribution of the Bed Material.....	51
Figure 4.2. Grain Size Distribution of Bank Material	51
Figure 4.3. Grain Size Distribution of Bed Material Based on Upstream Geology	52
Figure 4.4. Shields Parameters vs Reynolds Number (After Parker, 2004).....	55
Figure 4.5. Bankfull shear stress and median grain size D50 for gravel-bedded ($D > 1$ cm) and fine-grained ($D < 1$ cm) rivers (after Dunne & Jerolmack, 2020).....	55
Figure 4.6. Aspect Ratio of Target Rivers.....	56
Figure 4.7. Aspect Ratio Variation of Target Rivers	56
Figure 4.8. Aspect Ratio Variation of Target Rivers (Segment II-2 only) Based on Bed-Bank Material Condition (Table 4-1).....	57
Figure 4.9. Sinuosity and Aspect Ratio of Japan and Southeast Asian Rivers, Red Line Threshold Aspect Ratio 12-40, Sinuosity 1.5 (Rosgen, 1994), Green Line Threshold Aspect Ratio 25 (Church & Rood, 1983)	58
Figure 4.10. Meander Wavelength, Radius of Curvature and Aspect Ratio of Japan and Southeast Asian Rivers, Red Line Threshold Aspect Ratio 12-40, Sinuosity 1.5 (Rosgen, 1994), Green Line Threshold Aspect Ratio 25 (Church & Rood, 1983).....	59
Figure 4.11. Weighted mean silt-clay percentage (M) and Sinuosity	60
Figure 4.12. Weighted mean silt-clay percentage (M) and Aspect Ratio 12 and 40 (Red line) 25 (Green Line)	60
Figure 4.13. Width and Depth Prediction by Past Study (Julien & Wargadalam, 1995) ..	61
Figure 4.14. Dimensionless water surface width and water depth to dimensionless channel-forming discharge (after (Fukuoka, 2012)) including past study (after (Santoso, 2017))	62
Figure 4.15. Observed and Predicted Values of B/d_r and h/d_r Using Dimensionless Channel Forming Discharge Equation.....	62

Figure 4.16. Valley Slope and Stream Power (Modified from van den Berg (1995)).	64
Figure 4.17. Channel Pattern Determination by Using Stream Power and Median Grain Size (Modified from Kleinhans & van den Berg (2011))	64
Figure 4.18. River Patterns, Stream Power and Silt Clay Fraction of River Bank (Modified from Candel et al., (2021))	65
Figure 4.19. Channel Pattern Determination by Using Stream Power, Median Grain Size (Modified from Kleinhans & van den Berg (2011)) combined with Silt-Clay Percentage (Modified from Candel et al. (2021)).	66
Figure 4.20. Excess Shear Stress and Erosion Rate of Target Rivers	67
Figure 4.21. Sinuosity, Aspect Ratio, Bed-Bank Sediment Condition	69
Figure 4.22. Meander Wavelength, Radius of Curvature, Aspect Ratio, and Bed-Bank Sediment Condition - Red Line Threshold (Rosgen, 1994), Green Line Threshold (Church & Rood, 1983)	69
Figure 4.23. Straightened Rivers Condition in Type 2a	70
Figure 4.24. Past Condition of Oppe and Iruma (<i>Time Series Topographic Map, 2021</i>)	71
Figure 4.25. Cut-off Condition of Kano River (<i>Geospatial Information Authority of Japan, 2021</i>)	71
Figure 4.26. Cut-off Condition of Kuji River (<i>Geospatial Information Authority of Japan, 2021</i>)	71
Figure 4.27. Meandering Trace in Cimanuk River (45 km from river mouth)	72
Figure 4.28. M Value Condition Related to Aspect Ratio VS Sinuosity	73
Figure 5.1 Schematic diagram of flow velocity at bed load layer and erosion velocity ((Egashira et al., 1997) (Ahmad, 2020))	77
Figure 5.2 Particle Entrainment Model (Harada et al., 2019) (Modified by (Masbahul, 2020))	78
Figure 5.3 ICHARM Bank Erosion Model Computational Domain	78
Figure 5.4 Schematic of Grid Updating by Streachable Grid (Biswas et al., 2016)	79
Figure 5.5 Bank Grid Treatment	80
Figure 5.6 Erosion Rate Values for Numerical Simulation	81
Figure 5.7. Flood Alert Level Cimanuk River at Rentang Weir (Ministry of Public Works and Housing, 2021)	82
Figure 5.8. Daily Average Discharge at Rentang Weir (2003-2014)	83
Figure 5.9. Flow Duration Curve at Rentang Weir (2003-2014)	83

Figure 5.10. Numerical Simulation Result for Case 2a-1 SC Bank 91.46% Bed Material 0.05mm (a) Depth and Velocity Magnitude (b) Bank Shifting Distribution (c) Cross-Sectional Shape.....	85
Figure 5.11. Numerical Simulation Result for Case 2a-2 SC Bank 91.46% Bed Material 0.25mm (a) Depth and Velocity Magnitude (b) Bank Shifting Distribution (c) Cross-Sectional Shape.....	86
Figure 5.12. Numerical Simulation Result for Case 2a-3 SC Bank 45.29% Bed Material 0.25mm (a) Depth and Velocity Magnitude (b) Bank Shifting Distribution (c) Cross-Sectional Shape.....	87
Figure 5.13. Numerical Simulation Result for Case 2b-1 SC Bank 91.46% Bed Material 0.25mm (a) Depth and Velocity Magnitude (b) Bank Shifting Distribution (c) Cross-Sectional Shape.....	88
Figure 5.14. Numerical Simulation Result for Case 2b-2 SC Bank 91.46% Bed Material 0.05mm (a) Depth and Velocity Magnitude (b) Bank Shifting Distribution (c) Cross-Sectional Shape.....	89
Figure 5.15. Numerical Simulation Result for Case 2b-3 SC Bank 45.29% Bed Material 0.25mm (a) Depth and Velocity Magnitude (b) Bank Shifting Distribution (c) Cross-Sectional Shape.....	90
Figure 5.16. Forming Mechanism Type 2a Downstream of Lower Reach Segment II-2 ..	93
Figure 5.17. Potential Specific Stream Power of Numerical Simulation Cases	96
Figure 5.18. Forming Mechanism Type 2b Downstream of Lower Reach Segment II-1 ..	96
Figure 5.19. Active Erosion and Deposition of Cimanuk River	97

List of Tables

Table 2-1. Type of Sand-Mud Mixtures (Van Rijn, 2020)	19
Table 2-2. Summary of Aspect Ratio (F), Sinuosity (P) and M Values	21
Table 3-1. Target Rivers General Characteristics Summary	25
Table 3-2. The Ciliwung River Discharge with Different Return Period (Ministry of Public Works and Housing, 2008).....	31
Table 3-3. The Serayu River Discharge With Different Return Period (Ministry of Public Works and Housing, 2016).....	32
Table 3-4. Number of Data in Each River.....	41
Table 3-5. Geological Characteristics of Target Rivers	47
Table 4-1. Classification of Bed and Bank Material Condition	53
Table 4-2. B/d_r and h/d_r Estimation Coefficient for Each GSD Type.....	63
Table 4-3. Proposed Classification of Meandering Rivers (Modified (Soar & Thorne, 2001))	74
.....	
Table 5-1. Boundary Condition of Cimanuk River Bank Erosion Simulation	81
Table 5-2. Discharge Analysis for Cimanuk River Simulation	84
Table 5-3. Bank Shifting and Centerline Movement Summary	91
Table 5-4. Cross-Sectional Parameters and Aspect Ratio Summary for Case Type 2a	92
Table 5-5. Summary for Case Type 2a	93
Table 5-6. Cross-Sectional Parameters and Aspect Ratio Summary for Case Type 2b	95
Table 5-7. Summary for Case Type 2b	95

List of Symbol

AR or F	=	aspect ratio or width-depth ratio
B or W or W_{bf}	=	bankfull width (m)
H or h	=	depth (m)
K or P	=	sinuosity
I_o or S or S_c	=	channel slope
$\sqrt{D_{84}/D_{16}}$	=	grain size distribution uniformity
L_m	=	meander wavelength (m)
R_c	=	radius of curvature (m)
Q	=	channel forming discharge (m^3/s)
g	=	gravity acceleration (m/s^2)
d_r or D_{60}	=	representative diameter (m)
ω	=	stream power (W/m^2)
τ_0	=	bed shear stress (N/m^2)
τ_c	=	critical shear stress (N/m^2)
u	=	depth-averaged flow velocity (m/s)
ρ	=	density of water (kg/m^3)
Q_{bf}	=	bankfull discharge (m^3/s)
ω_{pv}	=	potential specific stream power (W/m^2)
S_v	=	valley slope
W_r	=	reference channel width (m)
α	=	relative standard deviation of sediment size distribution
D_{50}	=	median sediment diameter (m)
ω_{bm}	=	discriminator between a braided and meandering pattern
ω_{sc}	=	discriminator between scroll and chutes meandering
ω_{ia}	=	discriminator of inactive-active pattern transition
ω_{tm}	=	discriminator of tortuous–meandering pattern transition
ω_{it}	=	discriminator of the inactive–tortuous pattern transition
M	=	silt-clay index of channel perimeter (%)
C_{bank}	=	silt and clay percentages in channel banks (%)
C_{bed}	=	bed silt and clay percentages (%)
d	=	average depth (m)
τ_{bf}	=	bankfull fluid shear stress
τ_*	=	Shield parameter
H_{bf}	=	bankfull depth
τ_{*bf}	=	averaged bankfull Shield stress

R	=	assumed relative submerged grain density
ε	=	lateral fluvial erosion rate
k_d or K	=	erodibility coefficient
τ_{b0}	=	cross-sectional shear stress (N/m ²)
τ_{bc}	=	critical bank shear stress (N/m ²)
P_{SC}	=	Silt-clay percentage (%)
τ_{*bf50}	=	bankfull Shields number
Re_{p50}	=	particle Reynolds number

Chapter 1

Introduction

1.1 Background

Natural disaster has been increasing recently at a global scale, drawing more attention of research focusing on the extreme event analysis and the impact of climate change on the hydrological processes. Flood is one of the hydrological natural disasters which affects large portion of population among other natural hazard (Aerts et al., 2018). Evidence of the increasing number of floods around the world has also been described in many studies. A global analysis of flood event utilizing observation data from EM-DAT (Emergency Events Database) and DFO (Dartmouth Flood Observatory) indicated the increasing number of flood events on a global scale (Hu et al., 2018). In addition to that, the study also suggested a tendency of higher flood magnitude in a single event. Similar trend was identified through several regional studies, such as around Europe (Kundzewicz et al., 2018) and Asia (Dutta & Herath, 2004). Such increase has been projected through global climatic model which predicts that higher number of flood would likely to occur across Asia, South America, and some part of Africa (Hirabayashi et al., 2013). These studies also show that frequency of flood in Indonesia seems to be higher in the future. This condition increases flood risk because many cities in Indonesia are located around flood prone area.

Flood is one of the dominant hazards among the natural disasters in Indonesia, along with the tornado (Caksono, 2020). The Indonesia National Board for Disaster Management (BNPB) has also recorded hundreds to thousands of floods occurred across the nation. More than half of flood events were concentrated in the big cities such as Jakarta, Bandung, Surakarta, Semarang, and Medan (Figure 1.1). In Jakarta alone, more than 90 thousand of people were affected by flood events in the beginning of year 2020. Such flood in Jakarta have caused infrastructure losses of about 10 trillion Indonesian Rupiah (about 700 billion USD). Although the flood control facilities are being developed, the risk would be likely still to be high due to many influencing factors. The urbanization and population growth in big cities are in a positive trend, making the cities more vulnerable to such hazard. On the other hand, the annual national budget of the Directorate General of Water Resources in Indonesia (DGWR) for flood control is limited (Figure 1.2). Therefore, efficient strategies in flood management need to optimize the resources.

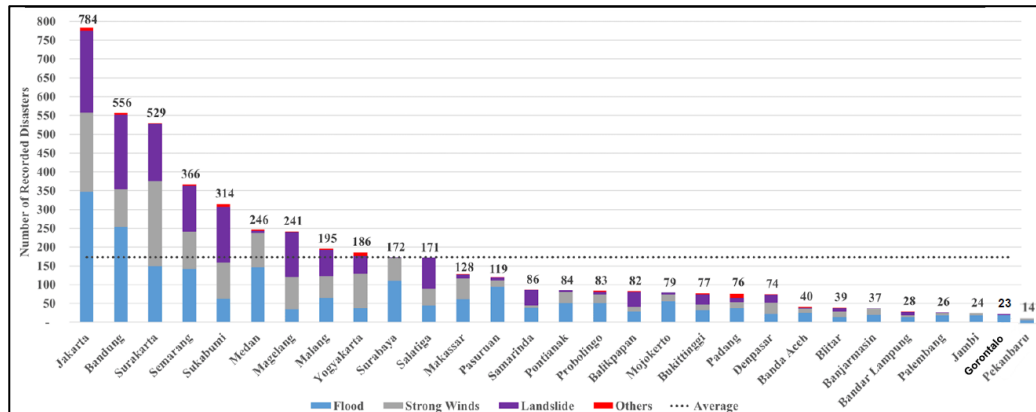


Figure 1.1 Disaster Events in Indonesia from 2003 – 2017 (BNPB Database)

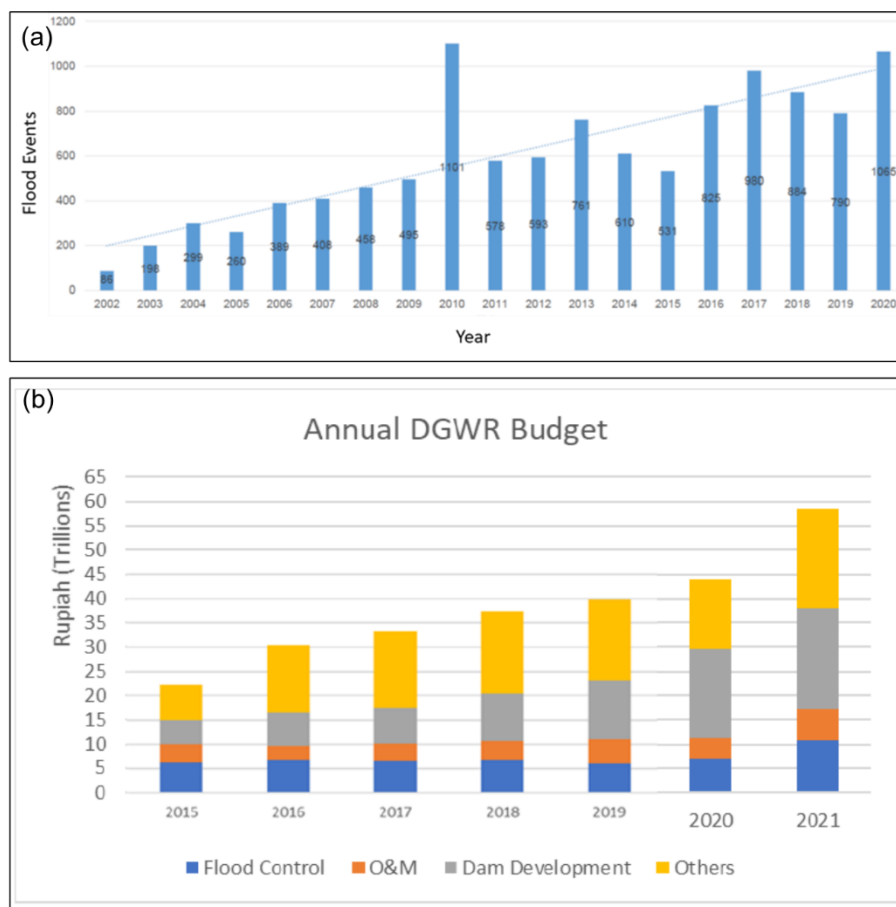


Figure 1.2 (a) Flood Events Trend in Indonesia (b) Annual DGWR Budget

Jakarta, the capital city of Indonesia, experienced the most frequent floods in the last decade (Figure 1.1). The flood disaster management in Jakarta is done by the floodway construction, river capacity improvements, and revitalization of retention ponds. Anticipating the higher risk in the future, the challenge in Indonesia, as well as other developing countries, is the optimization or prioritization of river works within limited available resources.

One of the most popular river improvement works in Jakarta is river capacity improvement by dredging and widening. However, the available space to do such work is

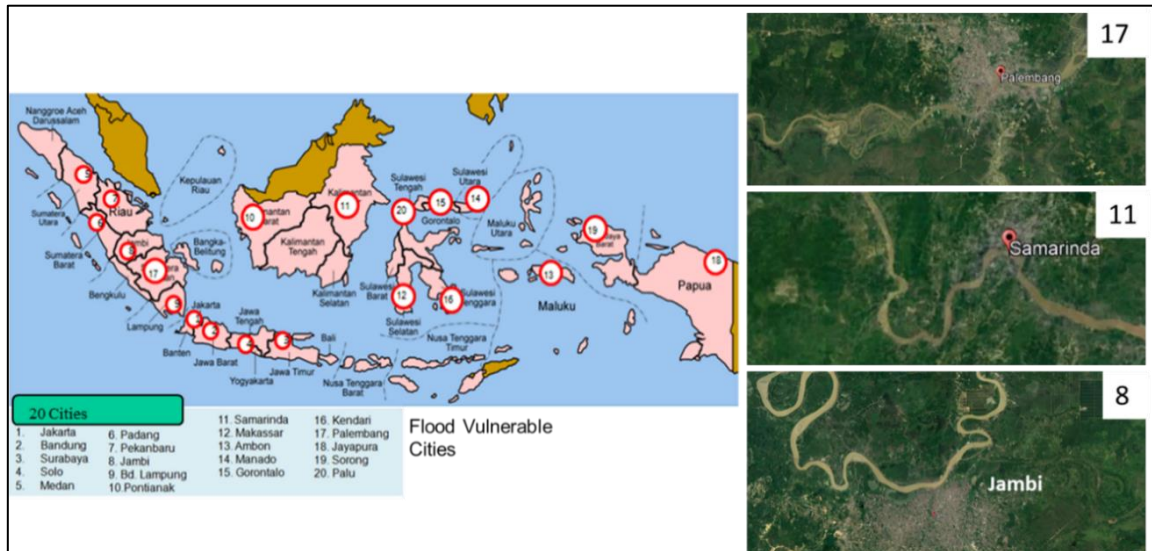


Figure 1.3 Cities with Meandering Rivers in Indonesia

limited, especially for river widening. Such challenge also occurs in other big cities which are usually located in the downstream. Moreover, areas in the downstream part are the meandering flood plain where meandering rivers exist (Figure 1.3). These situations increase the difficulty of river management due to the complex morpho-dynamics of the meandering channel. Planform dynamics of meandering rivers are complex, influenced by several factors, such as bed and bank material size, aspect ratio (width-depth ratio), bank erosion rate, shear velocities, bed shear stress and stream power, etc. The planform of meandering channel can be represented by meandering parameters such as sinuosity, radius of curvature and meander wavelength. These parameters also affect the planform dynamics, that means there are interactions. Therefore, understanding the mechanism of meandering river would be beneficial to the planning and design of river improvement works. Not only in Jakarta, but in other cities with similar physical characteristics, the knowledge on the mechanism can be applied.

One important factor in the plan of river works is the channel design. To optimize the channel design, it is necessary to consider the principles of both stable cross-sectional shape and the planform dynamics of meandering river simultaneously. Therefore, this study attempts to understand the mechanism of planform dynamics in maintaining the cross-sectional stable shape by focusing on aspect ratio (or width-depth ratio). We believe that elaborating this mechanism will be beneficial for the efficiency of river management works.

River managers can benefit from understanding of the processes and patterns of river bank erosion which determines the pattern of channel migration (Larsen et al., 2006). Despite the need for channel design principles in river management and restoration, the question “what controls the width of a river?” still remains unanswered (Dunne & Jerolmack, 2020). Therefore, it is important to understand the mechanism and phenomena among aspect ratio, sediment characteristics, hydraulic condition, bank erosion rate, planform and meandering

process. This study is trying to give comprehensive perspective about how to manage meandering rivers.

1.2 Objective

The objective of this research is to investigate individual characteristics of meandering channel and its stability by focusing on the interaction between sediment size characteristics and cross-sectional shape. Another important thing is how the regional characteristics affect the channel forming process which is related to cross-sectional shape. The difference of regional characteristics will be represented by the comparison of Japanese rivers and Southeast Asian rivers.

1.3 Methodology

This research covers three main methodologies as follows:

Field observation and Data Collection. Several target rivers were selected and the lower reach or around meandering flood plain are focused. Field observations has been carried out to collect cross-sectional and sediment data. Observation of satellite imagery, DEM, geological map and historical map is a method to complete the information about surrounding condition. In this part, channel parameters such as aspect ratio, sediment size, riverbed slope and discharge are main factors or parameters to prepare for comparison analysis. Meandering parameters such as sinuosity, radius of curvature, meander wavelength and centerline movement are also prepared to be analyzed.

Comparison and Analyzing Parameters. To understand the physical phenomena of each parameter, comparison among parameters was carried out. Parameters are aspect ratio, sinuosity, sediment sizes, silt-clay percentage, shear stress, stream power and bank erosion rate. During this process, understanding common characteristics and explaining them with the past classification of meandering channel are important. Target of this part is modifying the past classification of river channel in order to understand various condition of meandering channel.

Planform Change or Centerline Movement Analysis. This analysis tries to understand the interaction between sediment sizes and aspect ratio related to sinuosity and centerline movement. Numerical simulation was conducted by using iRIC Nays2DH ICHARM Bank Erosion Model. Target rivers was selected based on the modified classification. The validation was done based on the field observation data and the satellite image by checking bank erosion and centerline movement. The final targets are explaining aspect ratio stability of each channel type based on the modified classification and understanding the mechanism of planform dynamics affected by regional characteristics of bed-bank material.

1.4 Thesis Outline

This thesis is organized by five chapters. Chapter 1 explained about background and objectives of this study. Chapter 2 summarizes relevant literatures of the topics including past meandering classification. Information about target rivers and data collection method are introduced in Chapter 3. This chapter gives general information about catchment including catchment area and geological information. Chapter 4 is analyzing the relationship among parameters including how they are related to past meandering classification. After that, modified classification is proposed, and target rivers are classified. Chapter 5 gives information about numerical simulation and how it was validated with the observation data. By comparing the simulation results and the characteristics of each channel type, meandering process of each channel type is discussed. Chapter 6 is the summary of this thesis which consists of conclusion, recommendation and limitation of this study.

Literature Review

2.1 River Classification

One of the river classification systems is based on its geomorphological characteristics. Generally, the longitudinal profile of a river could be categorized into three parts: upstream, middle stream and downstream. Variation of rivers is governed by the complex interaction of sediment sizes, slopes and other influencing factors (Montgomery & Buffington, 1997). Figure 2.1 illustrates the general classification of river profile.

Different sediment size, slope and other river components create different characteristics of channel geomorphology from upstream to downstream as shown in Figure 2.2. The middle panel of Figure 2.2 shows the tendency of meandering river planform in the downstream area. The forming process of meandering river will be described in the next section.

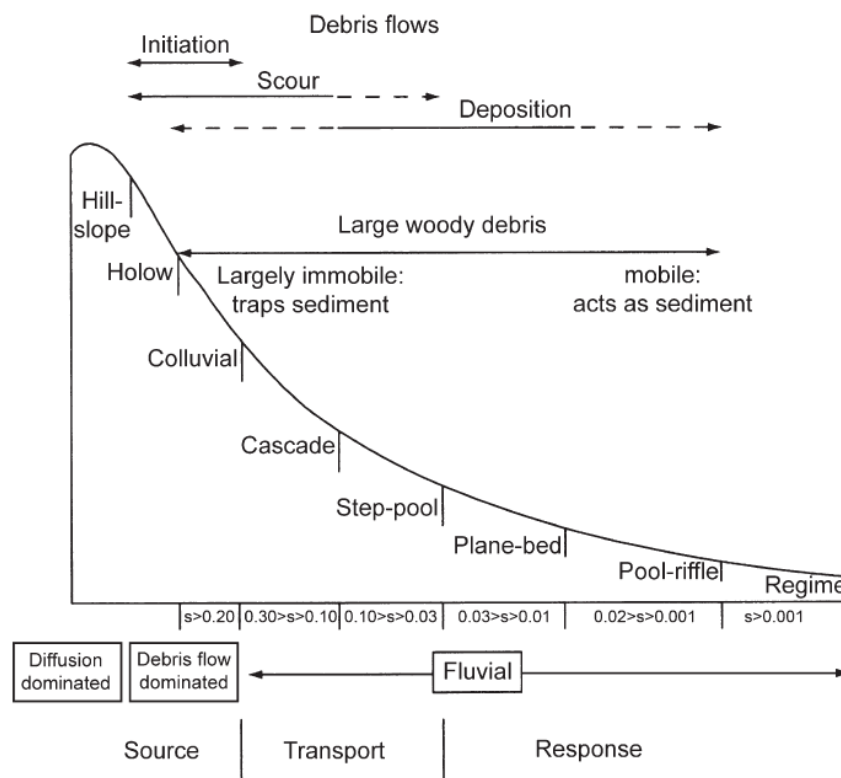


Figure 2.1. River channel types according to the longitudinal profiles (Montgomery & Buffington, 1997)

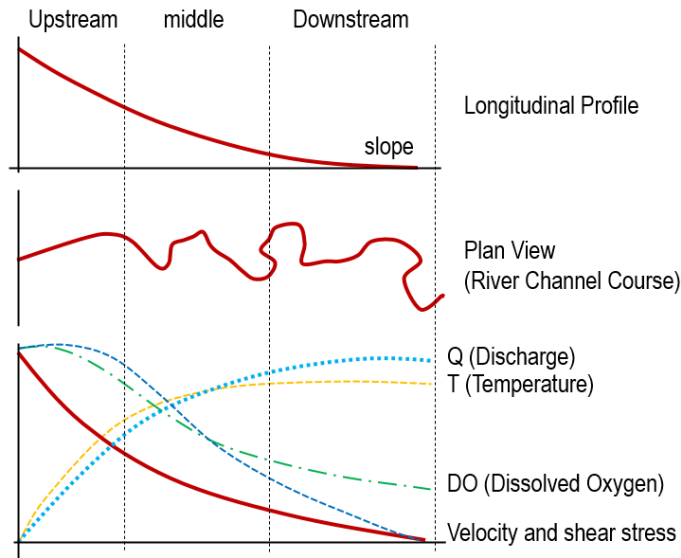


Figure 2.2. Longitudinal river profile from upstream to downstream and the different component characteristics. (modified from Maryono (2005))

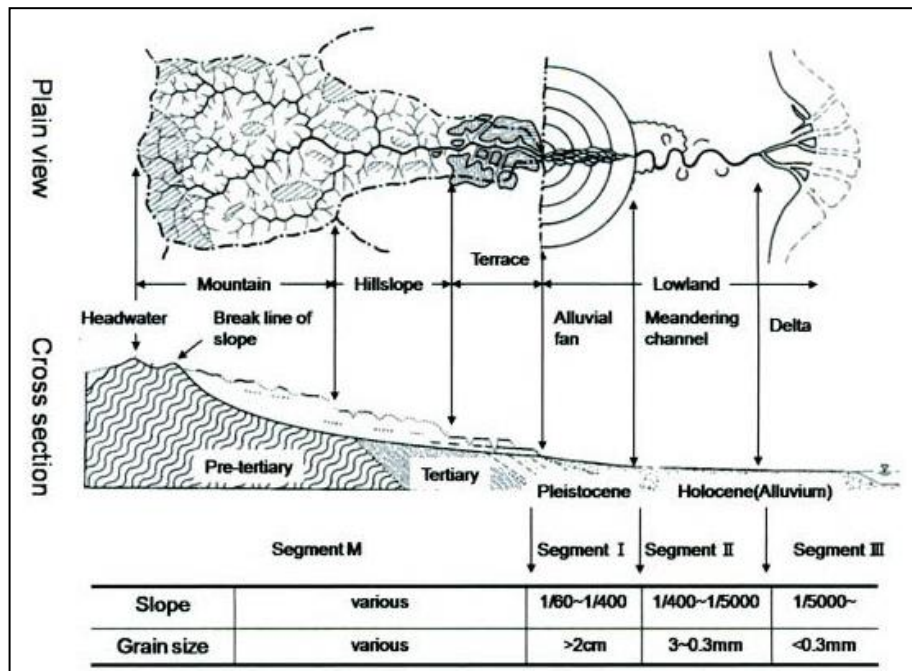


Figure 2.3. Fluvial geomorphology from mountain to the sea (modified from Suzuki (1997) and Yamamoto (2004))

Figure 2.3 shows another classification based on the river geomorphology which divides the river profile into four segments: Segment M (mountain), Segment I (alluvial fan), Segment II (meandering plain), and Segment III (delta area) (Yamamoto, 2004). This classification locates the meandering plain in Segment II. This segment is characterized by 1/400 - 1/5,000 slope and 3 cm - 0.3 mm sediment size. Based on the sediment size, this segment can be divided into two sub segments. In the first sub-segment (Segment II-1), sediment is ranging from 3 cm to 1 cm, while the second sub-segment (Segment II-2) has the sediment size ranging

from 1 cm to 0.3 mm. Meandering channel can be found both in Segment II-1 and II-2. These are the target segments of this study.

Research on meandering rivers has mainly attempted to explain the morpho dynamic evolution of meandering rivers governed by the interactions among water flow, sediment transport, channel planform, and bed morphology (Güneralp et al., 2012). Channel planform are evolving as results of interactions among flow, sediment transport, and channel form (Seminara, 2006).

Leopold & Langbein, (1966) showed that the effect of meanders is to introduce flow resistance due to curvature. In such a way, uniform utilization of energy occurs through the whole length of the meander reach. The meander pattern approaches more closely the condition of equilibrium, as defined by entropy concept, than the non-meandering one. Meandering is the most probable form of channel geometry which is more stable and natural than a straight channel (Chitale, 1973).

Meandering rivers can be classified based on channel planform, aspect ratio, riverbed slope and sediment size. There are three most referred categorizations of meandering rivers, which were suggested by previous studies (Brice, 1975; D. L. Rosgen, 1994; Schumm, 1963) as shown in Figure 2.4.

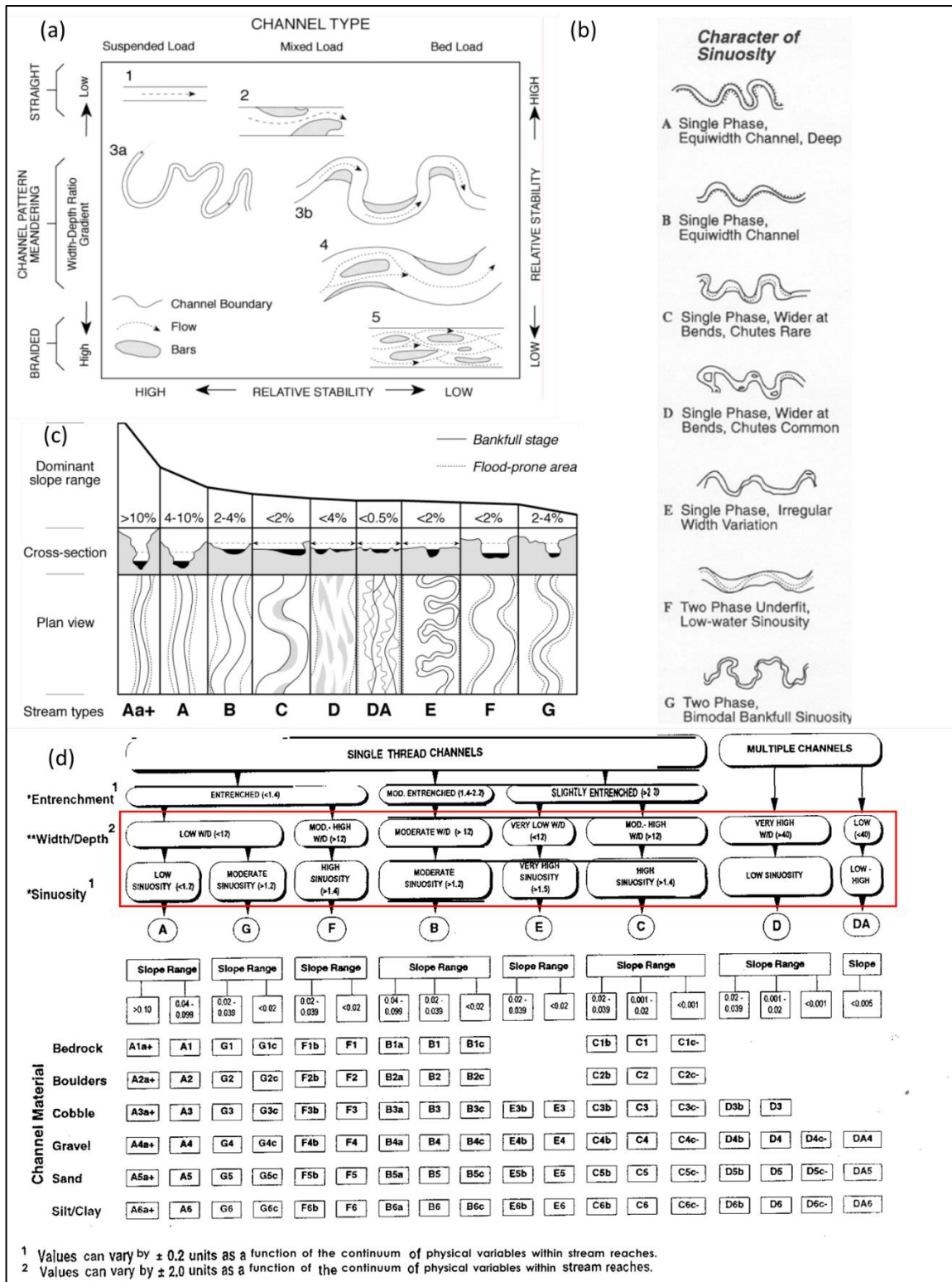


Figure 2.4. Categorization of Meandering Rivers (a) Channel Type (Schumm, 1963,1977) (b) Character of Sinuosity (Brice, 1975) (c) Geomorphic Characterization (Rosgen, 1994) (d) Morphological Description (Rosgen, 1994)

These studies summarized the type of stable single-thread channel (Soar & Thorne, 2001). Then three types could be defined through these studies, Type 1 for Equiwidth Meandering, Type 2 for Meandering with point bars, and Type 3 for Meandering with point bars and chute channels. Characteristics of three types shown in Figure 2.5 are summarized as follows (Soar & Thorne, 2001).

Type 1: Equiwidth meandering (Schumm’s Type 3a, Brice’s Type A/B and Rosgen’s Type E). This type is characterized by the low variability of channel width around the meander bends. This type has low width/depth ratio, erosion resistant banks, and fine-grain bed material (sand or silt). Banks are naturally stable and relatively low channel migration.

Type 2: Meandering with point bars (Schumm’s Type 3b, Brice’s Type C, and Rosgen’s Type C). This type is characterized by intermediate width/depth ratio, moderately erosion resistant banks, and medium grained bed material (sand or gravel). This type has well-developed point bars, but a few chute channels. Moderate channel migration rates are observed on this type, unless banks are stabilized.

Type 3: Meandering with point bars and chute channels (Schumm’s Type 4, Brice’s Type D and Rosgen’s Type C/D). This type is indicated by high width/depth ratios, highly erodible banks, medium-to-coarse grained bed material and (sand, gravel and/or cobbles). This type has well-developed point bars and frequent chute channels. Moderate channel migration rates is observed on this type, unless banks are stabilized.


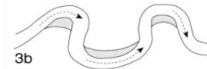
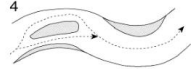
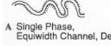




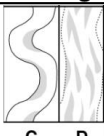
Classification of Meandering Rivers		
Type 1	Type 2	Type 3
Equiwidth Meandering • High Sinuosity • Low B/H Ratio • Bed Material Sand-Silt	Meandering with Point Bars • Moderate Sinuosity • Intermediate B/H Ratio • Bed Material Sand-Gravel	Meandering with Point Bars and Chute Channels • Low Sinuosity • Moderate to High B/H Ratio • Bed Material Sand-Gravel-Cobbles
Bed Material Load (Bed, Suspended, Wash Load) Type (Soar and Thorne, 2001)		
Low	Medium	Heavy
Bank Erosion (Soar and Thorne, 2001)		
Resistant	Moderately Resistant	Highly Erodible
Classification by Schumm (1963, 1977)		Fig. 2.5 (a)
		
Classification by Brice (1975)		Fig. 2.5 (b)
 A Single Phase, Equiwidth Channel, Deep	 C Single Phase, Wider at Bends, Chutes Rare	 D Single Phase, Wider at Bends, Chutes Common
Classification by Rosgen (1994)		Fig. 2.5 (c)
 E	 C	 C D

Figure 2.5. Classification of meandering river (based on Soar & Thorne, 2001).

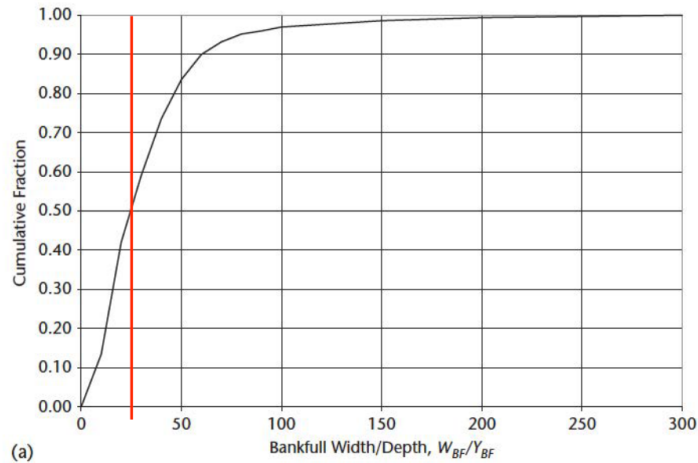


Figure 2.6. Cumulative frequency of 499 measurements of bankfull aspect ratios of natural channels (Church & Rood, 1983)

As is shown in Figure 2.5, width-depth ratio (aspect ratio), sinuosity and bed-bank material size are the important parameters for the planform. But the boundary among high, moderate or intermediate and low of these parameters is not clear. In order to find the quantitative boundary, key values for each parameter are analyzed respectively.

a) Aspect Ratio

In Figure 2.5, aspect ratio is an important parameter for channel planform. The threshold value of aspect ratio was determined by past study as follows; low aspect ratio is less than 12, moderate to high is 12-40, and very high aspect ratio is more than 40 (Rosgen, 1994). Another study investigated natural channels and mentioned that 50% of the distribution has a bankfull aspect ratio of more or less than 25 (Church & Rood, 1983). The condition of cumulative frequency of dataset is shown in Figure 2.6.

Related to other channel parameters such as tractive force and channel slope for bar formation, Kuroki & Kishi (1984) found the important boundary (Figure 2.7) that the aspect ratio between no bar and alternate bar is around 20-38 (Figure 2.7). This interpretation also related to single thread of meandering river that might be classified based on bar formation condition. 38 is similar with 40, but 20 to 25 can be another threshold. Figure 2.7, however, aspect ratios 20 corresponds to $I = 0.01$ and it is rather steep in meandering plain. Therefore, larger value seems to be better. The parameter includes channel slopes, but the boundary of the aspect ratio can be estimated (Santoso, 2017).

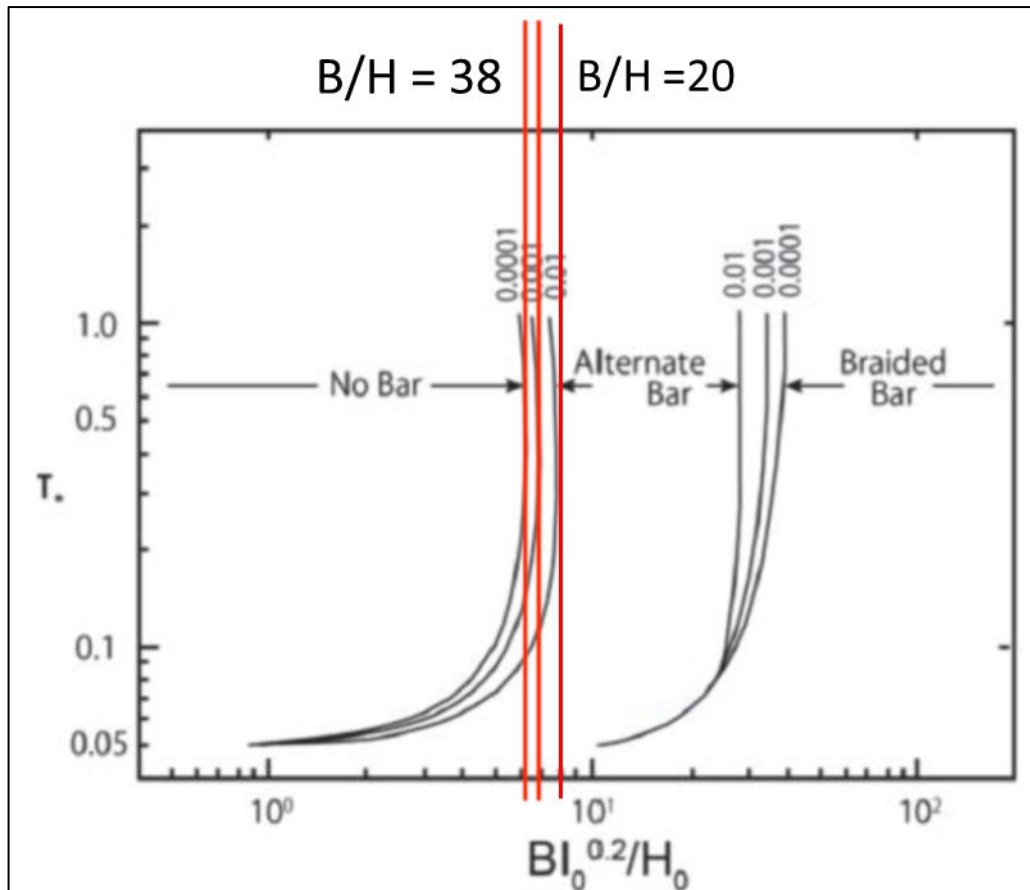


Figure 2.7. Kuroki-kishi Diagram (Kuroki & Kishi, 1984) and Aspect Ratio Interpretation (after Santos, 2017)

Based on overall studies above, an aspect ratio of 25 is considered as intermediate value of aspect ratio and the aspect ratio is classified into four categories: Low Aspect Ratio (<12), Low-Moderate (> 12 - < 25), Moderate – High (> 25 - < 40), and High (> 40).

b) Sinuosity

As shown in Figure 2.8, sinuosity is defined as stream length divided by valley length (Rosgen, 1996). Based on the classification by past study (Rosgen, 1994), river course is considered as low sinuosity if the value is lower than 1.2 (Figure 2.4 (d)). A value between 1.2 – 1.5 is considered to be moderate sinuosity (Rosgen, 1994), while river with sinuosity value more than 1.5 is categorized as high sinuosity. In this study, only 1.5 is used to define the boundary between high and low sinuosity in order to simply the classification.

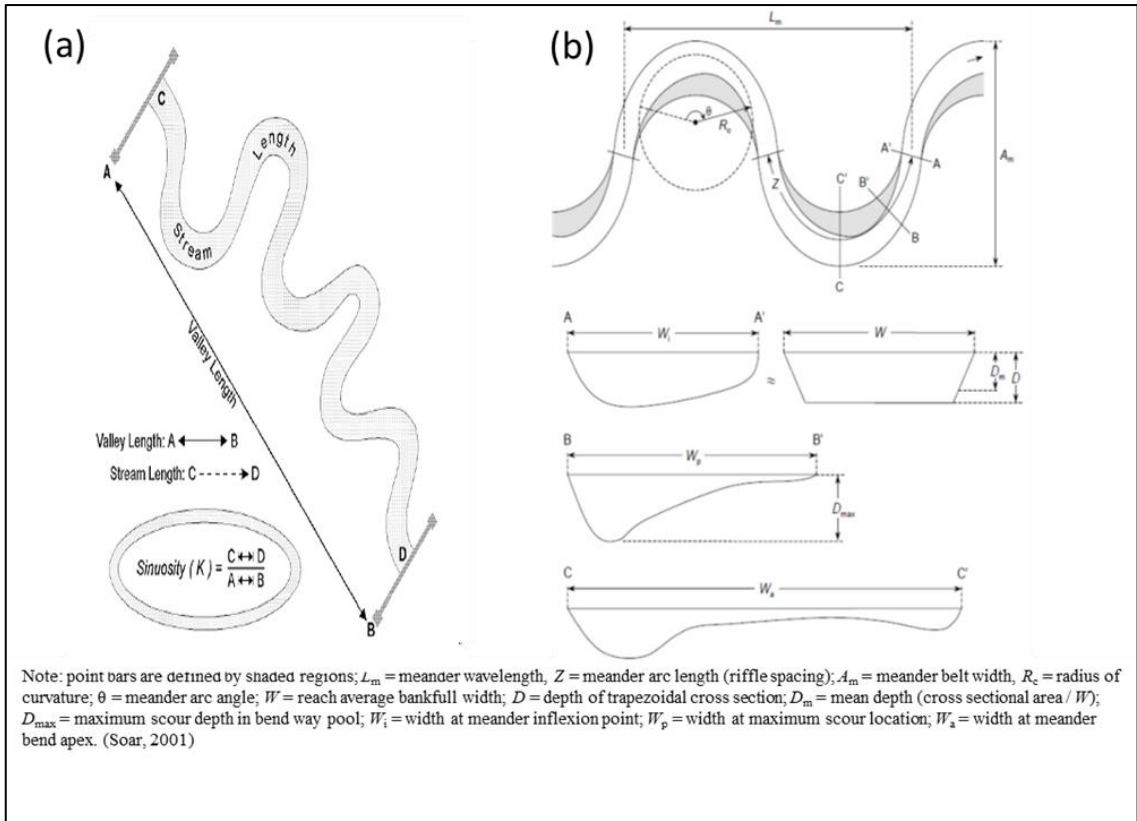


Figure 2.8. (a) Sinuosity (Rosgen, 1996). (b) Meandering Rivers Cross-Sectional Shapes (Soar & Thorne, 2001)

Past study divided each 10 km reaches to calculate sinuosity (Friend & Sinha, 1993). Similar methods were also applied for each around 1km of Ciliwung River reaches (Ramdhani & Setiawan, 2015) and around 3km of Cimanuk River reaches (Ramdhani et al., 2020) in past studies in Indonesia. In this study, sinuosity was calculated for each 3km of target rivers.

Other parameters for meandering characteristics are meander wavelength (L_m) and radius of curvature (R_c). Meander wavelength (L_m) could be estimated from channel width (W) as represented in equation (Soar & Thorne, 2001).

$$L_m = (11.26 \text{ to } 12.47)W \tag{1}$$

11.9 is the mean of 11.26 and 12.47 and will be used in this study.

Radius of curvature (R_c) is estimated by L_m as follows (Williams, 1986)

$$R_c = \frac{L_m K^{1.5}}{13\sqrt{K} - 1} \tag{2}$$

where K is sinuosity.

2.2 Regime Theory

The importance of “regime theory” has been widely discussed and several empirical relationships were introduced to investigate stability condition of channel shape. These studies tried to explain river width and depth by using discharge, sediment sizes, and slope. For example, Julien & Wargadalam (1995) suggested the following equations.

$$h = 0.2Q^{0.33}d_{50}^{0.17}S^{-0.17} \quad (3)$$

$$W = 1.33Q^{0.44}d_{50}^{-0.11}S^{-0.22} \quad (4)$$

Where h is river depth (m), W is river width (m), Q is bankfull discharge (m^3/s) d_{50} is median grain size diameter of the bed material (m), and S is channel slope.

However, unit of right and left side of these equations are different and it is difficult to understand the range of channel scale to apply the equation. Another study derived the relationship among dimensionless channel forming discharge, relative width and relative depth as follows (Fukuoka, 2010).

$$\frac{B}{d_r} = 4.25 \left(\frac{Q}{(gId_r^5)^{0.5}} \right)^{0.40} \quad (5)$$

$$\frac{h}{d_r} = 0.13 \left(\frac{Q}{(gId_r^5)^{0.5}} \right)^{0.38} \quad (6)$$

where B is width, h is depth, Q is channel forming discharge, d_r is representative diameter of the bed material in meters (usually d_{60}), g is gravitational acceleration, I is channel slope, and $Q/(gId_r^5)^{0.5}$ is dimensionless channel forming discharge. Applicability of these equations is shown in Figure 2.9.

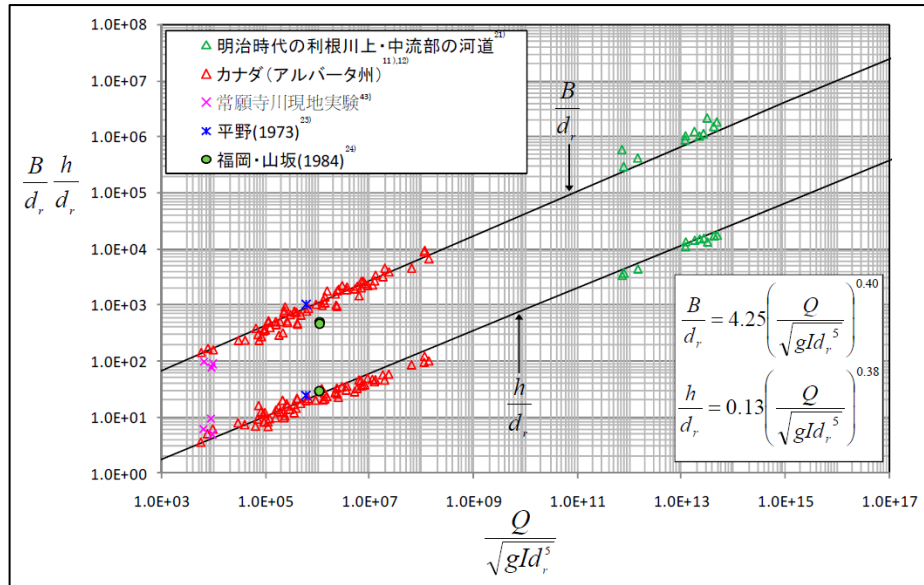


Figure 2.9. Dimensionless water surface width and water depth to dimensionless channel-forming discharge (Fukuoka, 2010)

2.3 Stream Power and Channel Pattern

Channel pattern is related to stream power. Stream power ω (W/m^2) is a power expenditure per unit width and length of stream bed (Bagnold, 1966). This parameter generally refers to bankfull condition and could be defined as follows.

$$\omega = \tau_0 u = \frac{\rho g Q_{bf} S_c}{W} \quad (7)$$

where τ_0 is the bed shear stress, u is the depth-averaged flow velocity, ρ is the density of water, g is the acceleration due to gravity, Q_{bf} is the bankfull discharge, S_c is the channel slope and W is the channel bankfull width (van den Berg, 1995). Figure 2.10 shows the relationship between unit stream power of bankfull flow and valley slope. It can be identified that braided channel and single thread channel with each P (sinuosity) parameter are determined by stream power and valley slope. Braided channel tends to have higher stream power and steeper slope.

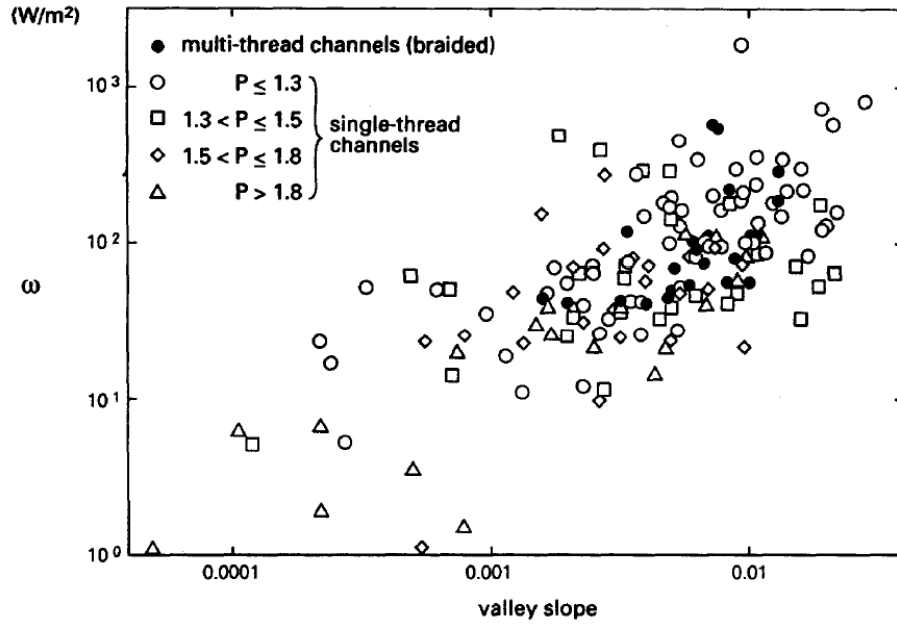


Figure 2.10. Unit Stream Power of Bankfull Flow versus Valley Slope (van den Berg, 1995)

Prediction of channel pattern was approached by potential specific stream power (Kleinhans & van den Berg, 2011). Potential specific stream power is defined as follows (van den Berg, 1995).

$$\omega_{pv} = \frac{\rho g Q S_v}{W_r} \quad (8)$$

Where ω_{pv} is the stream power for the potential maximum of the available flow energy corresponding to a minimum sinuosity $P = 1$, S_v is the valley slope (-), related to channel slope as $S = P S_v$, ρ is the water density (kg/m^3), g is the acceleration due to gravity (m/s^2), Q is the channel-forming discharge (m^3/s) (mean annual flood or bankfull discharge), and W_r is the reference channel width (m). The reference width W_r is predicted the by following empirical equation (Kleinhans & van den Berg, 2011).

$$W_r = \alpha \sqrt{Q} \quad (9)$$

where $\alpha = 4.7 \sqrt{\text{sm}^{-1}}$ for sand defined as $D_{50} < 2\text{mm}$ and $\alpha = 3.0 \sqrt{\text{sm}^{-1}}$ for gravel.

Figure 2.11 shows the classification of channel pattern based on the potential specific stream power (8) and D_{50} (Kleinhans & van den Berg, 2011). The definition of discriminators in the graph are ω_{bm} (discriminator between a braided and meandering pattern) = $900 D_{50}^{0.42}$ (blue line), ω_{sc} (discriminator between scroll and chutes meandering) = $\frac{900}{\sqrt{10}} D_{50}^{0.42}$ (green line), and ω_{ia} (discriminator of inactive-active pattern transition) = $90 D_{50}^{0.42}$ (red line).

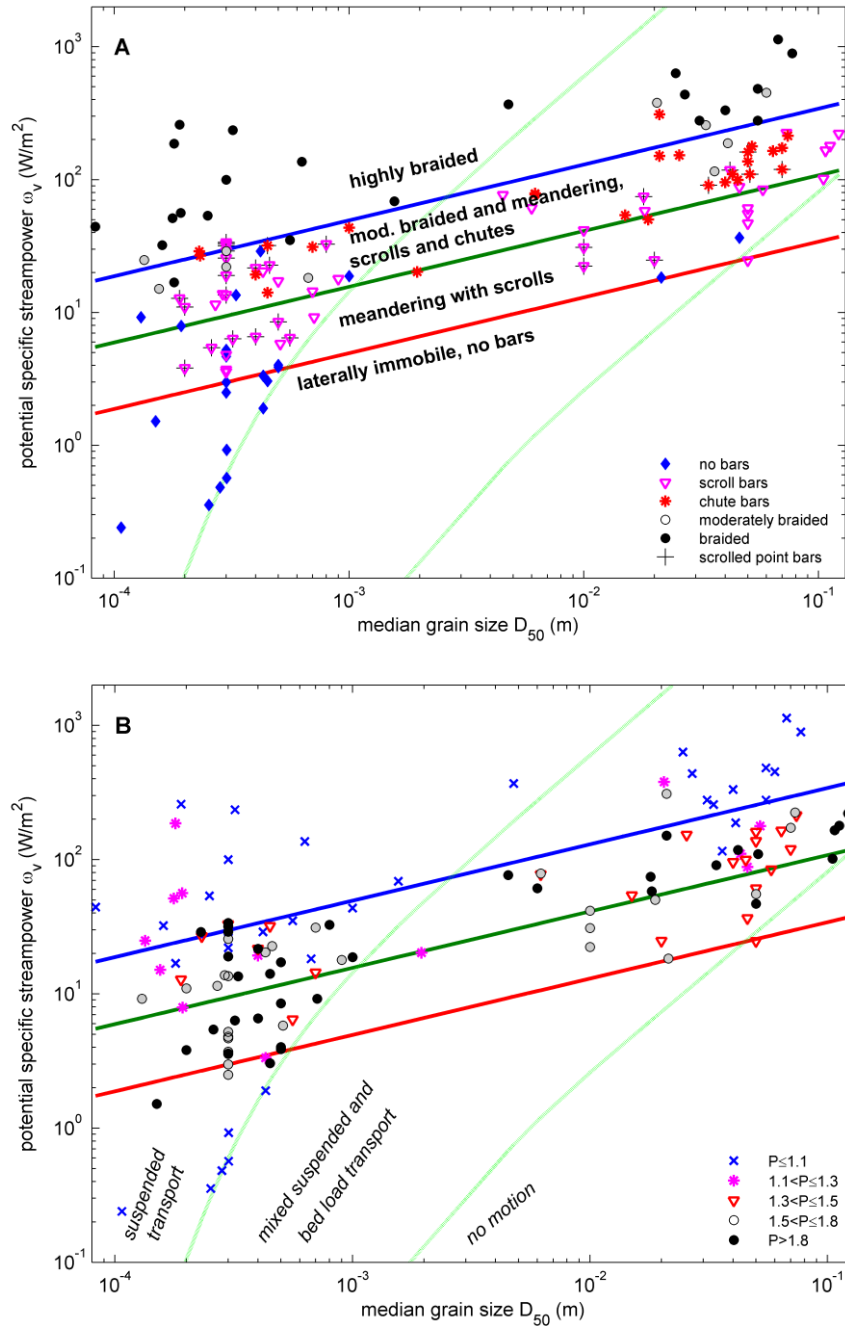


Figure 2.11. Patterns of equilibrium alluvial rivers plotted with the potential specific streampower related to valley gradient and predicted width. A. Data subdivided by bar pattern and B. Data subdivided by sinuosity (Kleinhans & van den Berg, 2011)

Figure 2.11 (A) shows that most rivers are correctly plotted above the applicable threshold and it can be used to predict channel pattern based on potential specific stream power and median grain size (D_{50}). Figure 2.11 (B) shows similar condition with sinuosity values and it can be explained that the threshold of potential stream power also correspond to meandering pattern. However, below the red line threshold where several pattern of sinuous river (bar or without bar) might still exist and it is necessary to re-interpreted.

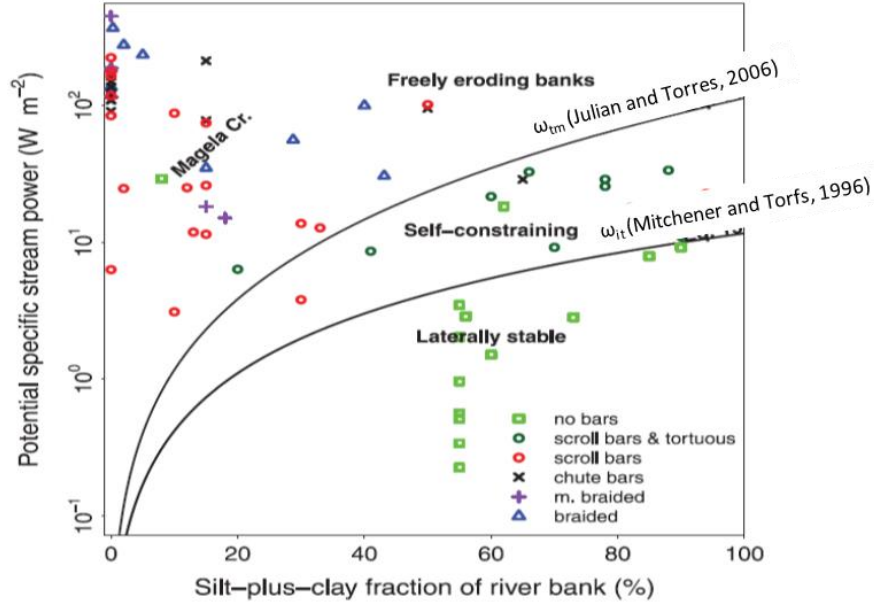


Figure 2.12. River Channel Pattern Prediction From Self-constraining Leading to a Tortuous Channel Pattern, and Freely Eroding Banks Leading to a Normal Meandering Channel Pattern (Candel et al., 2021)

Another effort to define additional discriminator was made by using silt-clay fraction in the river bank (Candel et al., 2021). Empirical relation between critical shear stress (τ_c) and silt clay (SC) fraction was derived as follows (Julian & Torres, 2006).

$$\tau_{c-tm} = 0.1 + 0.1779(SC) + 0.0028(SC^2) - 2.3E^{-5}(SC^3) \quad (10)$$

This equation was transformed into the relation between potential specific stream power and silt-clay fraction (Candel et al., 2021) and determined as ω_{tm} (discriminator of tortuous-meandering pattern transition) by using next equation,

$$\omega_{tm} = \frac{\tau_{c-tm}^{1.5} C}{\sqrt{\rho g}} \quad (11)$$

where C is chezy friction = 28 (Kleinhans & van den Berg, 2011).

Another relationship between critical shear stress (τ_c) and silt-plus clay (SC) fraction of river bank was delivered as follows (Mitchener & Torfs, 1996).

$$\tau_{c-it} = 0.1(SC) + 0.1 \quad (12)$$

This equation also was transformed into potential specific stream power (Candel et al., 2021) and determined as ω_{it} (discriminator of the inactive-tortuous pattern transition) by using next equation.

$$\omega_{it} = \frac{\tau_{c-it}^{1.5} C}{\sqrt{\rho g}} \quad (13)$$

where C is chezy friction = 28 (Kleinhans & van den Berg, 2011).

Detail of transformation process from silt-clay percentage into critical shear stress, to derive these discriminators (ω_{tm} and ω_{it}) are explained in the supplementary document provided by Candel et al., (2021). These discriminators (ω_{tm} and ω_{it}) are useful in order to improve channel pattern prediction for river with cohesive material which was not interpreted well in previous study (Kleinhans & van den Berg, 2011). This study defined both discriminators (ω_{tm} and ω_{it}) by using SC = 87.5% as middle value from upper range of of SC (75-100%) that has been introduced by Candel et al., (2021).

2.4 Silt-Clay Percentages in Bank and Bed Material

Bank strength is related to silt-clay percentage and cohesivity condition. The cohesive fraction of clay and very fine silt is defined as particles with diameters smaller than 8 μm (Van Rijn, 2020). The relationship between cohesiveness and silt-clay percentage could be defined as shown in Table 2-1. Then at least 20% percentage of silt could be interpreted as cohesive channel.

Table 2-1. Type of Sand-Mud Mixtures (Van Rijn, 2020)

Type of sediment	Percentage of organic material	Percentage of Clay+Fine Silt (< 8 μm)	Percentage of Silt (8 to 63 μm)	Percentage of Sand (> 63 μm)
Sand (non-cohesive)	0%	0%	0%	100%
Muddy Sand (weakly-cohesive)	0-10%	0-5%	20-40%	60-80%
Sandy Mud (cohesive)	0-10%	5-10%	30-60%	60-30%
Mud (cohesive)	0-20%	10-20%	50-70%	0-10%
Silty Mud (cohesive)	0-20%	10-40%	60-80%	0%
Clayey Mud (cohesive)	0-20%	40-60%	40-60%	0%

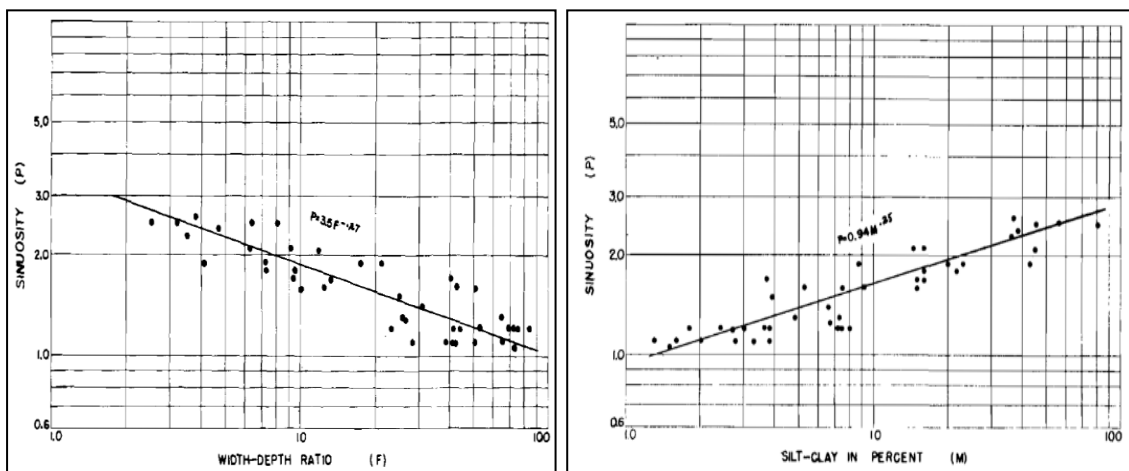


Figure 2.13 Relationship Sinuosity and Width-Depth Ratio (left) and Relationship Sinuosity and Silt-Clay Index (right) (Schumm, 1963)

Schumm (1963) stated that sinuous streams on the Great Plains are characterized by relatively narrow and deep channels, a higher percentage of silt-clay in the perimeter of the channel, and a gentler gradient than less sinuous streams. Relationship among sinuosity, width-depth ratio with silt-clay index of channel parameter (M) is shown in Figure 2.13.

Silt-clay index of channel perimeter (M) was introduced as weighted mean silt-clay percentages which represents the bed-bank material condition (Schumm, 1960). Silt-clay percentage is defined as percentage of passing material through the 200-mesh sieve or the portion smaller than 0.074 mm. M is derived by next equation:

$$M = \frac{C_{bed}(W)+C_{bank}(2d)}{W+2d} \quad (14)$$

Where C_{bank} is silt and clay percentages in channel banks, C_{bed} is bed silt and clay percentages, W is bankfull width, and d is average depth.

Based on the results shown in Figure 2.13, relationship among width-depth ratio (F), sinuosity (P), and weighted mean silt-clay percentages (M) were calculated as follows.

$$P = 3.5F^{-0.27} \quad (15)$$

$$P = 0.94M^{0.25} \quad (16)$$

Another relationship from previous study (Schumm, 1960) also was explained as follows.

$$F = 255M^{-1.08} \quad (17)$$

As mentioned in Chapter 2.1.b, Sinuosity (P) = 1.5 is considered to be an important threshold. If P = 1.5 is substituted in (15), F = 23 is obtained. This value is close to F = 25 that is also important threshold of aspect ratio. If P = 1.5 is substituted in (16), M = 6.5 obtained. But Schumm (1960) suggested another formula (17) that represents the relationship between F and M. In this case, M = 8.6 can be obtained by substituting F = 25.

These results also imply both sinuosity of 1.5 and aspect ratio 25 become significant boundary. By using (15) to (17), probable threshold value can be estimated as is shown in Table 2-2. P and M are derived from F in Table 2-2(a) by using (15) and (17). F and M are derived from P in Table 2-2(b) by using (15) and (16). F and P are derived from M in Table 2-2(c) by using (17) and (16). As the threshold value of M in Table 2-2(c), M = 20 was used because that is considered to be the boundary between cohesive and non-cohesive if bank and bed material is same. Based on Table 2-2, F = 10, P = 1.3, 1.8 and M = 5.6, 6.5, 8.6, and 17 are possible boundary to analyze the characteristics. These values should be checked when the field measurement data is analyzed.

Table 2-2. Summary of Aspect Ratio (F), Sinuosity (P) and M Values

<i>(a)</i>	<i>Aspect Ratio (F)</i>	<i>Sinuosity (P)</i>	<i>M Value</i>
	12 (Rosgen, 1994)	1.79	16.94
	25 (Church & Rood, 1983)	1.47	8.59
	40 (Rosgen, 1994)	1.29	5.56
<i>(b)</i>	<i>Sinuosity (P)</i>	<i>Aspect Ratio (F)</i>	<i>M Value</i>
	1.2 (Rosgen, 1994)	52.69	2.65
	1.5 (Rosgen, 1994)	23.06	6.48
<i>(c)</i>	<i>M Value</i>	<i>Aspect Ratio (F)</i>	<i>Sinuosity (P)</i>
	20 (Van Rijn, 2020)	10.03	1.99

*from predicted value

2.5 Bankfull Shear Stress, Excess Shear Stress, Silt-Clay Percentage and Erosion Rate

Figure 2.14 shows the schematic cross-section of alluvial river with bankfull condition. Bed and bank material can be identified and shear stress in the center of river channel is considered to exceeded the threshold motion. The cross-sectional geometry of fine-grained rivers is set by the threshold stress of cohesive bank-toe material, the structural anchor of the river bank (Dunne & Jerolmack, 2018). Bankfull fluid shear stress could be defined as follows.

$$\tau_{bf} = \rho g H_{bf} S \quad (18)$$

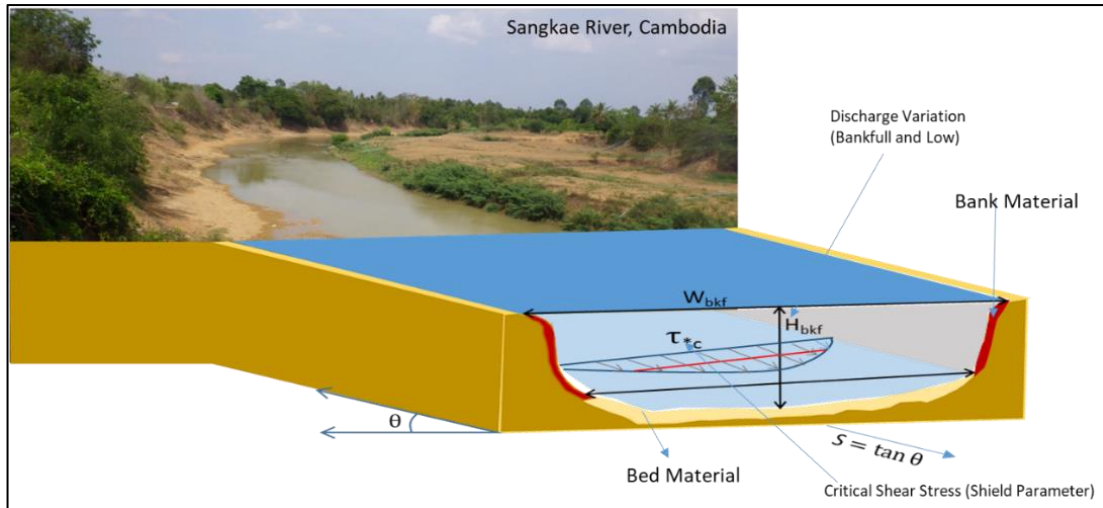


Figure 2.14 Schematic Cross-Section Under Bankfull Condition (Modified from (Dunne, 2020))

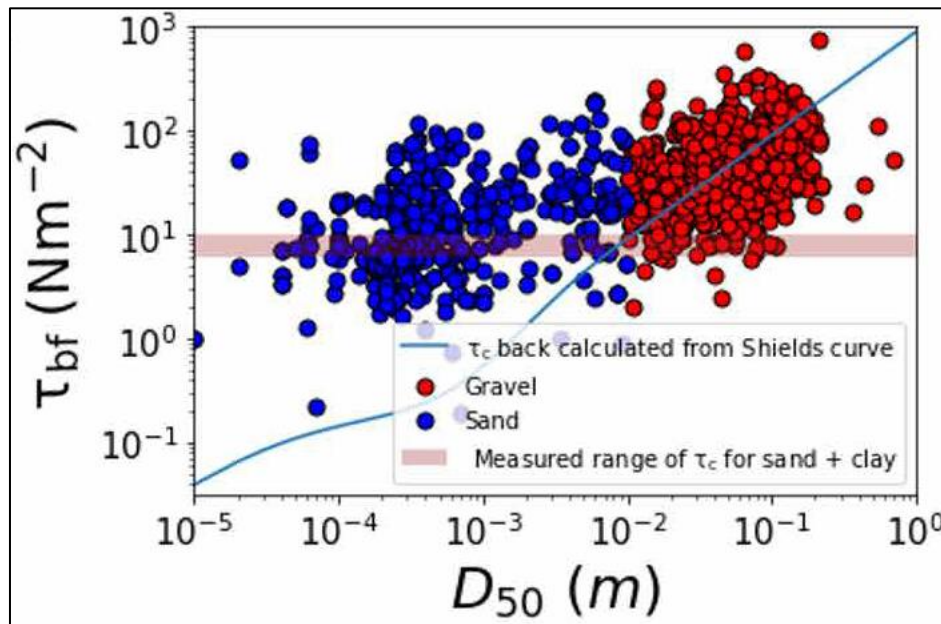


Figure 2.15 Bankfull shear stress τ_{bf} against median grain size D_{50} for gravel-bedded ($D > 1$ cm) and fine-grained ($D < 1$ cm) rivers (Dunne, 2020)

τ_{bf} and H_{bf} are bankfull fluid shear stress and depth under bankfull condition respectively and S is the river slope. τ_c is determined from fitted Shield-curve shown in blue line in Figure 2.15 (Van Rijn, 2020). Bankfull shear stress τ_{bf} of gravel-bedded ($D > 1$ cm with red plots) and fine-grained ($D < 1$ cm with blue plots) rivers is shown in Figure 2.15. Pink band obtained by Dunne (2020) from experiment determined the range of τ_c for sand-clay mixtures and the value is from 6 to 10 N/m^2 .

In case of pure bedload river, the channel is maintaining a stable and consistent width when the shear stress is at the threshold of motion for the material at the banks and slightly above the threshold of motion in the center (Parker, 1978). Another study extended the concept of Parker's model into the channel occupied by fine-grained materials based on the hypothesis that river channel geometries, and their subsequent sediment transport state are

either controlled by the erodibility of their beds or banks (Dunne, 2020). His research shows the coarser gravel is more difficult to be entrained than any cohesive bank material, while the finer sand is easier to be entrained than any cohesive bank material.

In bankfull condition, sediment transport capacity of a channel is often modeled as a function of the excess stress that is the difference between the bankfull and critical dimensionless shear stress ($\tau_{bf}^* - \tau_c^*$) (Luque R & Van Beek, 1976). The critical Shields stress (τ_c^*) describes the amount of stress needed to initiate median grain motion normalized by the grain size, and is generally between 0.03 and 0.08 (Pfeifer et al., 2017). Then the averaged bankfull Shields stress is calculated as follows (Dunne, 2020).

$$\tau_{*bf} = \frac{H_{bf}S}{RD_{50}} \quad (19)$$

where $R=1.65$ is assumed to be relative submerged grain density.

Related to bank erosion rate studies, excess shear stress ($\tau - \tau_c$) is the difference between shear stress by flow and critical shear stress for entrainment which defined by silt-clay percentages (Julian & Torres, 2006). If the fluid shear stress (τ) does not exceed the critical shear stress (τ_c) at which the soil particles are entrained, the soil remains stable (Osman & Thorne, 1988).

Past studies investigated the bank erosion rate in the Sacramento river (Ercan & Younis, 2009) and U-Tapao river (Patsinghasanee et al., 2015). Target area in the Sacramento River located in Segment II because it is around meandering plain and around 100 km from river mouth. While target area in the U-Tapao river is located in Songkhla Province, Thailand the segment of the target area is considered to be Segment II because d_{50} is around 0.34mm. Within the study sites of the U-Tapao River, riverbed and riverbank materials did not vary significantly with the silt-clay percentages in the riverbanks between 50.1% and 82.5%. Patsinghasanee et al., (2015) used polynomial equation which was developed by generated rating curve of silt-clay percentage (P_{SC}) (Julian & Torres, 2006) to get bank critical shear stress (τ_{bc}) for the U-Tapao River.

Bank erosion rate calculation of this study used following equations (Patsinghasanee et al., 2015).

$$\varepsilon = k_d(\tau_{b0} - \tau_{bc})^a \quad (20)$$

$$k_d = 10^{-7}\tau_c^{-0.5} \quad (21)$$

$$\tau_{b0} = \rho g D i \quad (22)$$

$$\tau_{bc} = 0.1 + 0.1779(P_{SC}) + 0.0028(P_{SC}^2) - 2.3E^{-5}(P_{SC}^3) \quad (23)$$

Where ε is the lateral fluvial erosion rate (m/s), a is the exponent generally considered to be 1 (Partheniades, 1965; Arulanandan et al., 1980) and k_d is the erodibility coefficient (m^3/Ns).

τ_{b0} is the actual or cross-sectional shear stress (Pa or N/m²), ρ is the density of water (1,000 kg/m³), D is the water depth (m), and i is channel slope.

Chapter 3

Field Observation and Data Collection

3.1 Target Rivers

This study covers 11 target rivers: 4 rivers located in Southeast Asia and 7 Rivers located in Japan (Table 3-1).

Table 3-1. Target Rivers General Characteristics Summary

Target Rivers (Country)	Location (City/ Prefecture/ Province)	Cathment Area (km ²)	Annual Rainfall (mm)	Discharge in m ³ /s (MAMD*) or (MAMDD**) or (Q ₂ ***)	Total Length (km)	Target Area Distance From River Mouth (km)	Slope of Target Area (m/m)
Kanogawa (Japan)	(Numazu, Mishima, Nagaizumi, Izunokuni) Shizuoka	852	2000 (middle to lower reach) 3000 (upstream)	927.75 (MAMD)	46	5-12	1/1921
Old Ara (Japan)	(Omiya, Urawa, Kawagoe, Chichibu,etc) Saitama	2,940	1400 (1200-1800)	1,627.1 (MAMD)	173	50-64	1/2500
Iruma (Japan)	(Kawagoe, Iruma, Hanno) Saitama	737.3	900-1500	404.17 (MAMD)	63	5-12.4	1/600-1/2500
Oppe (Japan)	(Kawagoe) Saitama	399.6	900-1500	634.2 (MAMD)	35.8 (Segment II)	0-15	1/600-1/3790

Target Rivers (Country)	Location (City/ Prefecture/ Province)	Cathment Area (km ²)	Annual Rainfall (mm)	Discharge in m ³ /s (MAMD*) or (MAMDD**) or (Q ₂ ***)	Total Length (km)	Target Area Distance From River Mouth (km)	Slope of Target Area (m/m)
Watarase (Japan)	(Kiryu) Tochigi (Ashikaga) Gunma	2,621	1790 (Ashio) 1240 (Kiryu)	980.88 (MAMD)	111.7	13.5-32.5	1/1700-1/4000
Naka (Japan)	(Naka, Hitachinaka, Mito. Hitachiomiya. Higashiibaraki, Nasukakarasuyama) Tochigi, Ibaraki	3,270	1300 (Mito) 2000 (Nasu)	2,167.2 (MAMD)	150	5-26	1/2500
Kuji (Japan)	(Hitachiota, Naka, Hitachiomiya, Daigocho, Tokaimura, Asakawa, Tana kura, Hanawa, Yamatsuri, Samegawamura, Otawara) Ibaraki	1,490	1400	889.62 (MAMD)	124	2-23	1/1200
Cimanuk (Indonesia)	(Majalengka, Indramayu) West Java	3,770	2800	636.28 (MAMDAD) 1,269.7 (Q ₂)	240	43-99	1/4000-1/5000
Ciliwung (Indonesia)	Jakarta, (Depok, Bogor) West Java	337	2500	217.41 (Q ₂)	109.7	22-70	1/4000
Serayu (Indonesia)	(Banyumas, Cilacap) Central Java	3,738	1700-4000	3,895.8 (Q ₂)	305.81	5-28.3	1/4000
Sangkae (Cambodia)	Battambang	3,707.5	1500-2000	634.28 (MAMDAD)	82	49-68	1/3000

*Mean Annual Maximum Discharge (MMAD)

**Mean Annual Maximum Daily Average Discharge (MMADAD)

***Flood Design Discharge 2 Year Return Period (Q₂)

3.2 Target Rivers in Southeast Asia

Segment classification for Southeast Asian rivers is not clear, but all rivers are considered to be classified in Segment II-2, while the sediment size is around 0.3mm.

a) Cimanuk River

The Cimanuk River is located in West Java Indonesia with the catchment area of around 3,770 km², and flows northward into Java Sea near Indramayu city area (Figure 3.1). The total length of the river is approximately 240 km with gradient, 1/150 to 1/500 in upper reaches, 1/2,000 to 1/3,000 in middle reaches and less than 1/5,000 in lower reaches.

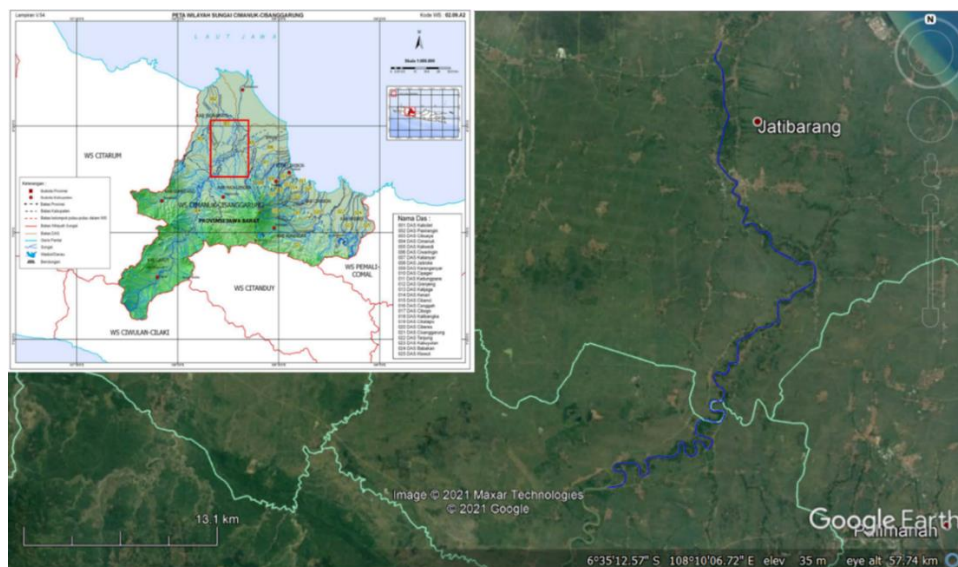


Figure 3.1 Cimanuk River Basin (Ministry of Public Works and Housing, 2017)



Figure 3.2 Target Area of The Cimanuk River (Ramdhani et al., 2020)

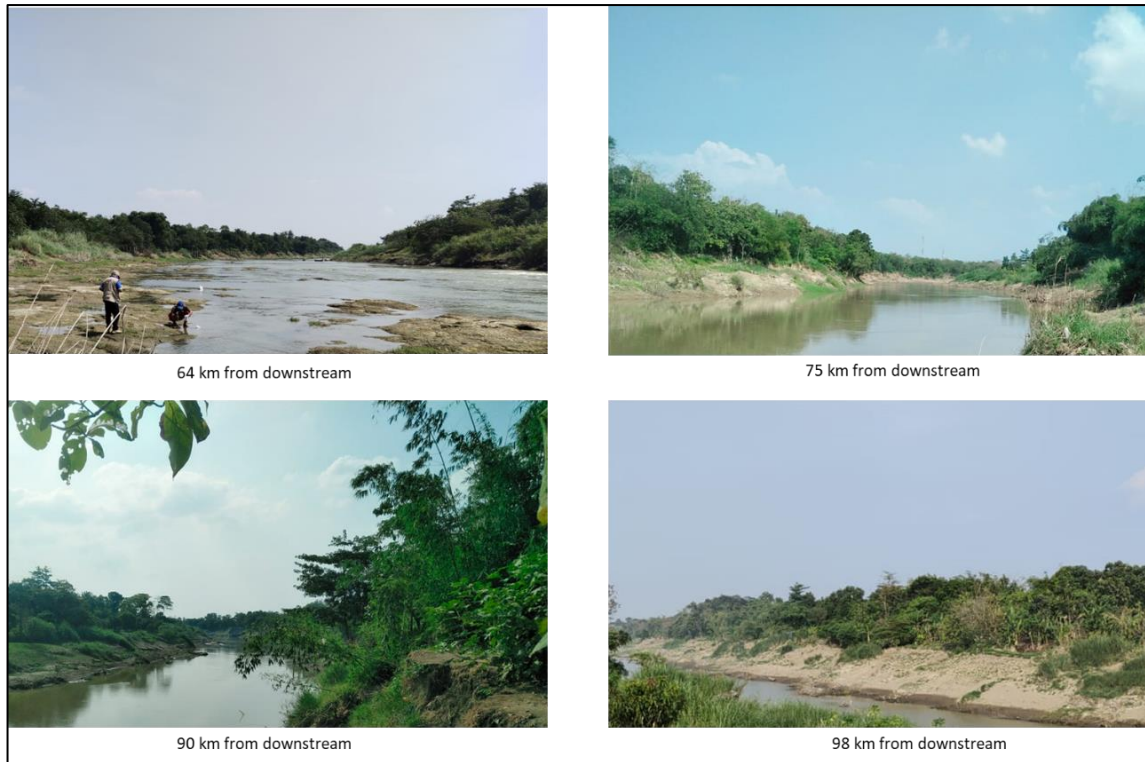


Figure 3.3 Pictures of the Cimanuk River

The study area is located in the lower reach of the Cimanuk River from Rentang Barrage to Rambatan Weir. The length of the study area is around 56 km (Figure 3.2) and the riverbed slope of the study area is around 1/4,000 – 1/5,000. The average annual rainfall is around 2,800 mm. Flood discharge of 2 years return period is around 1,269.7 m³/s (Cimanuk Masterplan, 2017). Figure 3.3 shows pictures of the study area.

Typical soils distributed in each sub-basin are summarized below (JICA, 2015):

- a. Upper basin: Regosol 32% (Clayey loam to sandy loam), Latosol 25% (heavy clay) and Andosol 17% (clay)
- b. Middle basin: Latosol, 70 % (heavy clay) and Alluvial (sandy loam, loam and clay)
- c. Lower basin: Gley 78%, (clay) Alluvial 18 %, (sandy loam, loam and clay) Mediterranean and Podzolic.

Geological Map of the Cimanuk River is shown in Figure 3.4.

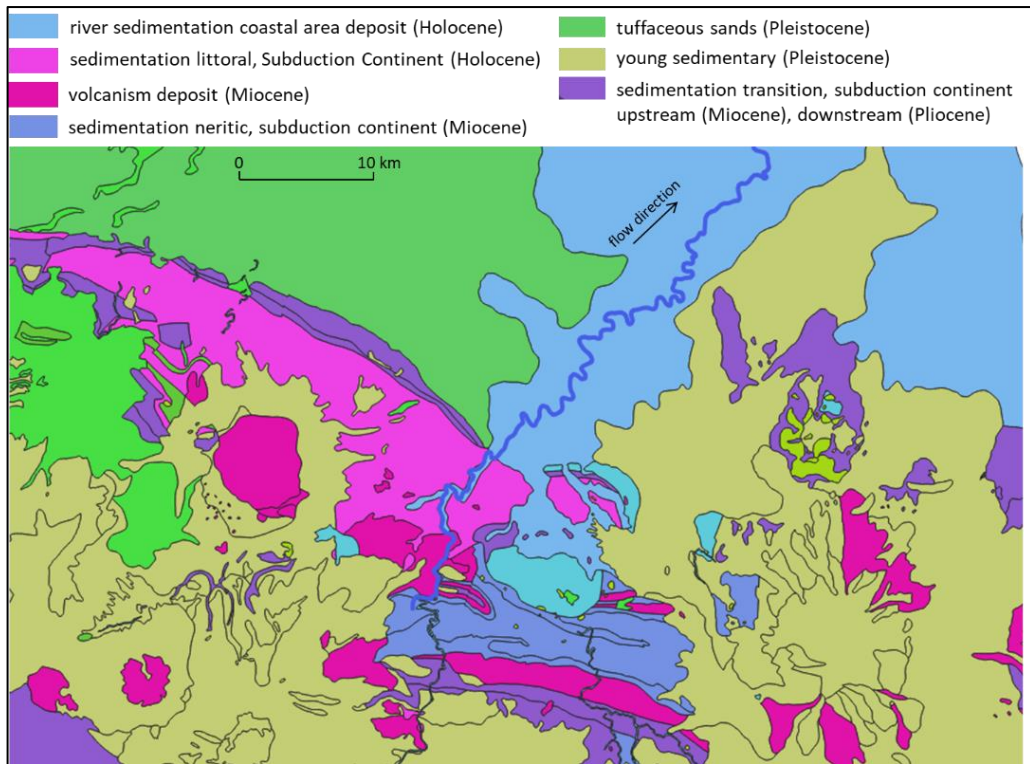


Figure 3.4 Geological Map of Cimanuk River

b) Ciliwung River

The Ciliwung River is located in Jakarta, Indonesia. Upstream origin of this river is located in Mount Gede-Pangrango, Bogor, and the river flows through Bogor, Depok, Jakarta and empties to Java Sea. The total length of the main river is 109.7 km and the river basin area is around 337 km² with annual rainfall, around 2,500 mm. Riverbed slope is around 1/4,000. Study area is from segment 4-6 in Figure 3.5 which is located around Depok and Jakarta. Pictures of the Ciliwung River condition are shown in Figure 3.6.

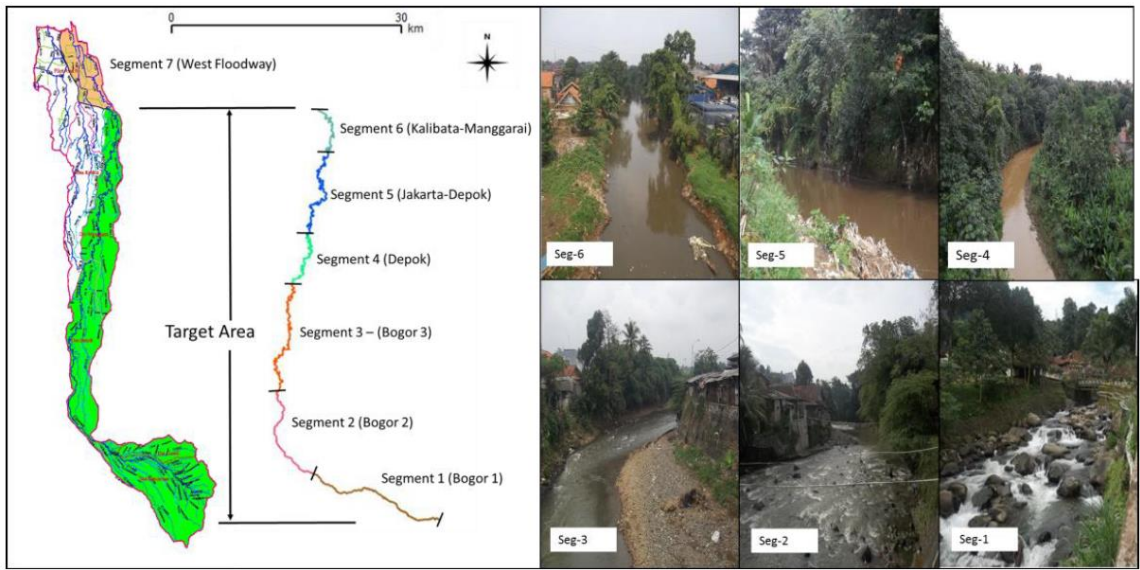


Figure 3.5 The Ciliwung River Basin (Ramdhani & Setiawan, 2015)



Figure 3.6 Pictures of the Ciliwung River

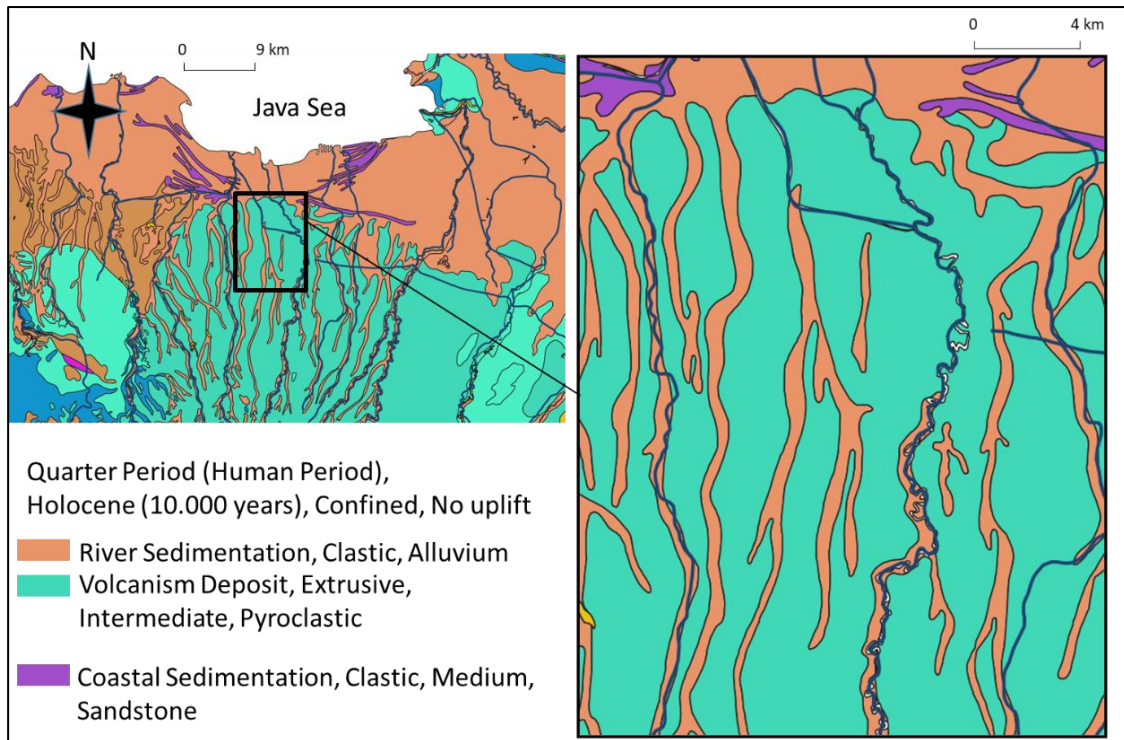


Figure 3.7 Geological Map of The Ciliwung River

Table 3-2. The Ciliwung River Discharge with Different Return Period (Ministry of Public Works and Housing, 2008)

Return Period (year)	1	2	5	10	20	25	50	100	1000
Discharge (m ³ /s)	105.31	217.41	308.12	361.68	391.41	417.47	454.05	492.87	585.96

Existing capacity of lower reach in the Ciliwung River is around 200 m³/s. The improvement work of the river capacity is on-going with target design capacity of 500 m³/s. Flood discharge is shown in Table 3-2.

Geological characteristics of this river are dominated by river sedimentation and volcanism deposit (Figure 3.7). Overall basin characteristics can be summarized as quaternary/holocene geological period with extrusive, intermediate and pyroclastic rock type.

c) The Serayu River

The Serayu River is located in Central Java, Indonesia. Catchment area of this river is around 3,738 km² with total river length of 305.81 km (Figure 3.8). Annual rainfall of this river from 1,700 mm to 4,000 mm and 2-year flood is around 3,895.8 m³/s (Table 3-3). Riverbed slope is around 1/4,000.

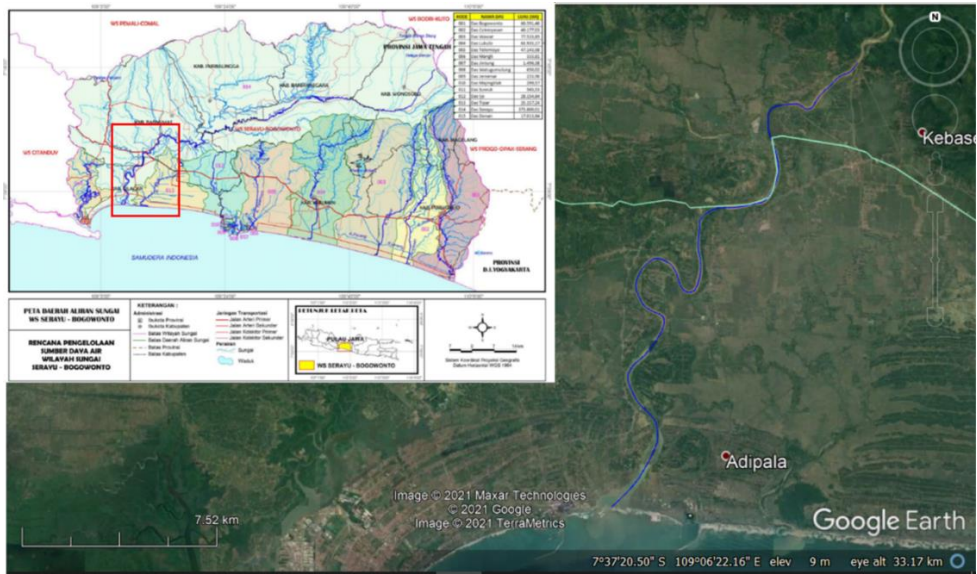


Figure 3.8 The Serayu River Basin (Ministry of Public Works and Housing, 2016)

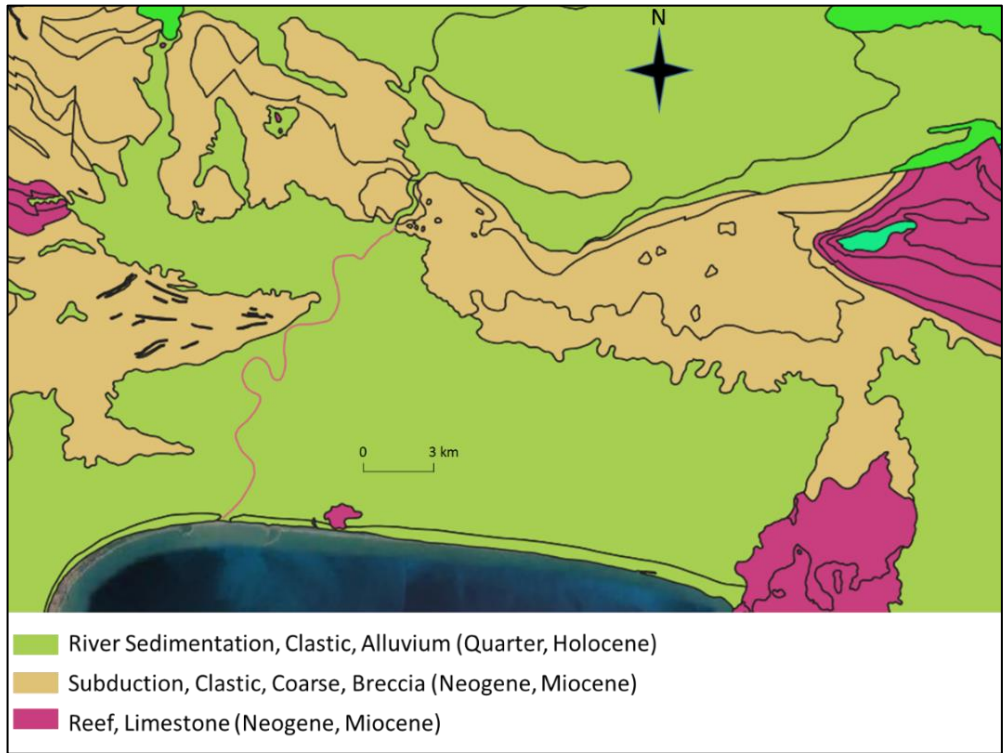


Figure 3.9 Geological Map of The Serayu River

Table 3-3. The Serayu River Discharge With Different Return Period (Ministry of Public Works and Housing, 2016)

Return Period (year)	2	5	10	25	50	100
Discharge (m ³ /s)	3.895,80	5.049,31	5.812,93	6.778,06	7.493,94	8.204,53

Geological characteristics of this river dominated by river sedimentation with alluvium rocktype (Figure 3.9). Overall basin characteristics can be summarized as quaternary/holocene geological period with clastic and alluvium rock type.

d) The Sangkae River

The Sangkae river has catchment area of 3,707.5 km² (Figure 3.10), average annual rainfall of 1,280.7 mm (2000-2011) with mean annual maximum daily discharge of 634.28 m³/s (JICA, 2013). The river originates in Phnom Kbal Lan (Pursat province) and extends for about 82 km from Battambang municipality to the Tonle Sap Lake (Diepart, 2015). Riverbed slope is around 1/3,000. Soil type in the Battambang province is alluvium tending to retain water much more water than rocky or sandy soils (JICA, 2013). Overall basin characteristics can be summarized as quaternary geological period with sandstone Triassic, colluviums and limestone rock type (Diepart, 2015). Pictures of the Sangkae River condition are shown in Figure 3.11.

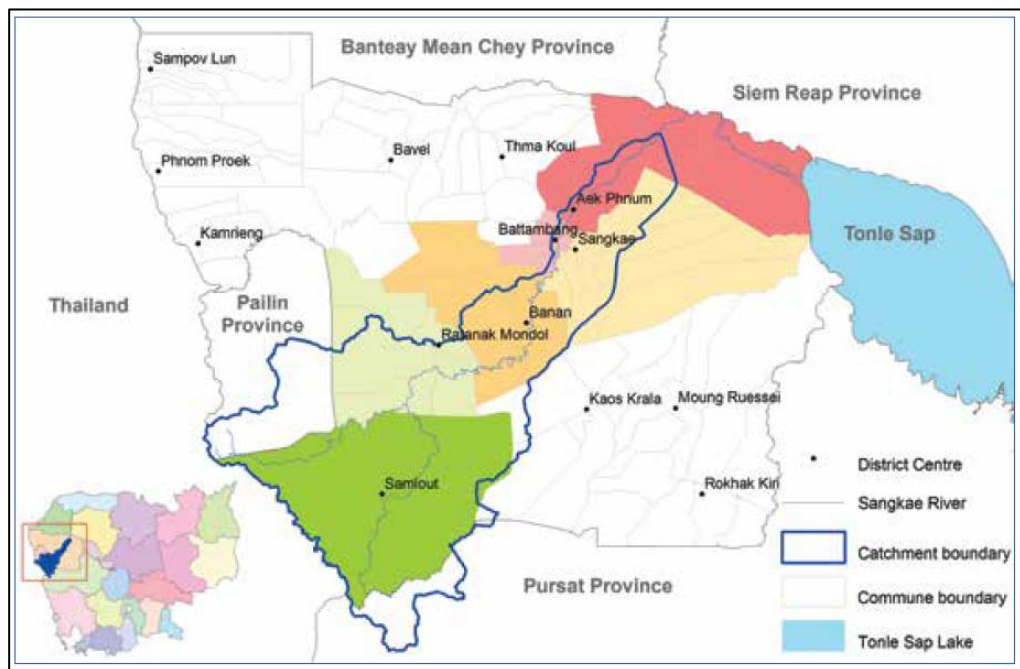


Figure 3.10 The Sangkae River Basin (Diepart, 2015)



Figure 3.11 Pictures of The Sangkae River Condition

3.3 Target Rivers in Japan

a) The Kano River

The Kano River is class A river which is located in Shizuoka Prefecture. This area has heavy rainfall, steep gradient, and it makes surrounding area prone to flooding in past. The Kano River starts from Mount Amagi in the center of Izu Peninsula to northern part into Suruga Bay at Numazu. This river has 46 km length and has a watershed of 853 km² (Figure 3.12). Segment II-1 in this river located from 12 km to 23 km and Segment II-2 is from 0-12 km from river mouth. Pictures of the Kano River condition are shown in Figure 3.13. Geology in Japan rivers is summarized in Table 3-5.

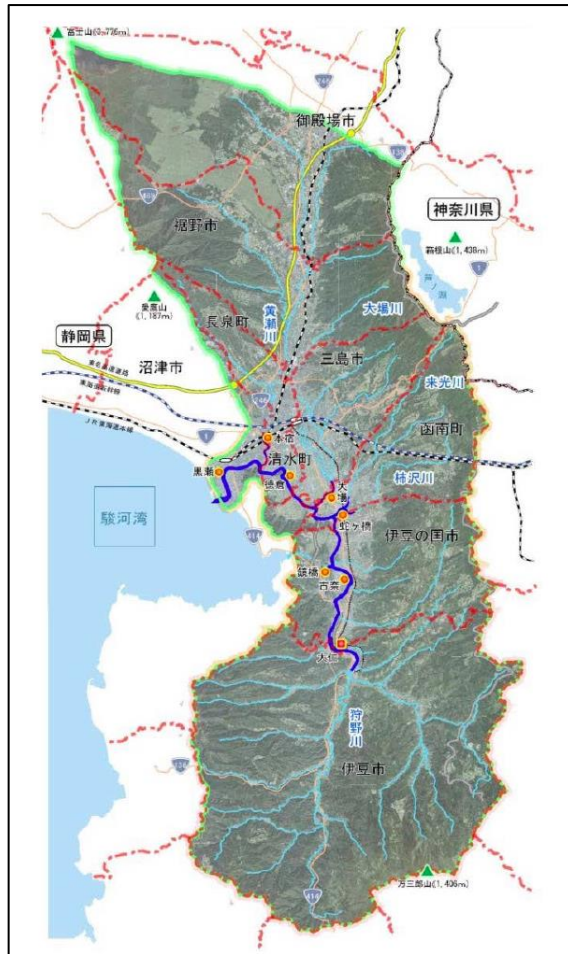


Figure 3.12 Kano River Basin (MLIT, 2012)



Figure 3.13 Pictures of The Kano River

b) The (Old) Ara River

In the past around four hundred years ago, several alignment and straightened works were done in the Ara River. Abandoned channels or oxbow lakes (Old Ara) also can be found in some locations. The Ara River is class A river and flowing through Saitama and Tokyo. Upstream origin of this river is located at Mount Kobushi in Saitama Prefecture, and the river flows into Tokyo Bay. This river has 173 km length and the drainage basin covers 2,940 km² (Figure 3.14). Segment II-1 is from 54-75 and segment II-2 is from 44 to 54 km from river

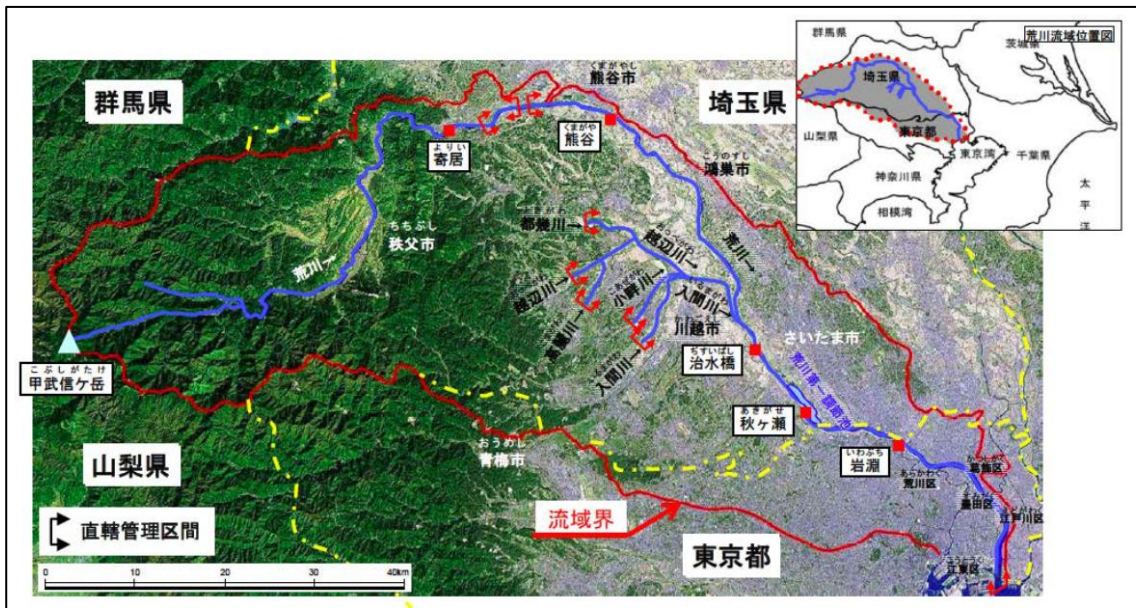


Figure 3.14 The Ara River Basin (MLIT, 2012)



Figure 3.15 Picture of The Old Ara River

mouth. The Old Ara which is the target area of this study located from 50 km to 64 km from river mouth. Pictures of the Old Ara River condition are shown in Figure 3.15.

c) Iruma River

The Iruma River is flowing from Mount Omochi in Saitama to Arakawa River at Kawagoe, Saitama. The catchment area around 721 km² with total length of the main channel is 63 km, 16 km belongs to Segment II. Segment II-1 is 2.4 km to 12.4 km and Segment II-2 0 to 2.4 km from the confluence with Arakawa River. Pictures of the Iruma River condition are shown in Figure 3.16.



Figure 3.16 Pictures of The Iruma River



Figure 3.17 Pictures of The Oppe River

d) Oppe River

The Oppe River is the main tributary of the Iruma River and has catchment area of 65.2 km² with total length 35.8 km. Segment II-2 is from from 0 km to 15 km from confluence with the Iruma River. Pictures of the Oppe River condition are shown in Figure 3.17.

e) The Watarase River

The Watarase River is the tributary of the Tone River which has 106.7 km in length and its catchment area is around 2,621 km² (Figure 3.18). Segment II-1 is 2 km to 32.5 km and Segment II-2 is 13.5 to 23 km from confluence with Tone River. The government of Japan categorizes it as a class A river. Upstream of this river is located in Mount Sukai on the boundary of the city of Nikkō in Tochigi Prefecture and it empties into the Tone at the boundary of the city of Koga in Ibaraki Prefecture and the town of Kitakawabe in Saitama Prefecture. Pictures of the Watarase River condition are shown in Figure 3.19.

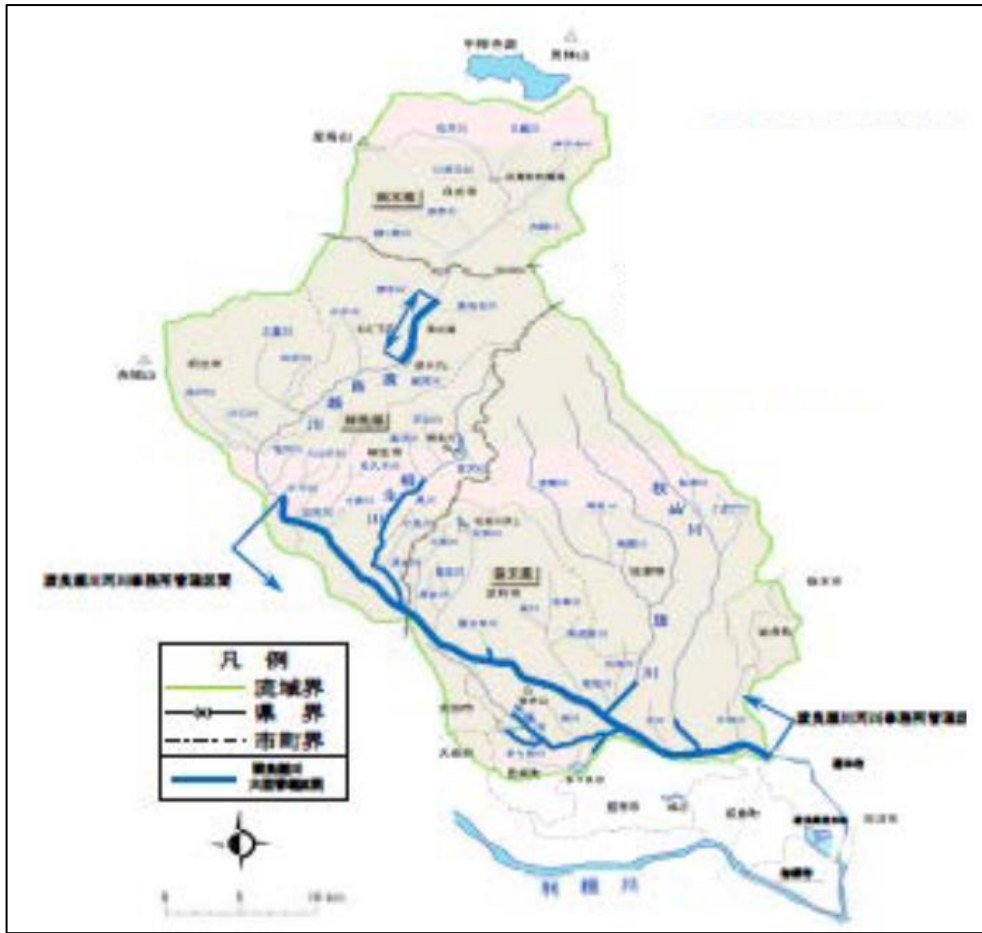


Figure 3.18 The Watarase River Basin (MLIT, 2012)



Figure 3.19 Pictures of The Watarase River

f) The Naka River

The Naka River is a class A river in the boundary between Fukushima and Tochigi Prefectures which has catchment area of around 3,270 km² (Figure 3.20). The Naka River flows to Pacific Ocean across 13 cities, 8 towns and 1 village. Total length is around 150 km and 76 km belongs to Segment 2. From 0 km to 20 km is Segment 2-2, and from 20 km to 76 km is Segment 2-1. Slope range in The Naka River from 1/2500 to 1/600. Picture of the Naka River condition is shown in Figure 3.21.

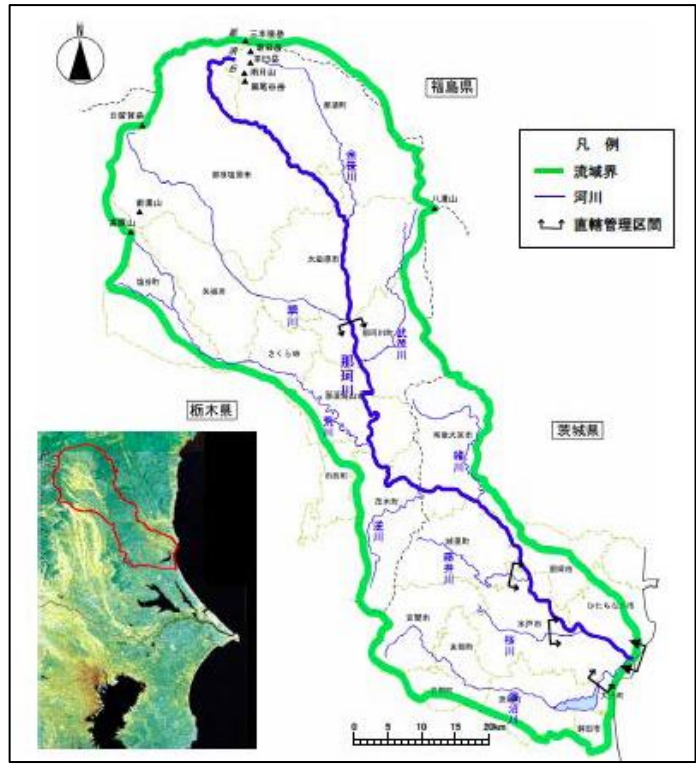


Figure 3.20 The Naka River Basin (MLIT, 2012)



7 km from downstream

Figure 3.21 Picture of The Naka River (Santoso, 2017)

g) The Kuji River

The Kuji River is a class A river which has 124 km length and a catchment area of 1,490 km² (Figure 3.22). This river is located in around the boundary of Fukushima, Tochigi and Ibaraki Prefectures and flows from Mount Hachiyoshi into the Pacific Ocean. Total length of Segment II of this river is around 31 km. From 0 km to 14km is Segment II-2, and from 14 km to 31 km is Segment 2-1. Slope range is around 1/2000 to 1/460. Picture of the Kuji River condition is shown in Figure 3.23.

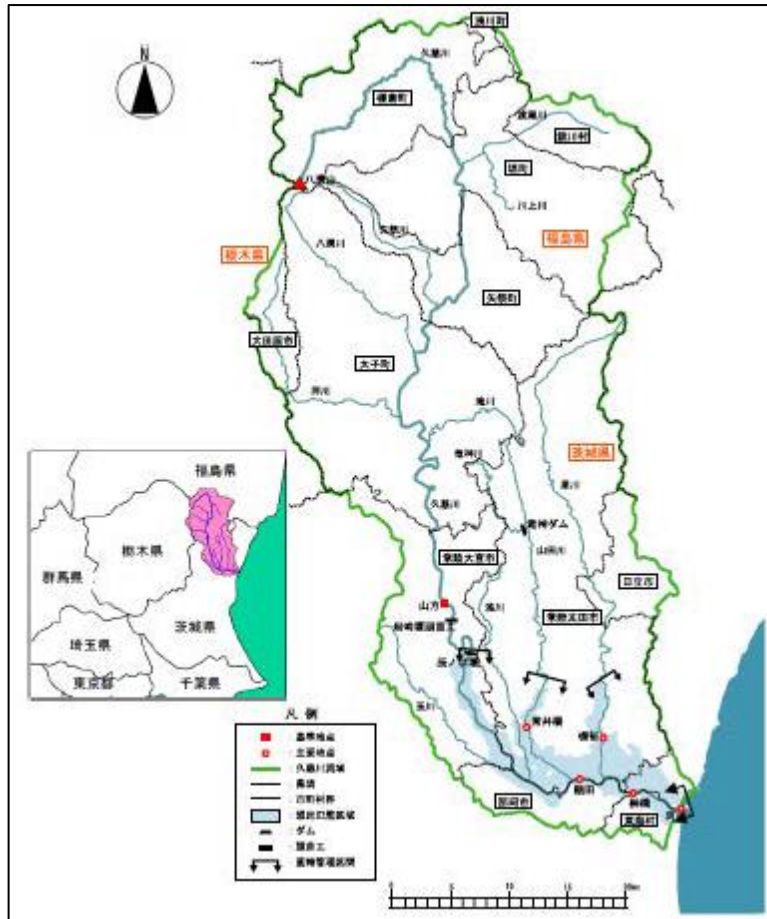


Figure 3.22 The Kuji River Basin (MLIT, 2012)



Figure 3.23 Picture of Kuji River (Santoso, 2017)

3.4 Data Collection

Number of cross-sections and sediment samples collected in target rivers are summarized in Table 3-4.

Bank material in the Serayu River could not be collected in this study, but the past study indicated that bank material is considered to be mostly sand because of sand mining activity (Purwono, 2018). This problem is also pointed out by South Java Flood Control Sector Project (ADB, 2007) and water resources masterplan for Serayu River (Ministry of Public Works and Housing, 2016). Bed sediment sampling was conducted in 2012 for the study about BOD-DO in downstream part of Serayu River (Herdyasrastiti, 2015).

Table 3-4. Number of Data in Each River

Target Rivers	Number of Cross-Sections Data (year)	Bed Material (Samples)	Bank Material (Samples)
Kanogawa	38 (2007)	2	2
Watarase	29 (2007)	3	3
Old Ara	8 (2007)	2	2
Oppe	75 (2012)	5	5
Iruma	38 (2012)	3	3
Kuji	53 (2011)	2	2
Naka	31 (2011)	2	2
Serayu	8 (2017)	8	N/A
Cimanuk	25 (2014)	4	4
Sangkae	7 (2013)	3	3
Ciliwung	24 (2013)	4	4

a) Cross-Sectional Data

Channel cross-section data of Japanese rivers was obtained from MLIT (Ministry of Land, Infrastructure, Transportation, and Tourism). The dataset from MLIT consists of channel



Figure 3.24. Field Measurement Using Total Station and Depth Measurement Device

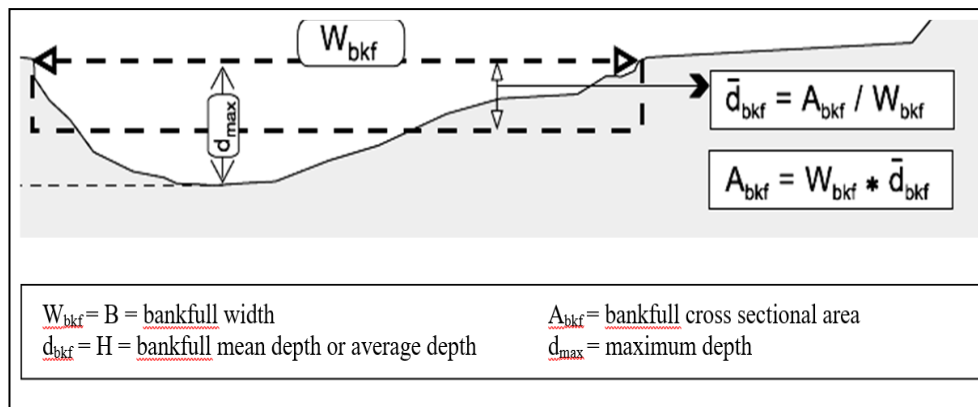


Figure 3.25 Cross-Sectional Dimension (D. Rosgen, 1996)

cross-sectional data for several yearly data. In case of the Old Ara River, some points of the current Ara River also contain the cross-sectional data of old channel. Field observations also were conducted to verify the obtained data of the old channel cross-section (Figure 3.24).

Cross-sectional data for Indonesian Rivers (Cimanuk, Ciliwung and Serayu) were obtained from Ministry of Public Works and Housing. The cross-sectional data of the Cimanuk River in 2007 and 2014, the Ciliwung River in the beginning of 2013, and the Serayu River in 2017 were collected. Survey for the Sangkae River in Cambodia was conducted from 2011 to 2013 by ourselves.

Cross-sectional data was analyzed to determine cross-sectional dimension (Figure 3.25). The essential part of this analysis is to determine the bankfull water level. After the bankfull water level is determined, then the cross-sectional area ($A_{b_{kf}}$) was calculated. B ($W_{b_{kf}}$) corresponds to the surface water width, and H ($d_{b_{kf}}$) corresponds to the average depth. Those parameters were calculated under bankfull discharge condition. Mean depth (H) was estimated as the division of channel area (A) by surface water width (B). It is necessary to use

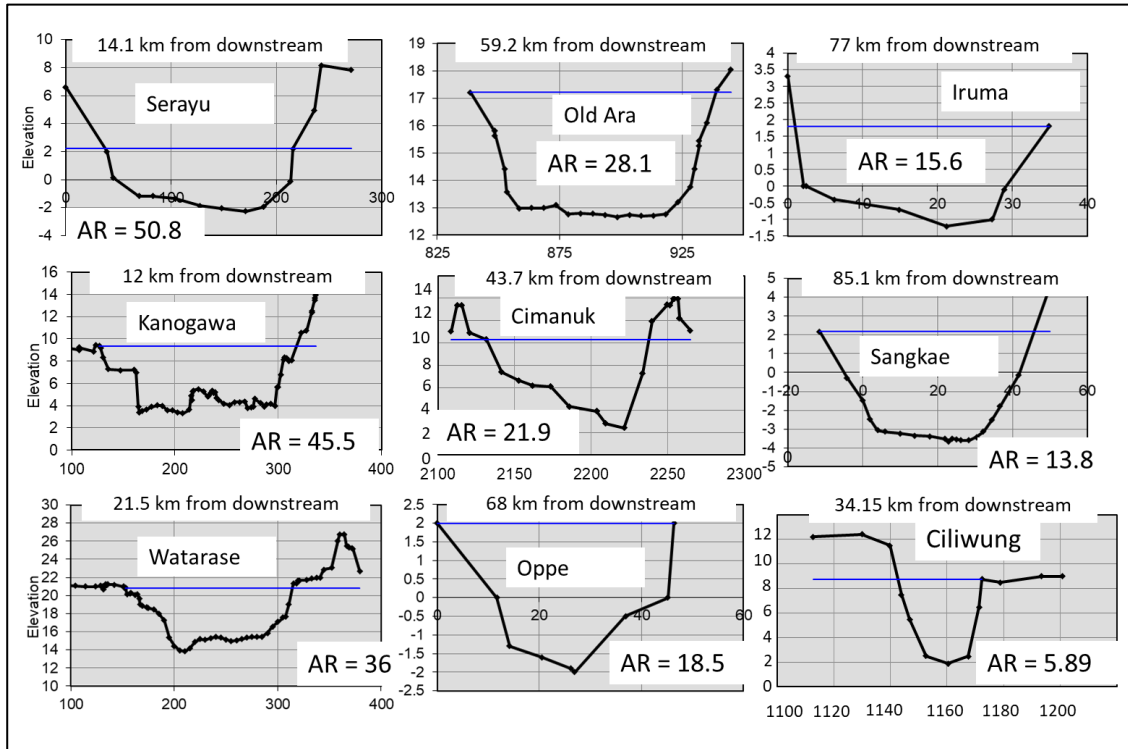


Figure 3.26 Samples Cross-Sectional Shapes for Each Rivers (AR is Aspect Ratio)

this method to get the representative depth values of irregular shape of riverbed. MS Excel spread sheet for cross-sectional shape parameters calculation (D. E. Mecklenburg & A. Ward, 2004)* was taken from USDA Stream Corridor Restoration Workgroup, output of the program is shown in Figure 3.26.

Definition of the bankfull discharge is based on bankfull water level at the bank edge. However, there is difference between bankfull discharge and mean annual maximum discharge, even though both are considered to be channel forming discharge. Figure 3.27 is the comparison of the bankfull and mean annual maximum discharge in target rivers. Aspect ratio for mean annual condition is higher than bankfull condition. However, in other cross-sections, aspect ratio for mean annual condition is lower than bankfull condition. Aspect ratio of bankfull condition might be decreased by channel deepening phenomena for channel with fine sand material. In this study, aspect ratio of bankfull condition is focused on. The reason is to ignore the effect of hydrological condition and the discharge variation.

*(<https://www.nrcs.usda.gov/wps/portal/nrcs/detailfull/national/water/?cid=stelprdb1043249>).

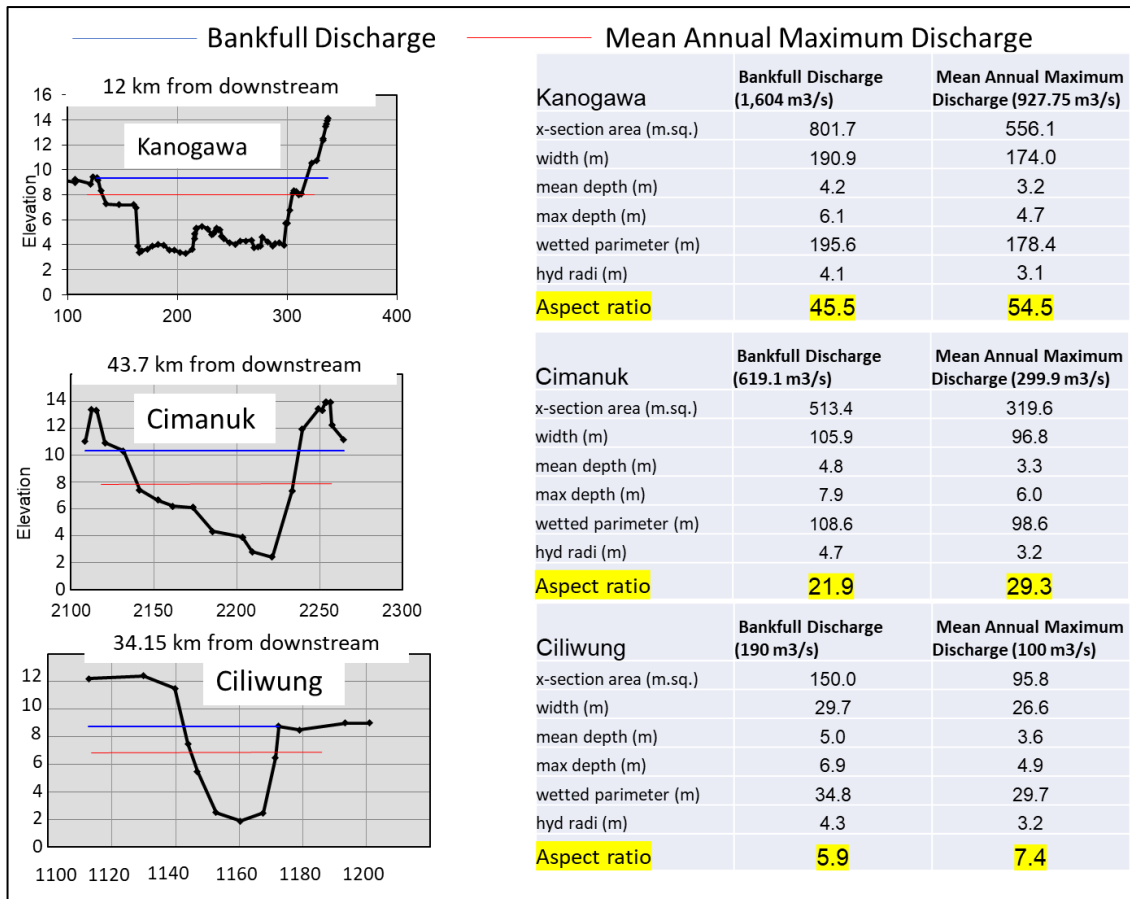


Figure 3.27 Bankfull and Mean Annual Maximum Discharge

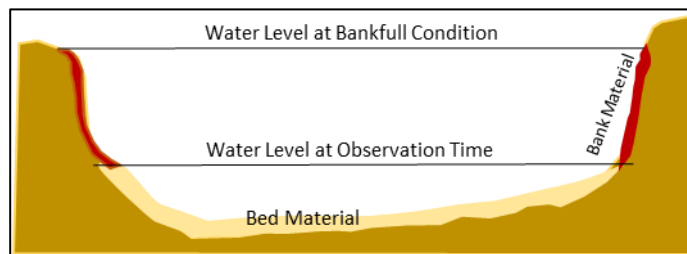


Figure 3.28 Schematic Condition of Bed-Bank Material

b) Sediment Data

Sediment was taken in riverbank and riverbed. River bank is the location between water level at bankfull flow condition and water level at observation time (normal flow condition). Riverbed is defined as the wetted perimeter under water level of observation time as shown in the Figure 3.28.

Scoop (Figure 3.29) was used to collect sample of bed material in shallow channel (Figure 3.30 right). If the channel is deep and scoop cannot be used, then Ekman Berge Sampler (Figure 3.29) was used to solve this problem (Figure 3.30). Bank material was also collected (Figure 3.31) to understand the bank condition. Samples of sediment material from each location were then put in a plastic container. Each collected sediment sample were used for

grain size analysis. This analysis was done by sieving method. Mass of each sieved sample was measured and then percentage distribution of sieved samples were obtained. Output of this analysis is grain size distribution curve based on ASTM D422-63 Standard Test Method for Particle-Size Analysis of Soils (ASTM D-422-63, 2007).

Burmister (1952) stated that any grain size between 0.05 mm and 0.1 mm could be used as the boundary between silt-clay and sand, and it is feasible to use either the 200-mesh (0.074 mm) or 230-mesh (0.0625 = 1/16 mm) sieves. Physical reasons for the selection of the 200-mesh sieve as the boundary between silt-clay and sand is that soil becomes less drained and capillarity increases with increase in material passing the 200-mesh sieve (Burmister, 1952). In this study, fine material with grain size smaller than 0.074 mm (200-mesh) was collected to calculate the weight percentage which was used for silt-clay index analysis.

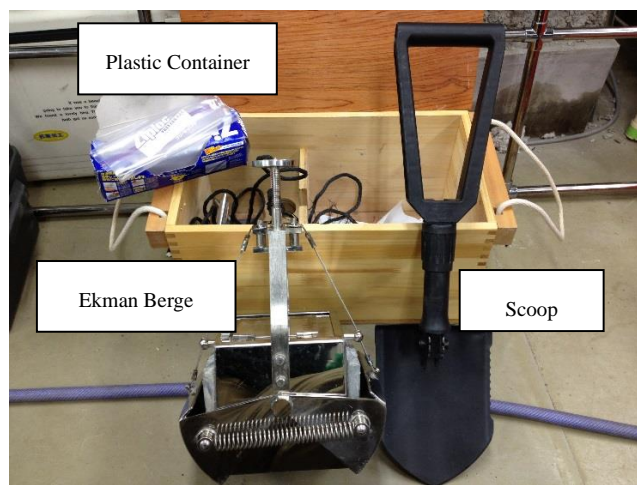


Figure 3.29 Ekman Berge Sampler and Scoop



Figure 3.30. Sample collection on riverbed by using Ekman Berge (left) and Scoop (right)



Figure 3.31. Sample collection on riverbank



Figure 3.32. River Centerline and Sinuosity Analysis

c) Satellite Imagery

Identification or delineation of river centerline was conducted based on the satellite imagery obtained from Google Earth. The historical imagery was also available at some rivers, and it was also possible to observe surrounding river environment in the satellite imagery. River centerlines were delineated and splitted into around 3km reach by using QGIS. After that, sinuosity was analyzed for each reach (Figure 3.32).

d) DEM Data

For Japanese rivers, DEM data with 5-meter resolution were obtained from Geospatial Information Authority of Japan (<http://maps.gsi.go.jp>). For Indonesian rivers, DEM data with 8-meter resolution were obtained from Indonesian Geospatial Agency (<https://tanahair.indonesia.go.id/demnas/#/demnas>). The DEM data for Java Island were obtained in 2011. The Sangkae River in Cambodia has SRTM DEM with 30-meter resolution.

e) Geological Map

Geological conditions of Japanese rivers were analyzed based on The Seamless Digital Geological Map of Japan provided by Geological Survey of Japan, AIST. Geological condition is shown on each grid and was accessed through website.

(https://gbank.gsj.jp/seamless/download/downloadIndex_e.html).

Geological conditions of Indonesian rivers were analyzed by regional geological map provided by Indonesian Geology Research Center. The Sangkae River's geological conditions were explained in the report "Learning for resilience: Insights from Cambodia's rural communities" (Diepart, 2015) and "PREPARATORY SURVEY ON THE PROJECT ON ADDITIONAL NEW WATER TREATMENT PLANTS FOR KAMPONG CHAM AND BATTAMBANG WATERWORKS IN THE KINGDOM OF CAMBODIA" (JICA, 2013)

Based on the geological map, characteristics of target rivers are summarized in Table 3-5.

Table 3-5. Geological Characteristics of Target Rivers

Target River	Aspect Ratio	Meander Classification	Geological Period/Epoch	Rock Type
Kanogawa	Moderate-High	Meandering with Point Bars and Chute Channel	Cretaceous	Volcanic Rock (not volcanoes)
Watarase	Moderate-High	Meandering with Point Bars and Chute Channel	Cretaceous	Volcanic Rock (not volcanoes)
Old Ara	Moderate-High	Meandering with Point Bars and Chute Channel	Jurassic	Sedimentary Chichibu-belt Jurassic
Oppe	Low-Moderate	Meandering with Point Bars (Old Channel)	Quaternary, Pleistocene	Jurassic Sedimentary
Iruma	Low-Moderate	Meandering with Point Bars (Old Channel)	Jurassic	Sedimentary Chichibu-belt Jurassic

Target River	Aspect Ratio	Meander Classification	Geological Period/Epoch	Rock Type
Kuji	Moderate-High	Meandering with Point Bars and Chute Channel	Middle to Late Jurassic	Accretionary complex
Naka	Moderate-High	Meandering with Point Bars and Chute Channel	Early Miocene to Middle Miocene	Sedimentary rocks (sandstone, slate) in the middle part, and Kanto loam on the downstream part.
Serayu	Moderate-High	Meandering with Point Bars and Chute Channel	Quaternary, Holocene	Sediment, Clastic, Alluvium
Cimanuk	Low-Moderate	Meandering with Point Bars	Quaternary, Holocene	Sediment, Clastic, Alluvium
Sangkae	Low-Moderate	Meandering with Point Bars	Quaternary	Sandstone Triassic, colluviums + limestone
Ciliwung	Low	Equiwidth Meandering	Quaternary, Holocene	Sediment, Clastic, Alluvium Extrusive, Intermediate, Pyroclastic

f) Old Map

Several historical maps were investigated in this study, especially for Japanese rivers. The purposes of this investigation are mainly to identify the old river course and surrounding condition. Also from the maps, the width variation of old river channel could be checked.

This is the list of historical maps that were used for this study

1. 1899 Historic Agriculture Environment, Released by Japan National Institute for Agro-Environmental Sciences (Figure 3.33).
2. Time Series Topographic Map (Figure 3.34) browsing site "今昔マップ on the web" provided by TANI Kenji's Laboratory Human Geography, Faculty of Education, Saitama University (<http://ktgis.net/kjmapw/index.html>).



Figure 3.33. Historical Map - 1899 Historic Agriculture Environment



Figure 3.34. Time Series Topographic Map Website Interface

Results and Discussion

4.1 Sediment Size Variation

The sediment samples from the field survey were tested in a laboratory to obtain the sediment characteristics. This section describes the grain size distribution of the bed and bank material. Grain size distributions of the sampled sediments obtained through the laboratory test are shown in Figure 4.1 and Figure 4.2.

The bed material of the target rivers could be divided into 3 types based on the grain size of main component: coarse sand (0.5-2mm), fine sand (0.075-0.5mm), and silt-clay (< 0.075mm). The coarse and fine sand were found in both Japanese and Southeast Asian rivers. Cohesive material is typically found in a narrow and deep channel such as the Ciliwung and the Sangkae Rivers.

The bank material could be categorized into 2 types: cohesive and non-cohesive bank. Cohesive material here is same with the silt-clay in bed material. All the river banks in Japan and Southeast Asia can be classified in these two categories. In general, rivers in Japan have less cohesive banks than the Southeast Asian rivers. Therefore, river banks of Southeast Asian Rivers are considered to be more stable than those of Japanese rivers.

While Japanese rivers have less silt-clay percentage compared with Southeast Asian rivers, the grain size distribution of sand (0.075-2mm) of the riverbank in Japan and Southeast Asian is nearly identical to each other. In these rivers, 0.075-1mm material that is a main component of the bank is transported as suspended material. Grain size distribution in the Old Ara River seems to be different but it may be due to dropped pebbles in the abandoned river channel (oxbow lake).

The difference of bed material is affected by upstream geological condition (Figure 4.3). Volcanic rivers in Japan can produce large amount of fine material compared to sedimentary rivers. On the other hand, sedimentary rivers in Japan can produce 1mm to 1cm material that is rare in other rivers. Fine sand in Southeast Asian rivers similar with sizes of bank material in Japan, because fine sand material are suspended material

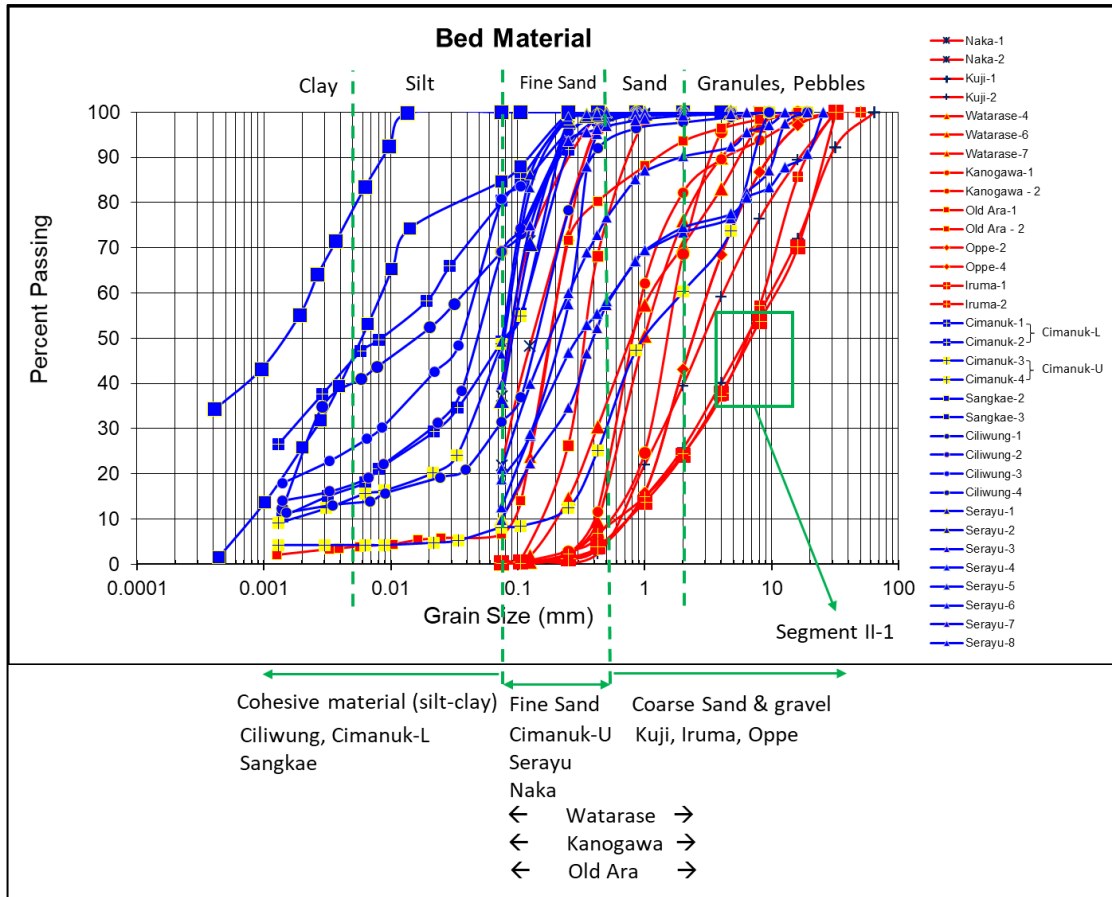


Figure 4.1. Grain Size Distribution of the Bed Material

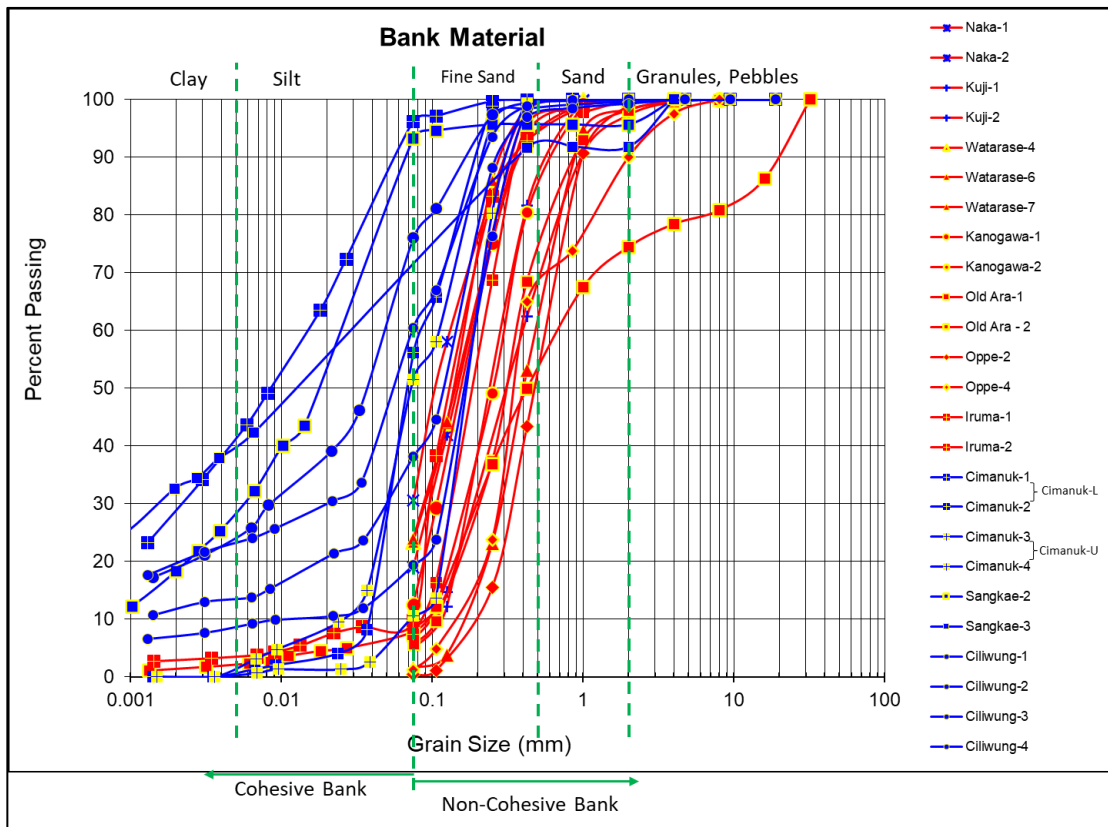


Figure 4.2. Grain Size Distribution of Bank Material

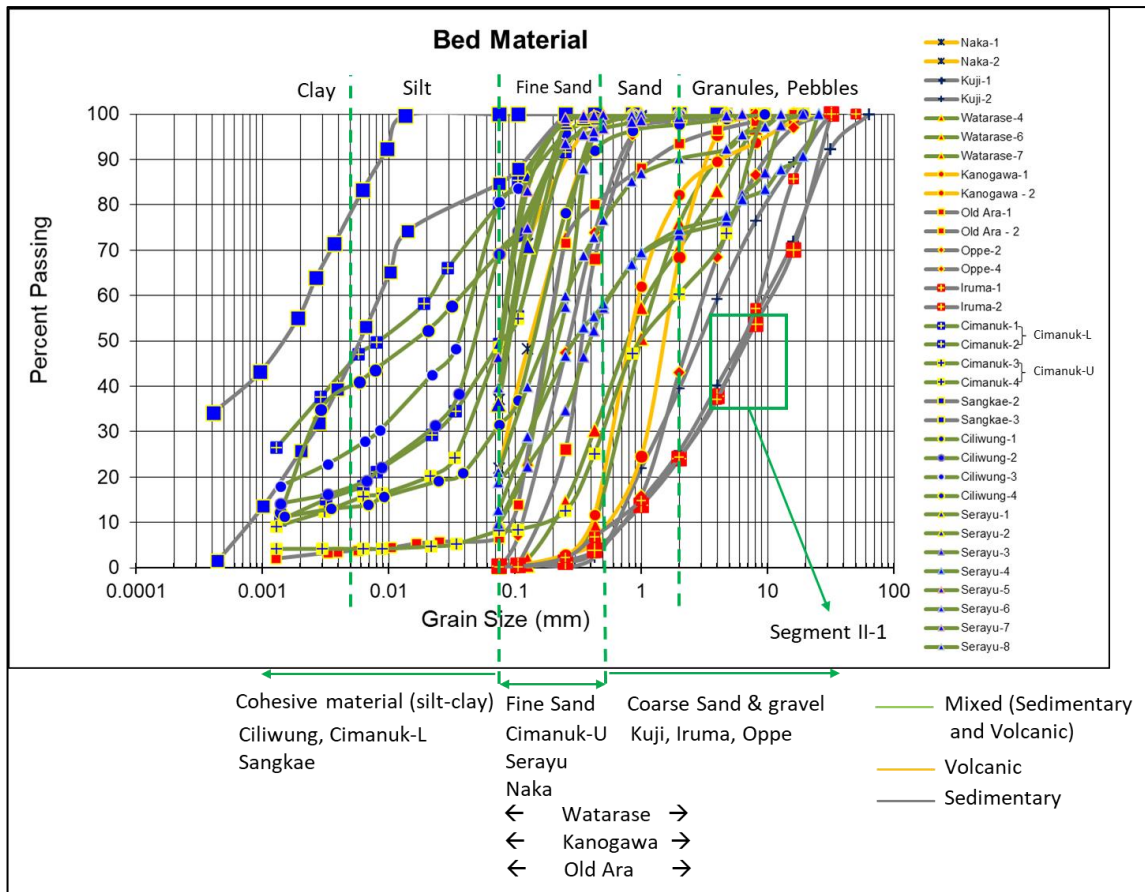








Figure 4.3. Grain Size Distribution of Bed Material Based on Upstream Geology

Table 4-1 summarized the condition of bed-bank material. Each type is represented by red, green, yellow, brown and blue color in order to clarify the plots of each type in the graphs shown later. This classification is considered to be important for evaluation of other parameters such as sinuosity and aspect ratio.

Table 4-1. Classification of Bed and Bank Material Condition

Bed	Coarse Sand With Coarse Gravel	Fine Sand	Silt-Clay
Bank Fine Sand	<p>I-1 </p> <p>Iruma-1 (d_{50bed}: 7.06mm, d_{50bank}: 0.20mm)</p> <p>Iruma-2 (d_{50bed}: 6.56mm, d_{50bank}: 0.14mm)</p> <p>Iruma-3 (d_{50bed}: 6.19mm, d_{50bank}: 0.19mm)</p> <p>Oppe-1 (d_{50bed}: 2.92mm, d_{50bank}: 0.24mm)</p> <p>Oppe-2 (d_{50bed}: 2.25mm, d_{50bank}: 0.51mm)</p> <p>Oppe-3 (d_{50bed}: 5.92mm, d_{50bank}: 0.17mm)</p> <p>Oppe-5 (d_{50bed}: 6.05mm, d_{50bank}: 0.13mm)</p> <p>Kuji-1 (d_{50bed}: 6.56mm, d_{50bank}: 0.35mm)</p> <p>Kuji-2 (d_{50bed}: 3.06mm, d_{50bank}: 0.29mm)</p> <p>Watarase-6 (d_{50bed}: 0.99mm, d_{50bank}: 0.15mm)</p> <p>Watarase-7 (d_{50bed}: 0.84mm, d_{50bank}: 0.41mm)</p> <p>Kano-1 (d_{50bed}: 0.86mm, d_{50bank}: 0.17mm)</p> <p>Kano-2 (d_{50bed}: 1.58mm, d_{50bank}: 0.25mm)</p> <p>Cimanuk-4 (d_{50bed}: 1.089mm, d_{50bank}: 0.185mm)</p>	<p>I-2 </p> <p>Oppe-4 (d_{50bed}: 0.26mm, d_{50bank}: 0.36mm)</p> <p>Watarase-4 (d_{50bed}: 0.19mm, d_{50bank}: 0.14mm)</p> <p>Naka-1 (d_{50bed}: 0.13mm, d_{50bank}: 0.11mm)</p> <p>Naka-2 (d_{50bed}: 0.093mm, d_{50bank}: 0.17mm)</p> <p>Old Ara-1 (d_{50bed}: 0.34mm, d_{50bank}: 0.32mm)</p> <p>Old Ara-2 (d_{50bed}: 0.19mm, d_{50bank}: 0.43mm)</p> <p>Serayu-1 (d_{50bed}: 0.094mm, d_{50bank}: fine sand)</p> <p>Serayu-2 (d_{50bed}: 0.075mm, d_{50bank}: fine sand)</p> <p>Serayu-3 (d_{50bed}: 0.384mm, d_{50bank}: fine sand)</p> <p>Serayu-4 (d_{50bed}: 0.302mm, d_{50bank}: fine sand)</p> <p>Serayu-5 (d_{50bed}: 0.079mm, d_{50bank}: fine sand)</p> <p>Serayu-6 (d_{50bed}: 0.217mm, d_{50bank}: fine sand)</p> <p>Serayu-7 (d_{50bed}: 0.089mm, d_{50bank}: fine sand)</p> <p>Serayu-8 (d_{50bed}: 0.188mm, d_{50bank}: fine sand)</p> <p>Ciliwung-4 (d_{50bed}: 0.152mm, d_{50bank}: 0.124mm)</p>	<p>I-3 </p> <p>Ciliwung-2 (d_{50bed}: 0.051mm, d_{50bank}: 0.178mm)</p>
Cohesive (Silt-Clay)	<p>II-1 </p> <p>-----</p>	<p>II-2 </p> <p>Cimanuk-3 (d_{50bed}: 0.081mm, d_{50bank}: 0.073mm)</p>	<p>II-3 </p> <p>Ciliwung-1 (d_{50bed}: 0.017mm, d_{50bank}: 0.038mm)</p> <p>Ciliwung-3 (d_{50bed}: 0.036mm, d_{50bank}: 0.059mm)</p> <p>Sangkae-2 (d_{50bed}: 0.006mm, d_{50bank}: 0.022mm)</p> <p>Sangkae-3 (d_{50bed}: 0.002mm, d_{50bank}: 0.017mm)</p> <p>Sangkae-4 (d_{50bed}: 0.002mm, d_{50bank}: 0.013mm)</p> <p>Cimanuk-1 (d_{50bed}: 0.008mm, d_{50bank}: 0.009mm)</p> <p>Cimanuk-2 (d_{50bed}: 0.078mm, d_{50bank}: 0.070mm)</p>

4.2 Sediment Mobility and Transport Type

The sediment mobility and sediment transport type of bed material could be expressed by using the Bankfull Shields parameter and particle Reynolds number (Parker, 2004). Bankfull Shields number (τ_{*bf50}) and particle Reynolds number (Re_{p50}) is derived from (24) and (25).

$$\tau_{*bf50} = \frac{H_{bf}S}{RD_{50}} \quad (24)$$

$$Re_{p50} = \frac{\sqrt{RgD_{50}}D_{50}}{\nu} \quad (25)$$

where $R=1.65$ is assumed to be relative submerged grain density.

Figure 4.4 shows the relationship between these parameters in our study rivers. Initiation of motion is indicated by red line and suspension condition boundary is indicated by blue line. Green line is proposed by Yamamoto (2004) to show the relationship in Japanese rivers. Japanese target rivers tend to follow the stability theory by Yamamoto. Yamamoto clarified that U_*^2 under mean annual maximum discharge in Segment II tend to be almost constant and is around $0.02(\text{m/s})^2$. Y axis of Figure 4.4 is not U_*^2 but Shields number, therefore X and Y values on green line is inversely proportional. As shown in Figure 4.4, all Southeast Asian rivers and some of Japanese rivers, the Naka River, the Watarase River, and the Old Ara River with smaller bed material are located in suspension condition. Southeast Asian rivers and some Japanese rivers have suspended material that coming from upstream of volcano basin. But this study clarified that, both Southeast Asian rivers and Japanese rivers follow Yamamoto's theory regardless of river size.

To explain more details about sand and mud (silt-clay) in these rivers, it is necessary to consider bankfull shear stress ($\tau_{bf} = \rho g H_{bf} S$) condition as shown in Figure 4.5 (Dunne & Jerolmack, 2020). Blue line is Shields curve. τ_c , critical shear stress for sand-clay mixtures as experimentally measured (Dunne, 2020) and this threshold (pink line range) is important for South East Asian Rivers which have cohesive bank materials. Dunne (2020) also explained that gravel-bed rivers which follow the Shields curve are in condition of bed sediment control, while fine-grained rivers are consistent with cohesive bank control. Another approach from Yamamoto's theory (green line) also explained that stability under mean annual maximum discharge. As is mentioned above, U_*^2 is around $0.02(\text{m/s})^2$ and that means τ_{bf} is around 20N/m . It is also close to measured range for sand and clay in past study (pink line). From these results, it was clarified that both Japanese and Southeast Asian rivers follow the line of $U_*^2 = \sqrt{gHS} = \tau_{bf} / \rho$ as was introduced by Yamamoto (2004) and Dunne (2020). But the line of Yamamoto's theory cannot explain the condition of fine material well. The stability condition which controlled by bed sediment and cohesive bank will also affect the aspect ratio and its variation.

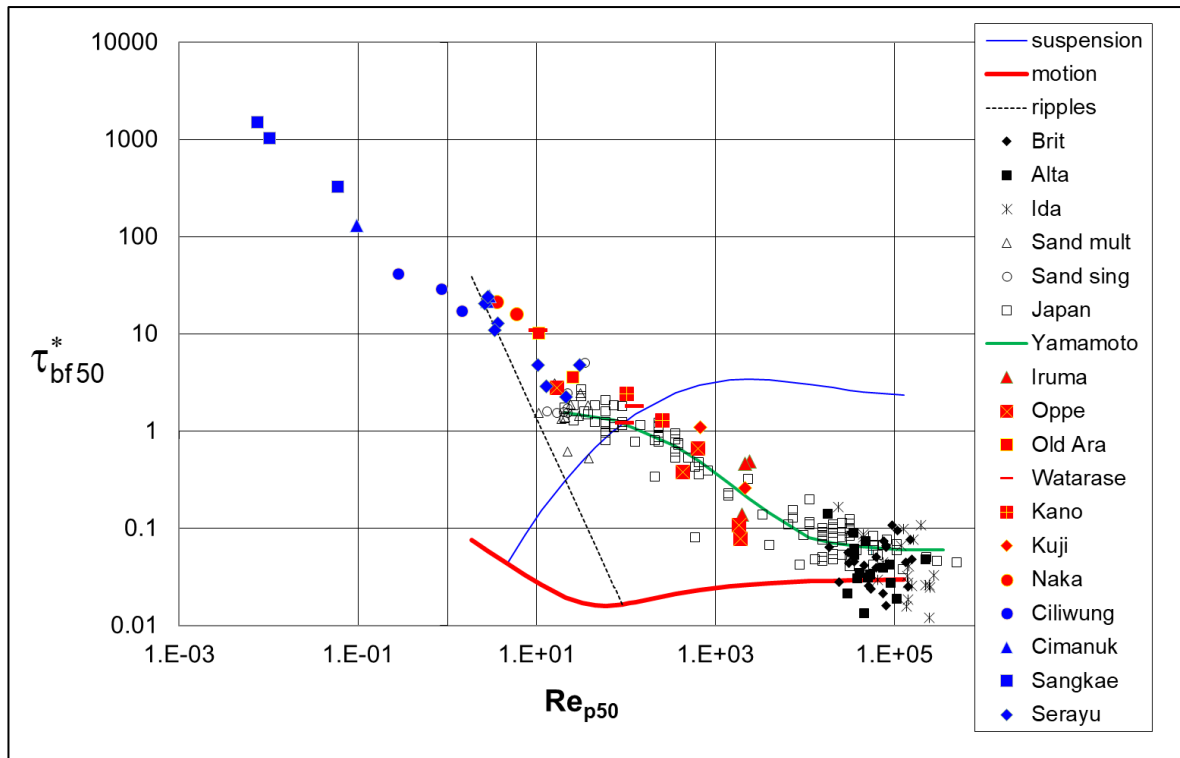


Figure 4.4. Shields Parameters vs Reynolds Number (After Parker, 2004)

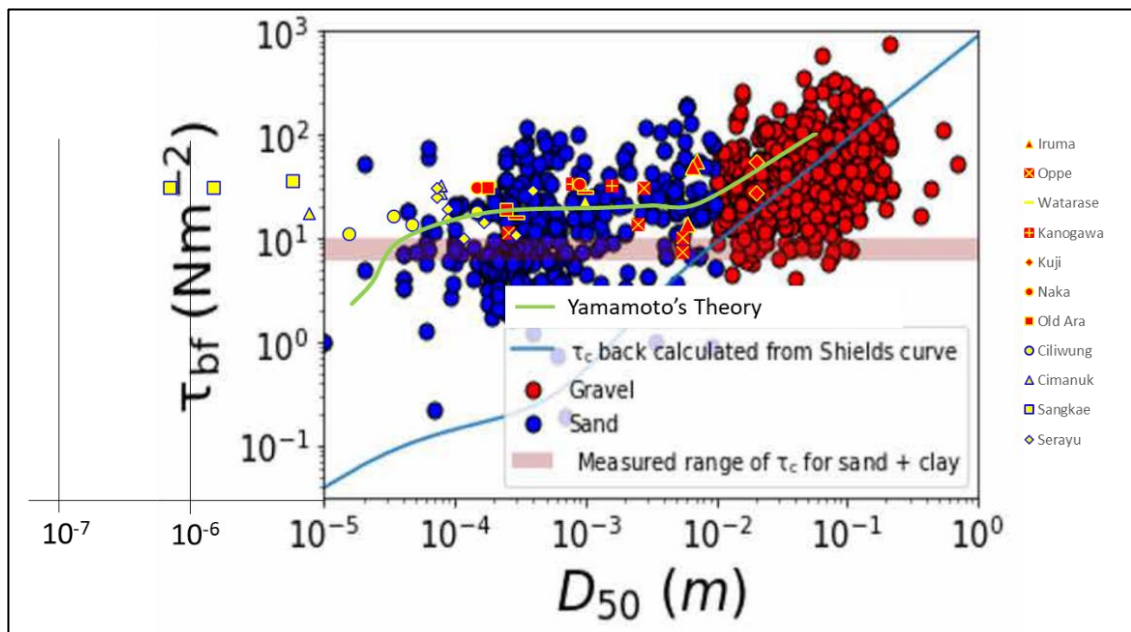


Figure 4.5. Bankfull shear stress and median grain size D_{50} for gravel-bedded ($D > 1$ cm) and fine-grained ($D < 1$ cm) rivers (after Dunne & Jerolmack, 2020)

4.3 Aspect Ratio Variation

Aspect Ratio of all target river could be summarized as Figure 4.6 based on distance from downstream end which could be river mouth or confluences. Figure 4.7 shows the results of

aspect ratio variation. Most of Japanese rivers have relatively large and diverse variation of aspect ratios except for the Iruma River, lower reach of the Oppe River and lower reach of the Kano River. The Serayu River in Indonesia shows wide variation in aspect ratio that might be caused by sand-bed rivers that usually has wide channel. Other rivers such as Cimanuk, Ciliwung and Sangkae show smaller values of aspect ratio that might be caused by cohesive bank. Figure 4.8 shows aspect ratio variation based on bed-bank material condition (Table 4-1) and it can be identified that rivers with non-cohesive bank (red and green square mark) mostly have aspect ratio more than 25 with large aspect ratio variation. On the other hand, rivers with cohesive bank (yellow and blue square mark) mostly have aspect ratio lower than 25 with small aspect ratio variation. However, some red marks such as the Kuji, the Kano, the Iruma and the Cimanuk-U rivers that have coarse sand with occasional gravel on bed and non-cohesive bank show smaller aspect ratio than green marks.

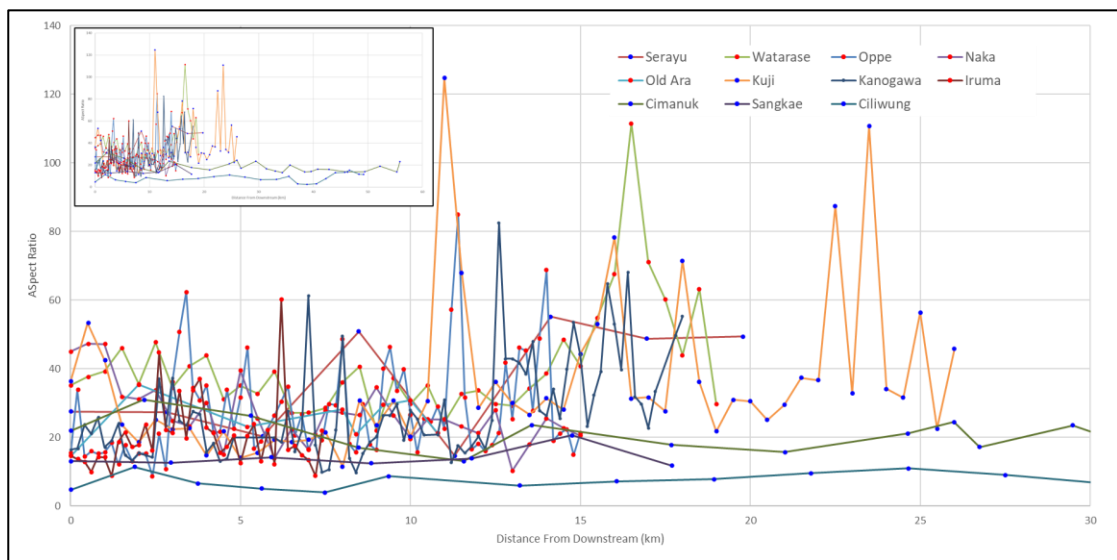


Figure 4.6. Aspect Ratio of Target Rivers

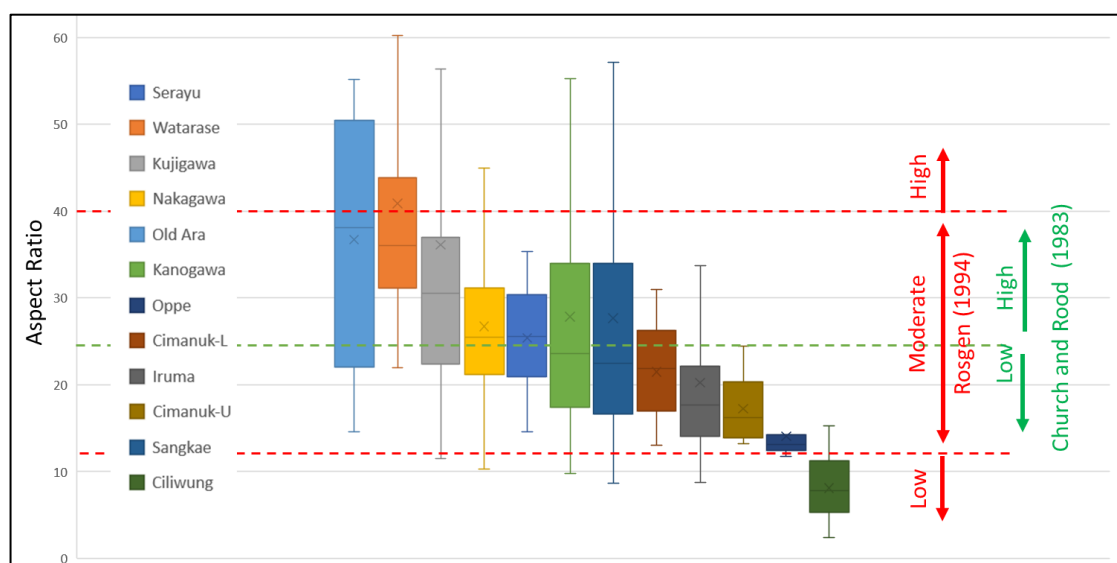


Figure 4.7. Aspect Ratio Variation of Target Rivers

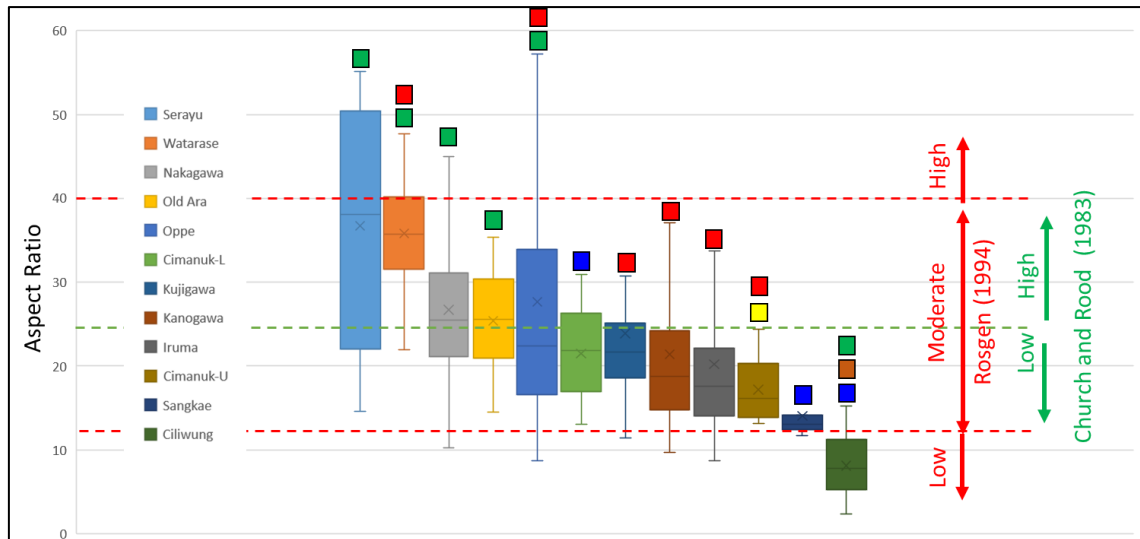


Figure 4.8. Aspect Ratio Variation of Target Rivers (Segment II-2 only) Based on Bed-Bank Material Condition (Table 4-1)

Their banks are less cohesive than those of Southeast Asian rivers, but they show similar condition with Southeast Asian rivers regardless of its non-cohesive bank. This result shows the order of aspect ratio is green and red marks higher than other color marks.

As this result shows, the order of aspect ratio is green and red marks higher than other color marks. The Ciliwung river also show green mark, but aspect ratio is much lower than any other rivers and has characteristics as equiwidth meandering (Type 1 see Chapter 2.1) explained by Soar & Thorne (2001). Figure 4.8 also implied that the Cimanuk River may have several channel patterns and in the transition between red mark and blue mark. In order to explained relationship among parameters, classification of target rivers will represent by green, red, yellow and blue mark plots.

4.4 Sinuosity, Meander Wavelength, Radius of Curvature and Aspect Ratio Variation

Most of Southeast Asian Rivers have more sinuous reach compared with Japanese rivers (Figure 4.9 and Figure 4.10). Japanese rivers also tend to have high aspect ratio as well as low sinuosity. These feature are consistent with the theory that river with low sinuosity has wide and shallow channel (Schumm, 1963). On the other hand, narrow and deep channel such as Ciliwung River has high sinuosity. And moderate condition can be found between aspect ratio values of 12 and 40 (Rosgen, 1994)). Figure 4.9 shows that both Southeast Asian rivers and Japanese rivers are plotted between aspect ratio of 12 and 25 and have various sinuosity. Figure 4.10 shows that the relationship between aspect ratio and radius of curvature or meander wavelength. As this figure shows, these parameters of the Ciliwung River have the lowest value and it can be considered as the narrow and deep channel characteristics. Other rivers with aspect ratio value of 12 to 40 show gradually increasing value of radius of curvature

and meander wavelength which might be related to channel pattern of each river. However, the trend is not clear when aspect ratio is more than 40.

As these results show, the characteristics can be summarized as follows. If the aspect ratio is lower than 12, then sinuosity is more than 1.5 as is indicated by Schumm (1963). The radius of curvature and meander wavelength in this case are small and constant. On the other hand, if the aspect ratio is more than 25, then sinuosity is less than 1.5. This is also indicated by Schumm. The radius of curvature and meander wavelength are diverse and no clear trend is found. If the aspect ratio is between 12 and 25, however, sinuosity is quite diverse. The radius of curvature and meander wavelength are proportional to the aspect ratio. It is considered to be due to bar formation and intermediate condition is found when aspect ratio is between 25 and 40

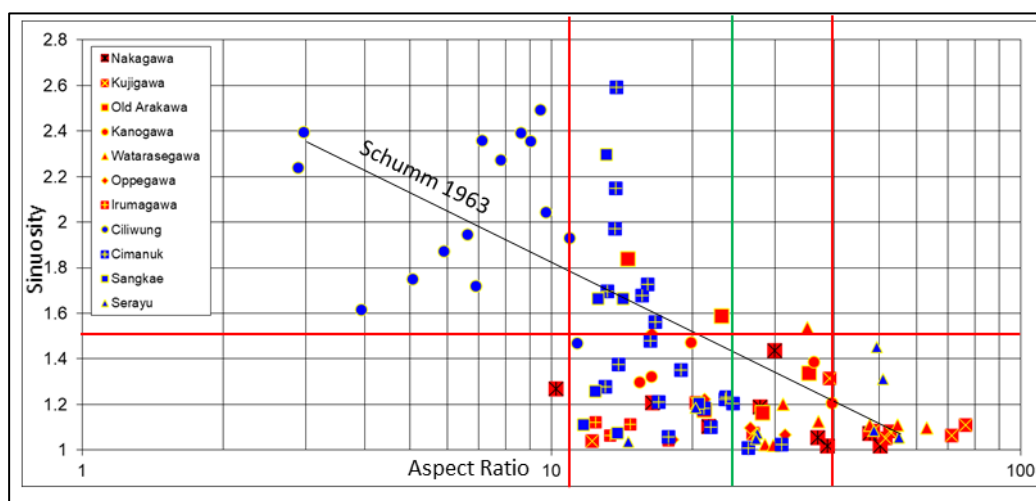


Figure 4.9. Sinuosity and Aspect Ratio of Japan and Southeast Asian Rivers, Red Line Threshold Aspect Ratio 12-40, Sinuosity 1.5 (Rosgen, 1994), Green Line Threshold Aspect Ratio 25 (Church & Rood, 1983)

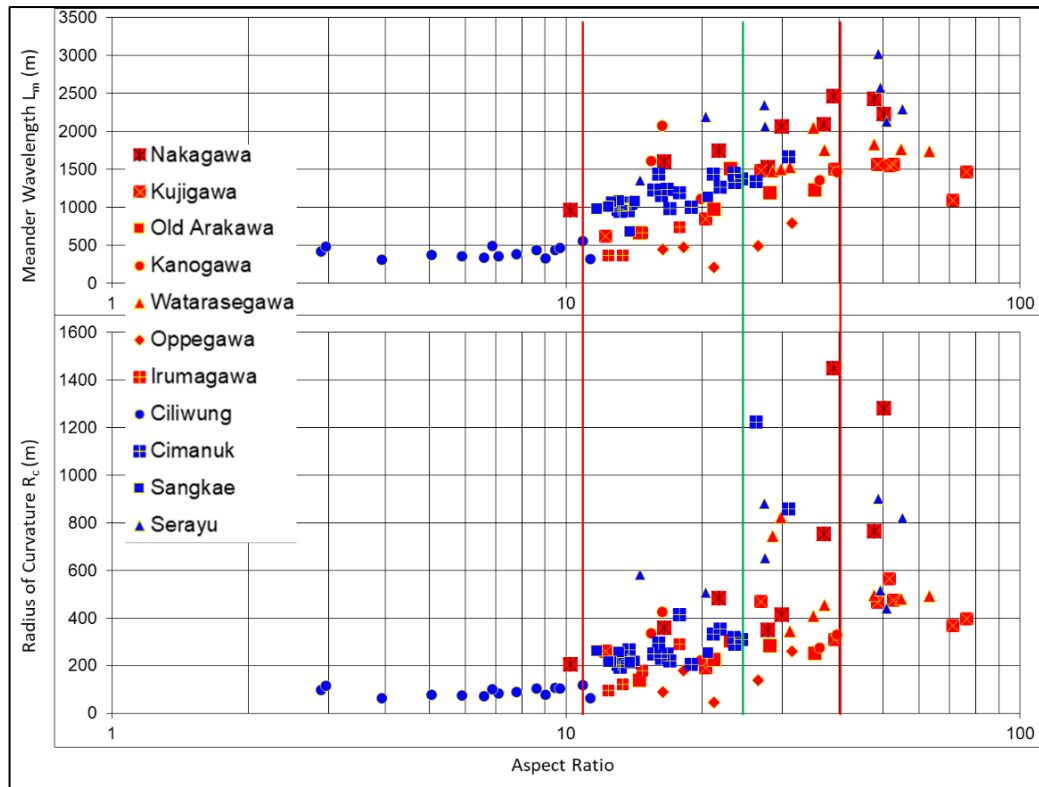


Figure 4.10. Meander Wavelength, Radius of Curvature and Aspect Ratio of Japan and Southeast Asian Rivers, Red Line Threshold Aspect Ratio 12-40, Sinuosity 1.5 (Rosgen, 1994), Green Line Threshold Aspect Ratio 25 (Church & Rood, 1983)

4.5 Silt-Clay Percentage, Aspect Ratio and Sinuosity

Figure 4.11 shows comparison between the target rivers and past studies related to the weighted mean silt-clay percentage (M value in (14), see Chapter 2.4 Figure 2.13). This comparison showed that the condition of all rivers is diverse and does not always follow the relationship between sinuosity and M value shown by Schumm (1963). Schumm (1963) did not investigate the river with M value lower than 1. In this study, most of M values in Japanese rivers are lower than 10, but high sinuosity still could be identified in Old Ara River and the Kano River (See Figure 4.11). On the other hand, low sinuosity were found even though M value is high. Related to this phenomenon, it can be assumed that high M value does not always represent high sinuosity.

Aspect ratio in comparison with M value in Figure 4.12 shows diverse condition in low, moderate, and high. As with Figure 4.11, green line and red line show the aspect ratio of 40, 25 and 12 respectively with possible threshold values (see Chapter 2.4).

Possible boundaries of M values such as 2.6, 5.6, 6.5, 8.6, 16.9 (these values predicted from Schumm's theory), and 20 (from Table 2-1) were obtained. In the target rivers, sinuosity and aspect ratio were not affected by M value which is derived from Schumm's theory as is mentioned above (only the Ciliwung River has weak correlation). Therefore, M values of 2.6, 5.6, 6.5, 8.6 and 16.9 cannot classify the rivers well. Schumm's theory was developed only from sinuous stream in Great Plain US and it might have some limitation to be applied in

general condition, hence the meaning of other values especially less than 10 is not clear and it is considered not to affect the cross-sectional shape. However, M value of 20 which is the boundary between cohesive and non-cohesive (see Chapter 2.4) can classify the cohesive bank (Southeast Asia river and the Naka River) and non-cohesive bank (other Japanese rivers) well.

It can be concluded that the impact of M value on aspect ratio and sinuosity cannot be identified when it is less than 20. Schumm showed the good agreement even if it is less than 10, but it is implied that sinuosity and aspect ratio is affected by other factors in the target sites. Even if M value is high, Schumm's line does not show good agreement.

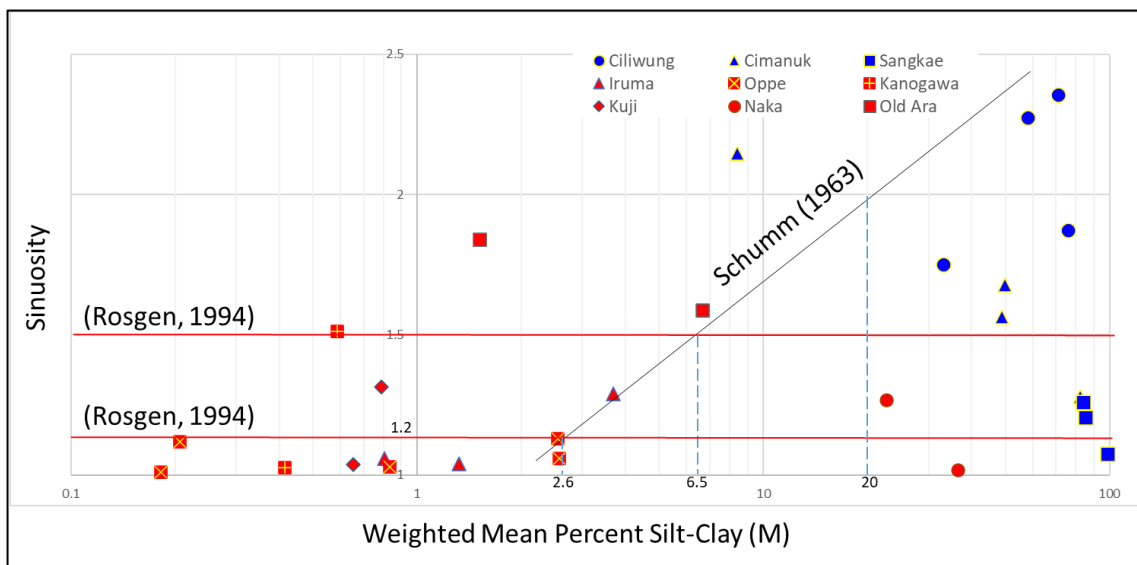


Figure 4.11. Weighted mean silt-clay percentage (M) and Sinuosity

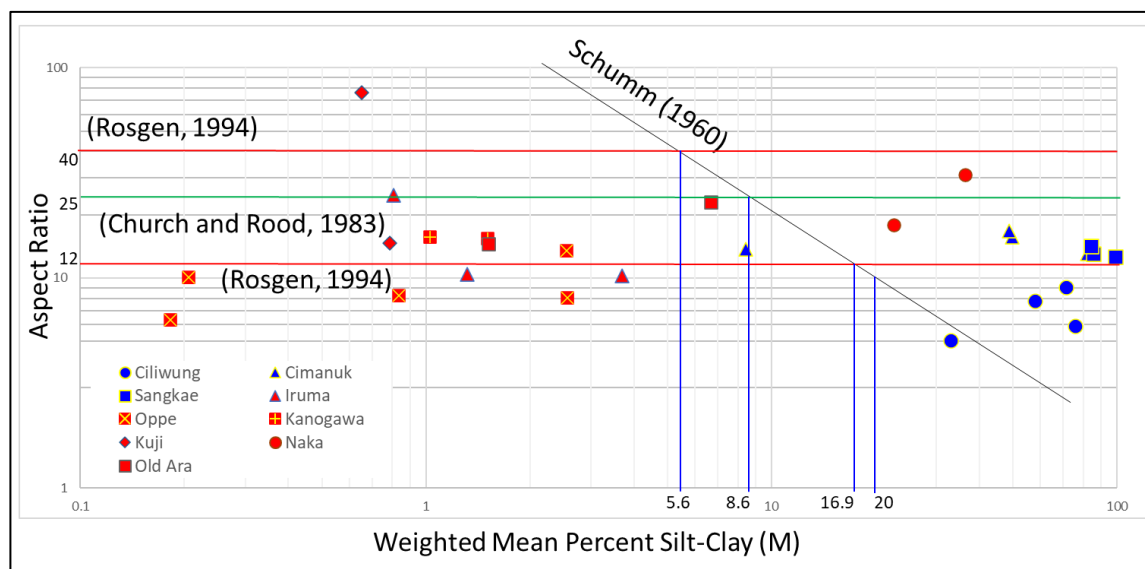


Figure 4.12. Weighted mean silt-clay percentage (M) and Aspect Ratio 12 and 40 (Red line) 25 (Green Line)

4.6 Applicability of Regime Theory

As seen in Figure 4.13, predicted value of width and depth using (3) and (4) tend to be higher than the observed values. Figure 4.14 shows the relationship between dimensionless water surface width (B/d_r) and water depth (h/d_r) to dimensionless channel-forming discharge. The figure also shows the same relationships presented by Santoso (2017), who focused on Segment II rivers in similar site in this study. As investigated by Santoso, equation (6) can predict h/d_r , but predicted B/d_r from equation (5) tends to be lower than Fukuoka (2010) and it might be caused by different definition of water surface which was levee to levee distance in the original study. However, strong correlation between measured B/d_r and dimensionless discharge ($Q/(gId_r^5)^{0.5}$) is found in Figure 4.14 and it can be used for predicting channel width even for finer and cohesive material. This proposed estimation of B/d_r can be represented by this equation.

$$\frac{B}{d_r} = 1.37 \left(\frac{Q}{\sqrt{gId_r^5}} \right)^{0.41} \quad (26)$$

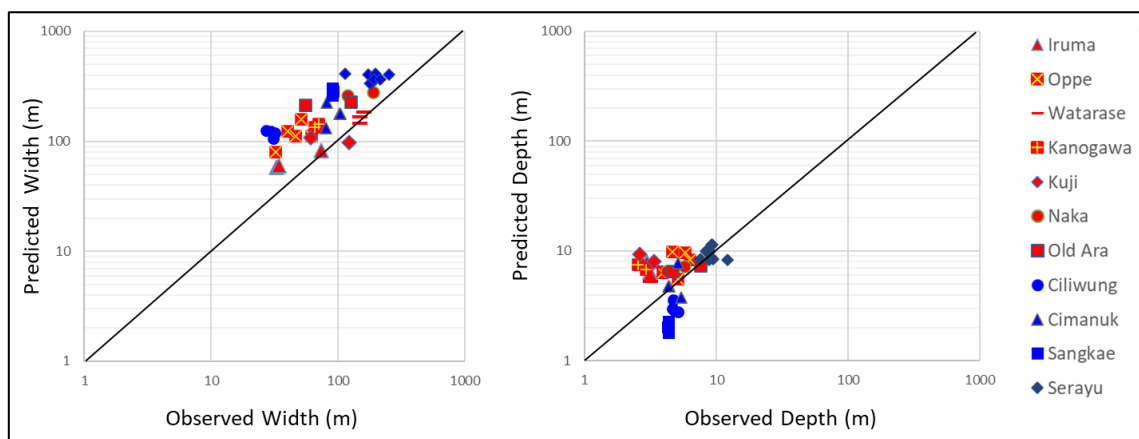


Figure 4.13. Width and Depth Prediction by Past Study (Julien & Wargadalam, 1995)

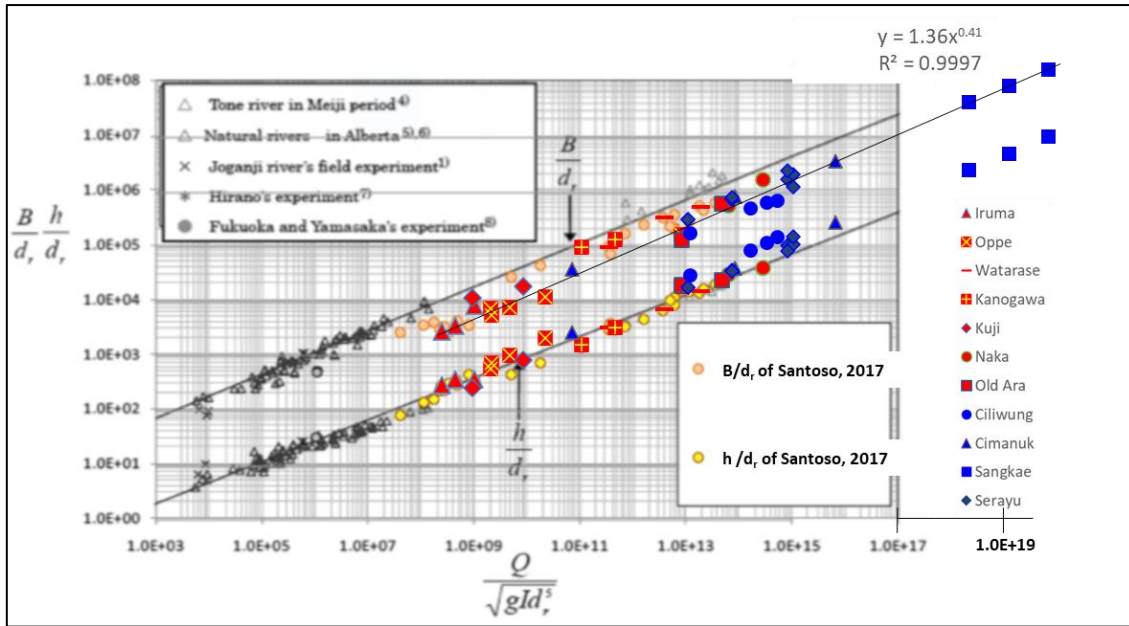


Figure 4.14. Dimensionless water surface width and water depth to dimensionless channel-forming discharge (after (Fukuoka, 2012)) including past study (after (Santoso, 2017))

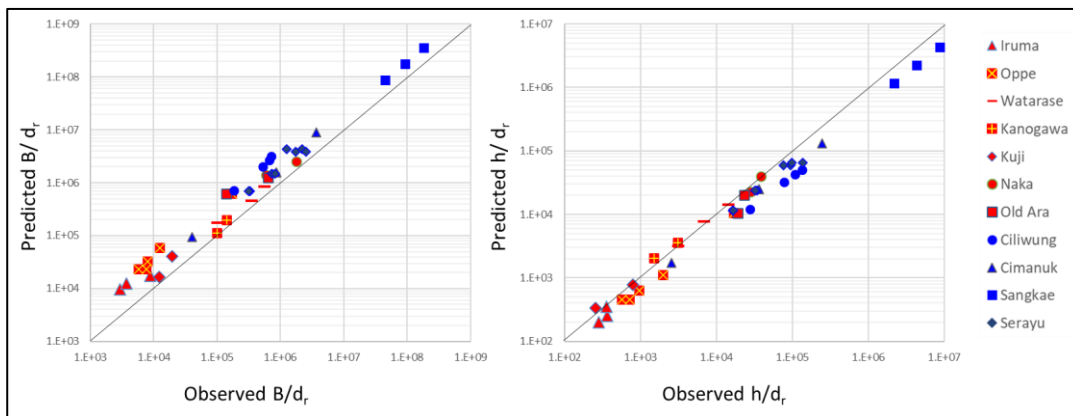


Figure 4.15. Observed and Predicted Values of B/d_r and h/d_r Using Dimensionless Channel Forming Discharge Equation

Prediction of B/d_r and h/d_r by using equation (5) and (6) is shown in Figure 4.15. h/d_r are relatively predicted well, but as bed material is getting finer it is underestimated, as seen in the blue plots (Southeast Asian rivers) which has lower M value compared to Japanese rivers. By considering equation (6), h can be estimated for coarser material. Results for finer material maybe underestimated because the past study by Fukuoka (2010) did not targeted low flow channel but total river width under much larger discharge. In case of gravel bed river, the same equation can be applied in low flow channel. On the other hand, the equation cannot be applied in Segment II rivers which have different bed and bank material or cohesive material.

Proposed B/d_r estimation coefficient (1.37) by this study in equation (26) has value almost one-third compared to past study coefficient (4.25) by Fukuoka (2010). It is explained

the difference of water surface definition between this study and original study Fukuoka (2010). To understand each estimation coefficient that related to each type of grain size distribution (see Chapter 4.3), it can be explained as follows in Table 4-2

Table 4-2. B/d_r and h/d_r Estimation Coefficient for Each GSD Type

Type	I-1 ■	I-2 ■	II-2 ■	II-3 ■
B/d _r Estimation $B/d_r = cB(X)^{0.40}$	$cB = 0.28$ to 1.34 Mean $cB = 0.72$	$cB = 0.31$ to 1.00 Mean $cB = 0.62$	$cB = 0.55$ to 0.71 Mean $cB = 0.63$	$cB = 0.28$ to 0.71 Mean $cB = 0.53$
h/d _r Estimation $h/d_r = ch(X)^{0.38}$	$ch = 0.03$ to 0.09 Mean $ch = 0.06$	$ch = 0.04$ to 0.1 Mean $ch = 0.06$	$ch = 0.0598$ to 0.0609 Mean $ch = 0.0604$	$ch = 0.06$ to 0.11 Mean $ch = 0.09$
$X = Q/(gI d_r^5)^{0.5}$				

4.7 Classification of Channel Pattern by Using Stream Power

Past study (van den Berg, 1995) explained about the relationship between valley slope and stream power. Japanese rivers have diverse as Figure 4.16 shows, target rivers of this study have milder slope and high stream power. It implies discharge in the target rivers is higher than past study (van den Berg, 1995).

Therefore, it is necessary to understand how to distinguish their characteristics, especially by analyzing the relationship between stream power and channel pattern. This study is trying to use past empirical channel pattern discriminator which is determined by potential specific stream power, median grain size (Kleinhans & van den Berg, 2011), and silt-clay percentage in river bank (Candel et al., 2021). Firstly, target rivers are plotted along with past study (Kleinhans & van den Berg, 2011) as shown in Figure 4.17. It could be identified that more than half of target rivers are located between ω_{ia} and ω_{bm} (see Chapter 2.3). Some rivers are closely located in the boundary of a highly braided condition and moderate braided and meandering scroll and chutes. It might be caused by steep slope (Segment II-1). Another possibility is transition between mixed and suspended sediment transport that is necessary to be considered. Ciliwung and Sangkae with cohesive bed need to investigate with silt-clay fraction discriminator.

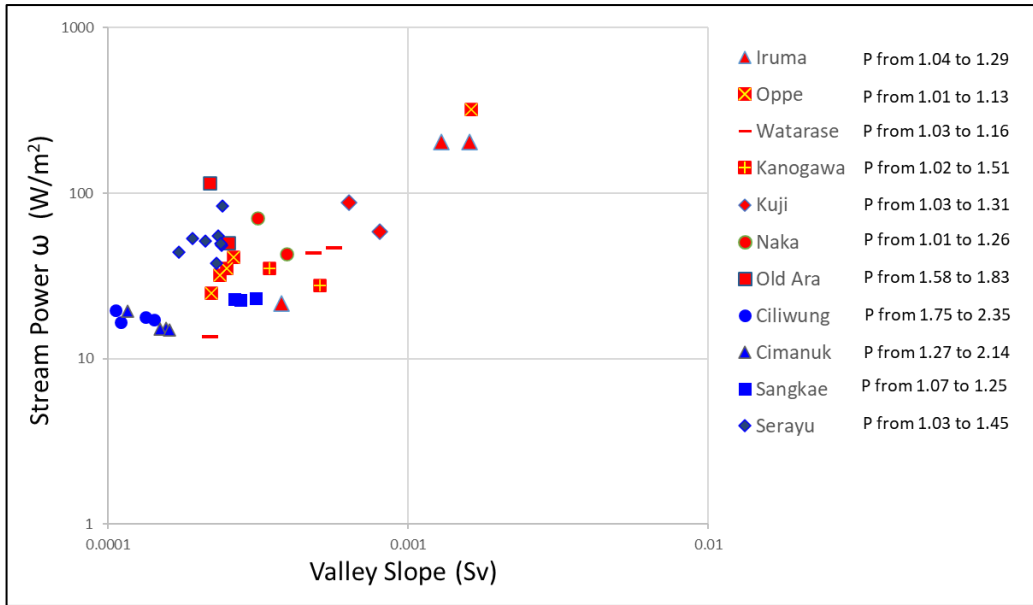


Figure 4.16. Valley Slope and Stream Power (Modified from van den Berg (1995)).

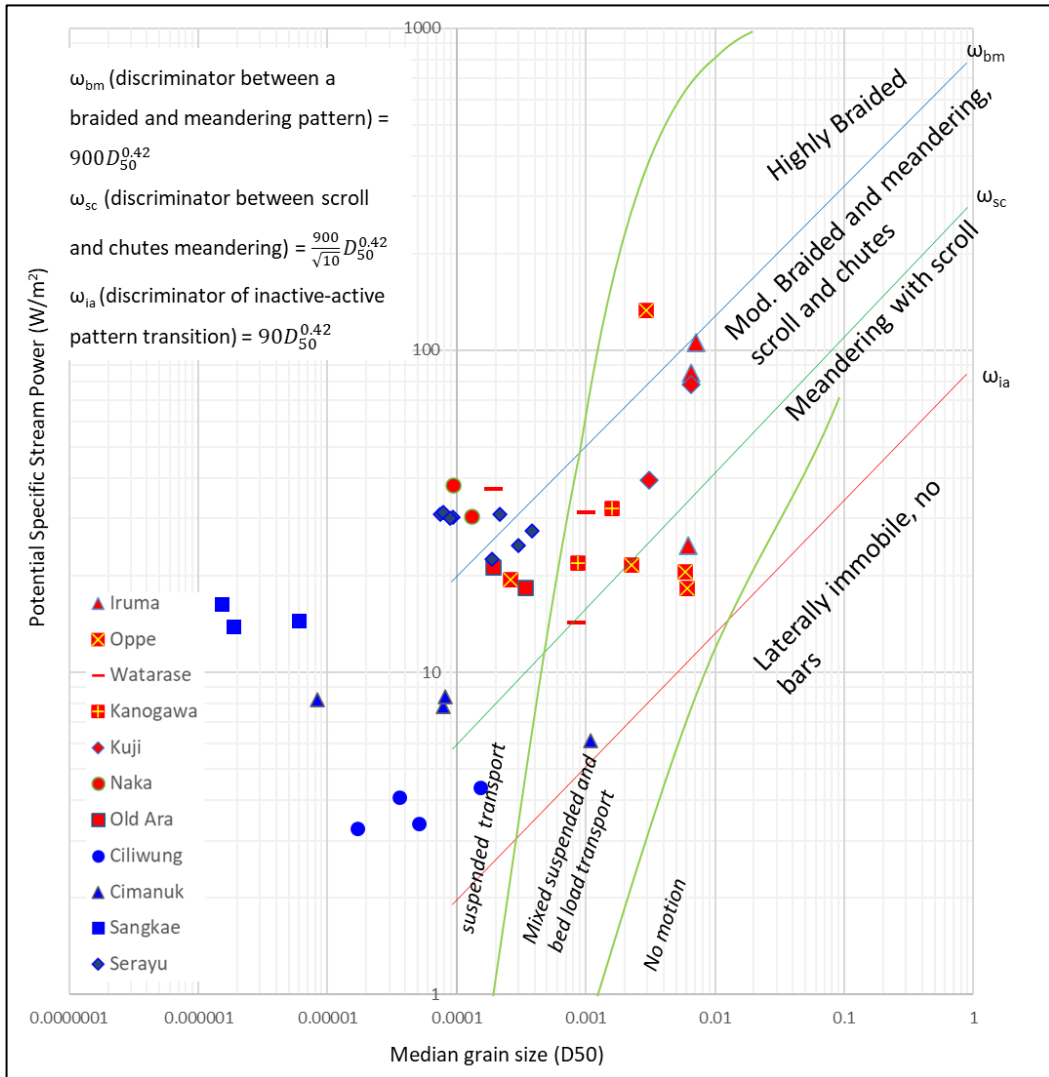


Figure 4.17. Channel Pattern Determination by Using Stream Power and Median Grain Size (Modified from Kleinhans & van den Berg (2011))

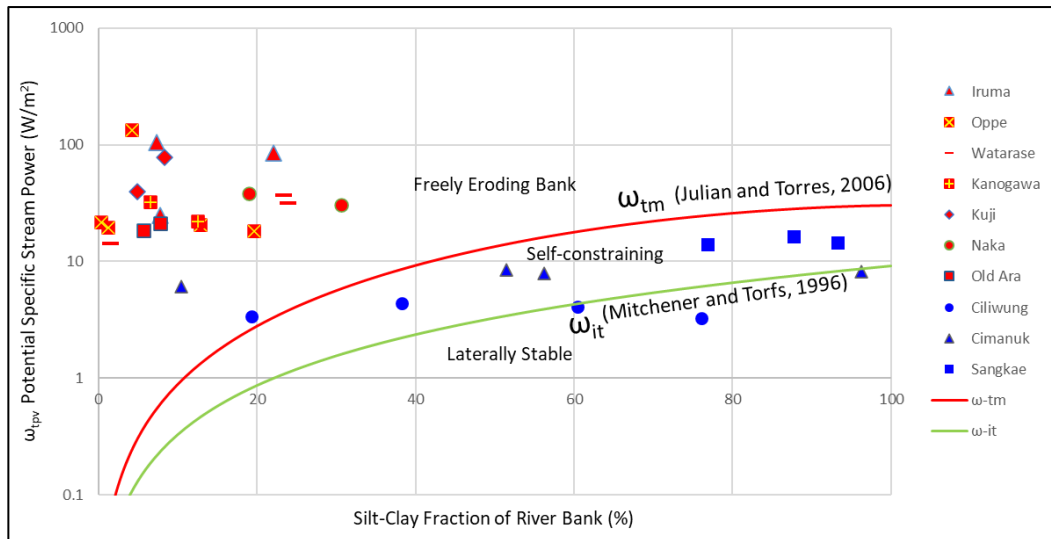


Figure 4.18. River Patterns, Stream Power and Silt Clay Fraction of River Bank (Modified from Candell et al., (2021))

Figure 4.18 shows that all Japan rivers with low silt clay fraction are categorized as freely eroding bank, while mostly Southeast Asian rivers defined as self-constraining which lead to tortuous channel pattern, and some parts of Ciliwung River are categorized as laterally stable rivers. Laterally stable and no bar condition can be confirmed in Ciliwung River and Sangkae river, but actual characteristics of tortuous and scroll bars are found. Cimanuk river has transition characteristics that may have meandering with scroll and laterally immobile at the same time. It means, even though has scroll bar, meandering reaches of Cimanuk river tend to have stability especially in lower reaches.

Japanese rivers such as the Naka River, the Oppe River and the Watarase River tend to be stable if bed material are fine and in suspended condition. Increasing discharge or increasing river capacity will lead to increasing stream power and channel pattern tend to have chutes. Interesting part is that past conditions of some rivers such as Oppe, Iruma and Naka still could be identified as meandering channel (detail in Chapter 4.9). Some parts of this channel are not changing and remaining as original meandering river shape even though the sinuosity were changed because of straightening works.

Figure 4.19 shows the combination of channel pattern predicted by past studies. The graph was modified to represent stream power, median grain size and silt clay percentage which is represented by ω_{tm} and ω_{it} . By using this modified graph, rivers that have cohesive material with high silt-clay percentage in river bank could be represented.

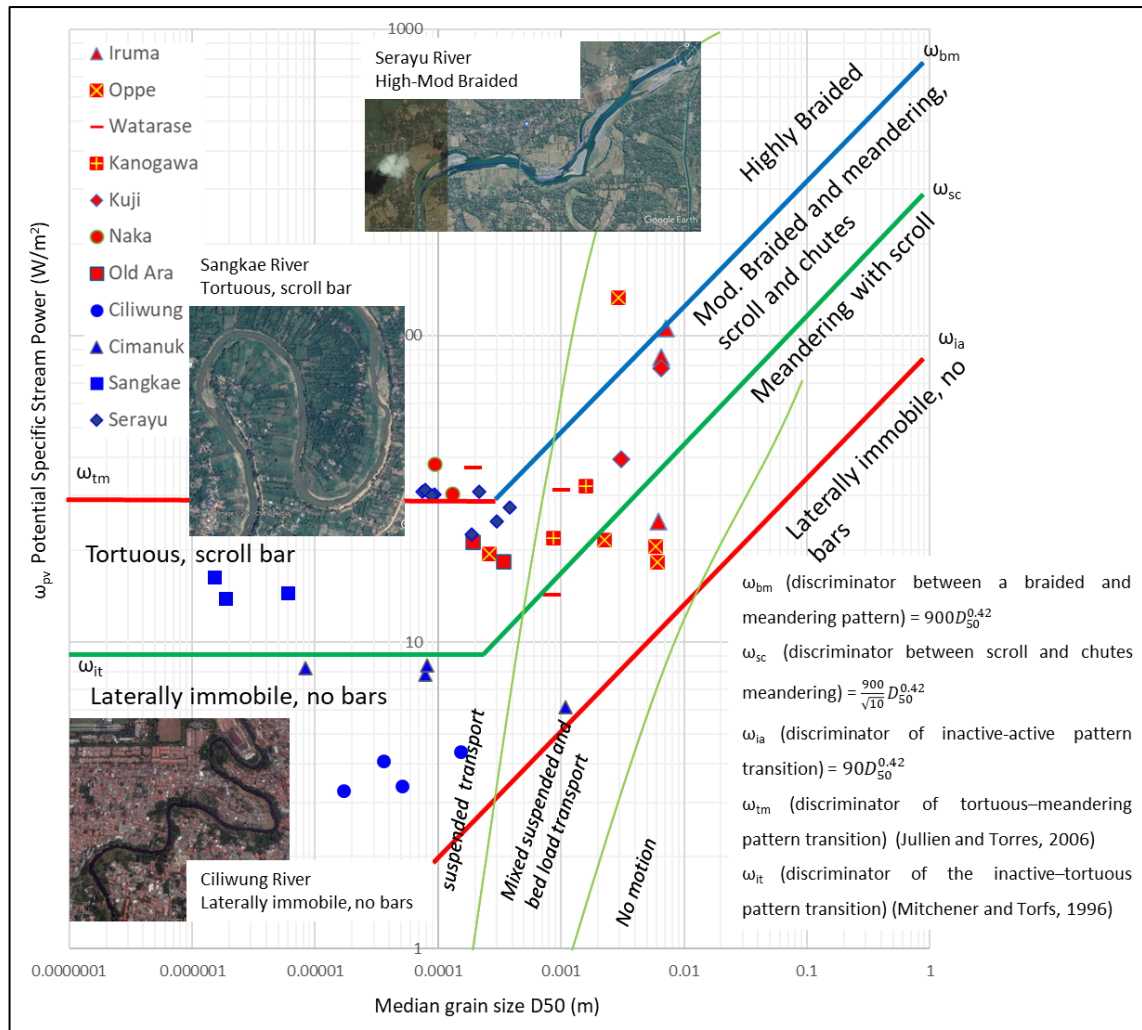


Figure 4.19. Channel Pattern Determination by Using Stream Power, Median Grain Size (Modified from Kleinhans & van den Berg (2011)) combined with Silt-Clay Percentage (Modified from Candel et al. (2021)).

4.8 Bank Erosion Rate and Silt—Clay Percentage

Past study (Julian & Torres, 2006) used material of both banks (left-right bank) to calculate silt-clay percentage and τ_{bc} value for their observation material. This study used single location of bank sample to calculate silt-clay percentage and τ_{bc} value for bank material. Excess shear stress and erosion rate was calculated by using equations (20) to(23). Excess shear stress and erosion rate from target rivers as is shown in Figure 4.20.

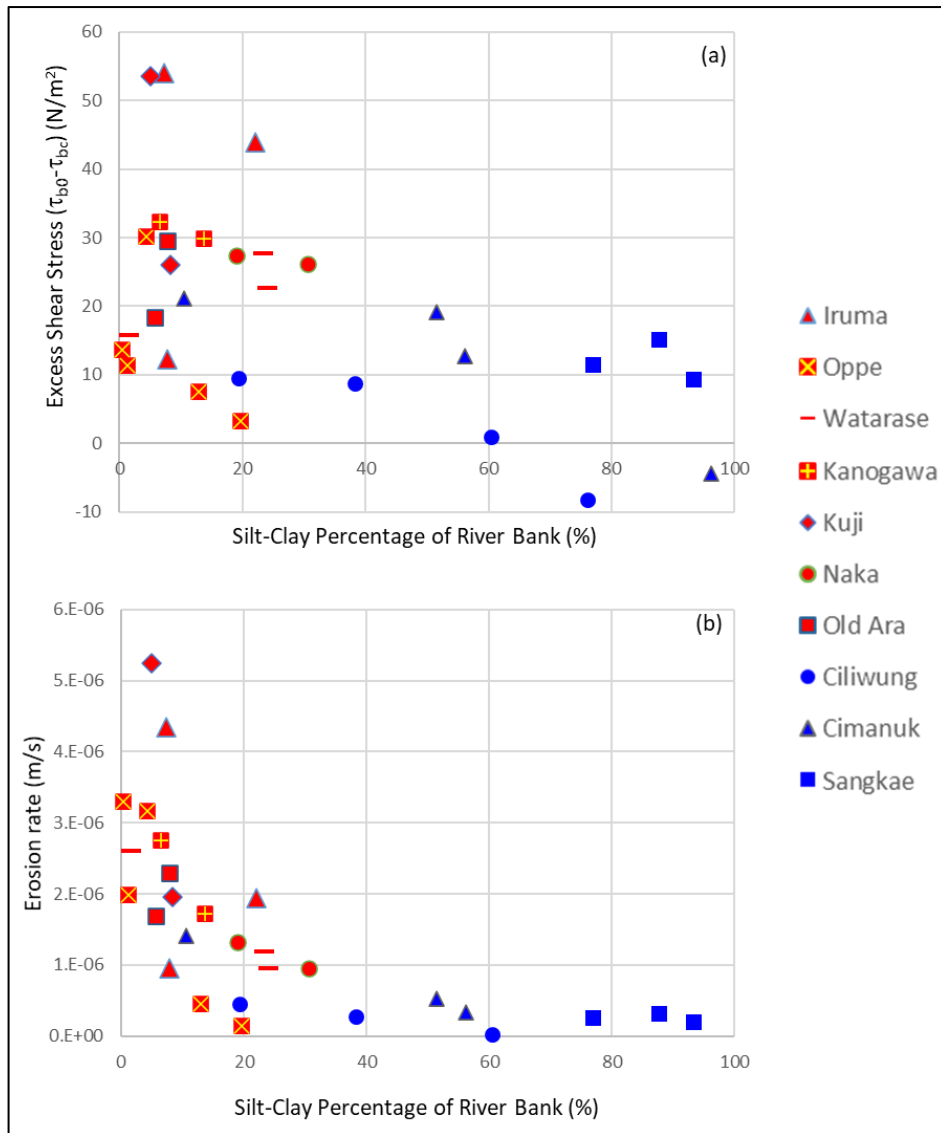


Figure 4.20. Excess Shear Stress and Erosion Rate of Target Rivers

If the fluid shear stress (τ_{b0}) does not exceed the critical shear stress (τ_{bc}) at which the soil particles are entrained, the soil remains stable (Osman & Thorne, 1988). At shear stress levels below the critical shear stress, relatively little erosion takes place (Arulanandan et al., 1980). The negative value of the excess shear stress gives the negative value of the fluvial erosion rate, which has no physical meaning (Patsinghasanee et al., 2015). Any negative values of excess shear stress were modeled to be zero since τ_{bc} represents a threshold that must be exceeded in order to have excess shear stress (Julian & Torres, 2006). In this study, some negative values of excess shear stress values could be detected in Cimanuk and Ciliwung. Results of erosion rate are diverse and Southeast rivers have lower erosion rate due to cohesive bank. Erosion starts to increase drastically when it comes to 20% of silt-clay percentage. Some values are lower in some reaches of the Iruma River, the Oppe River (both straightened), and the Ciliwung River which might be caused by narrow and deep channel characteristics.

4.9 Proposed Classification of Meandering River

Figure 4.21 shows that bed and bank condition could be classified into 4 types and represented with blue, yellow, green and red colors. Compared with past studies about aspect ratio and meandering classification, 4 groups also can be identified. Left upper part with narrow-deep channel with cohesive bed-bank (Type 1 plotted with blue color) and related to channel pattern it should be laterally immobile and sometimes scroll bar. On the other side, in many Japanese rivers, aspect ratio is more than 25 and sinuosity is less than 1.5. If both bank and bed material are fine sand, it is plotted with green color. This type is classified as Type3 and many green marks are located here. In terms of channel pattern, it should be braided meandering with chutes or scroll and sometimes highly braided.

Type2 is intermediate condition between Type 1 and 3. This type show the diversity in sinuosity and it can be divided into two types, 2a with low sinuosity 2b with high sinuosity. After the results examined, it was found that the difference between bank and bed is important. Related to aspect ratio in Type1 and Type2b, cohesion of the bed in type2b is less than type1 and aspect ratio increases. Moreover, if bed material is coarser than bank material it is plotted in yellow color and concentrated in type2b. On the other hand, if riverbed is coarse sand with occasional gravels, it is plotted with red color

Plotted target rivers based on meander wavelength, radius of curvature and bed-bank sediment condition can be shown in Figure 4.22. It can be identified the transition of channel pattern that shows laterally immobile river (the Ciliwung river with blue plots), tortuous and scroll bar rivers (the Cimanuk river and the Sangkae river with yellow and blue plots), moderately braided with scroll and chutes rivers (with red, green, and yellow plots), and highly braided rivers (green and red plots).

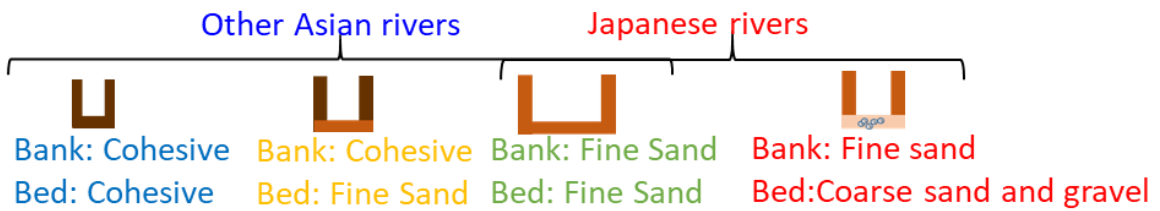
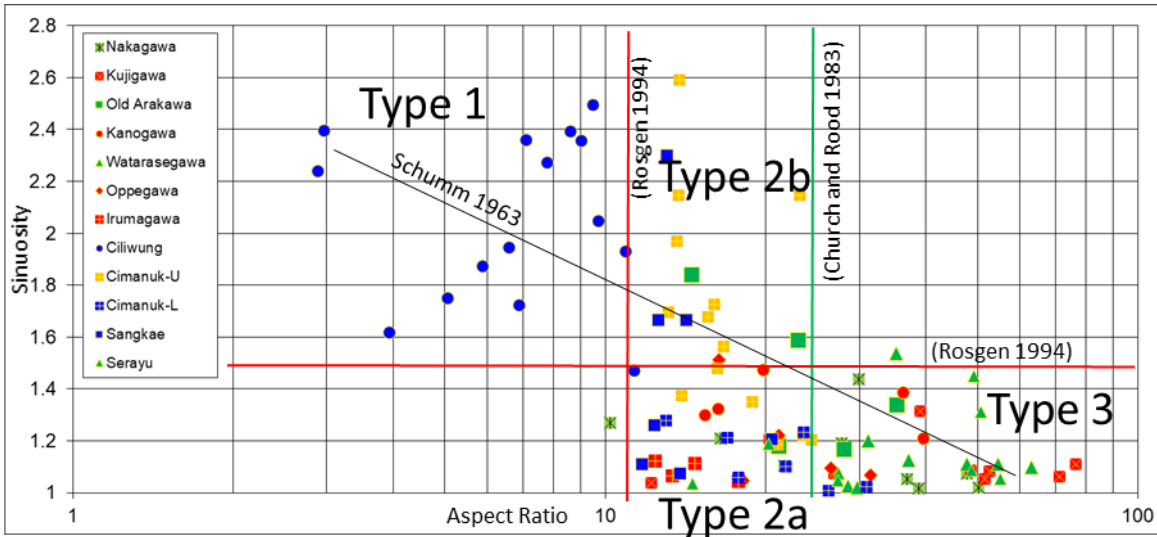


Figure 4.21. Sinuosity, Aspect Ratio, Bed-Bank Sediment Condition

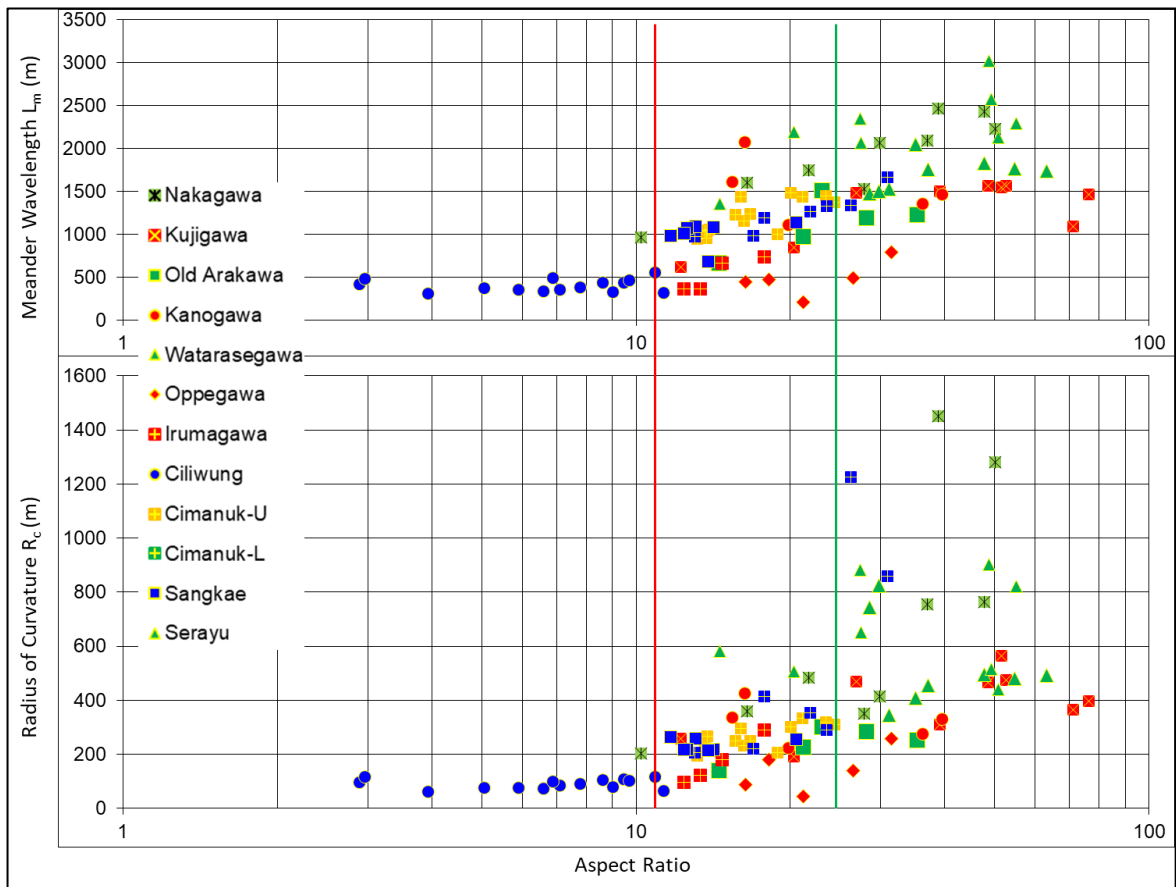


Figure 4.22. Meander Wavelength, Radius of Curvature, Aspect Ratio, and Bed-Bank Sediment Condition - Red Line Threshold (Rosgen, 1994), Green Line Threshold (Church & Rood, 1983)

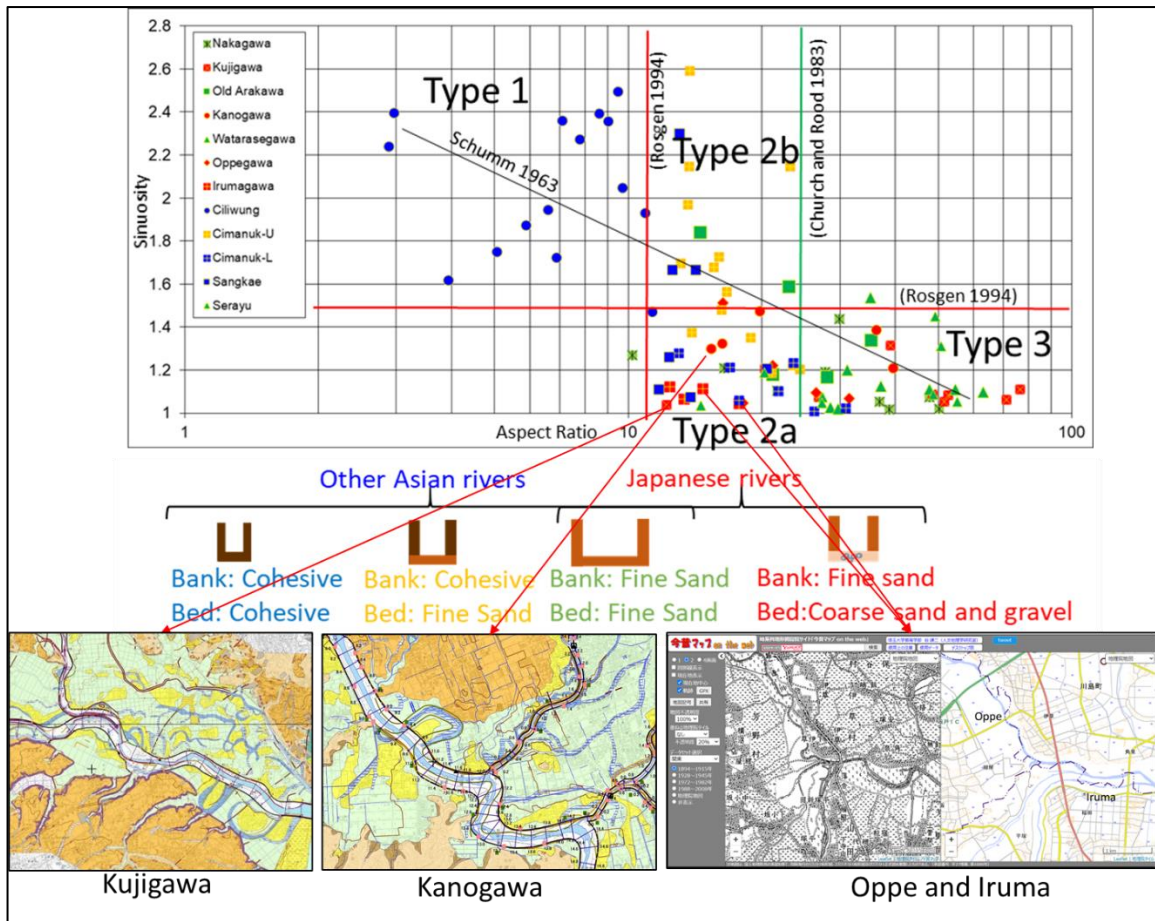


Figure 4.23. Straigtended Rivers Condition in Type 2a

There are some explanations about aspect ratio in type 2 and type 3, existence of occasional on coarse sand makes aspect ratio lower. Some rivers with red marks are classified as 2a due to the straightening, but old maps implied they were sinuous rivers before (Figure 4.23). It means they were type 2b before and these rivers are always red plots that contains gravel on bed.

For example, Figure 4.24 shows the boundary of city/town and old paths of the Oppe and the Iruma rivers. As seen in the figure, these rivers had meandering reaches in the past. Figure 4.25 shows the old channel condition and cut-off channel of the Kano River around 9 km to 11 km upstream from the river mouth. Figure 4.26 shows old channel condition and cut-off channel of the Kuji River. Figure 4.27 shows meandering trace in Cimanuk River.

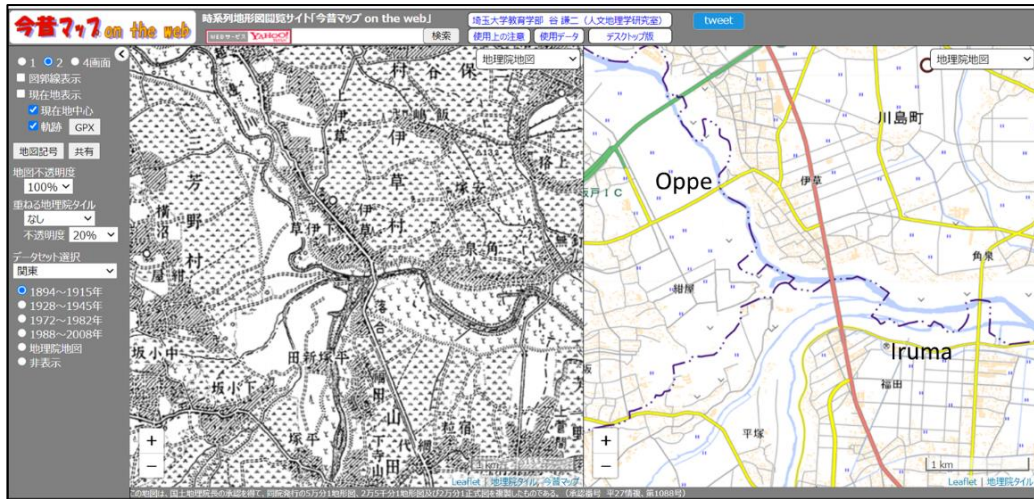


Figure 4.24. Past Condition Map of Oppe and Iruma (Time Series Topographic Map, 2021)

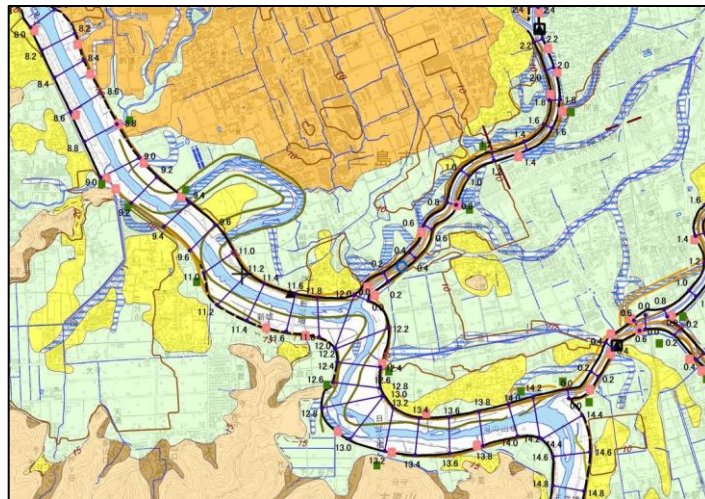


Figure 4.25. Cut-off Condition of Kano River (Geospatial Information Authority of Japan, 2021)

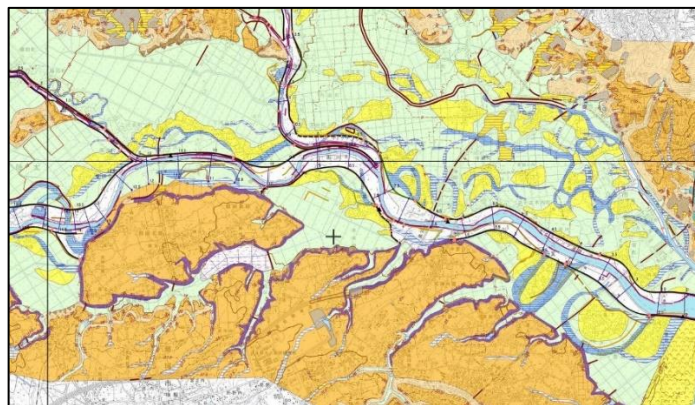


Figure 4.26. Cut-off Condition of Kuji River (Geospatial Information Authority of Japan, 2021)

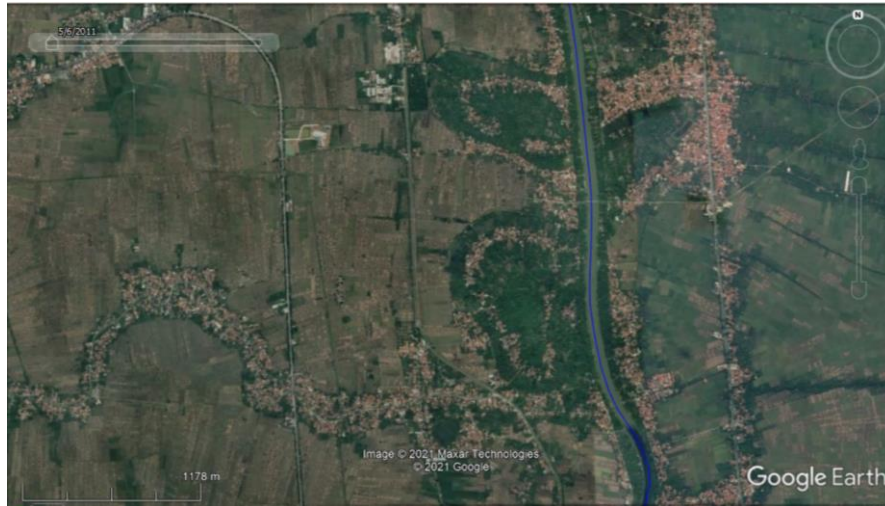


Figure 4.27. Meandering Trace in Cimanuk River (45 km from river mouth)

In order to give comprehensive view related to aspect ratio and sinuosity, M value was also compared (Figure 4.28). As mentioned in Chapter 4.5, several possibilities of M value can be identified and higher possible value is 20. Type 1 and Type 2b which may have M upper than 20 and it tends to follow Schumm's theory about narrow and deep channel with cohesive material. But Type 2a might have different characteristics. In this study, some of them were identified as straightened channel (Figure 4.23). But even though it was meandering rivers in the past (originally Type 2b), these rivers has M value lower than 20 and this characteristic is different from Schumm's theory.

On the other hand, some plots of the Naka River and the Sangkae River also can be identified in Type 2a, these rivers have M value upper than 20. The explanation of this phenomena still cannot be clarified yet, but it might be affected by larger discharge from river basins that create larger channel capacity. Therefore, aspect ratio is larger compared to Type1 even though river channel has cohesive characteristics. These phenomena also might be explained from stream power viewpoint (Figure 4.19) for the Naka River that has high stream power and existing possibility of bar formation which make aspect ratio become larger.

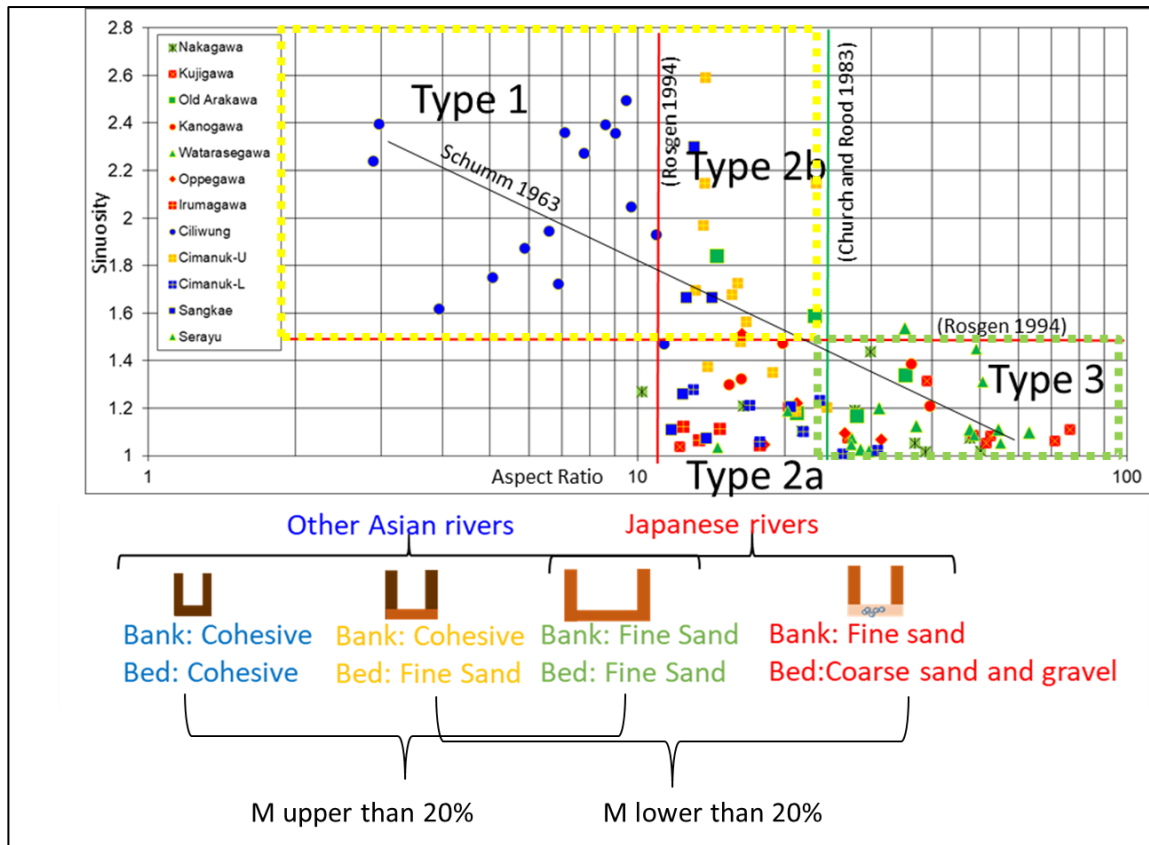






Figure 4.28. M Value Condition Related to Aspect Ratio VS Sinuosity

Based on this overall comparison condition, this study proposed new classification as follows to modify previous classification (Soar & Thorne, 2001). Diverse variation on Type 2 is necessary to explain more detail, therefore in this study it is divided into Type 2a and Type 2b. Table 4-3 shows that proposed classification and this is improved table of Figure 2.5. This proposed classification also give additional parameter or characteristics that expected to be helpful for understanding meandering rivers characteristics.

Table 4-3. Proposed Classification of Meandering Rivers (Modified (Soar & Thorne, 2001))

Characteristics	Type 1 Equiwidth Meandering	Type 2a Meandering with Point Bars	Type 2b Meandering with Point Bars	Type 3 Meandering with Point Bars and Chute Channel
Bar Existence and Planform	No Bar 	Unclear Bar 	Stable Clear Bar 	Unstable Clear Bar 
Bed and Bank Material	Bank: Cohesive Bed: Cohesive (High clay percentage)	Bank: Cohesive Bed: Cohesive (Low clay percentage)	Bank: Cohesive Bed: Fine sand (Non-cohesive) or Bank: Fine sand Bed: Coarse sand and gravel	Bank: Fine sand Bed: Fine sand
Sinuosity (Planar Shape)	High (> 1.5)	Low (< 1.5)	High (> 1.5)	Low (< 1.5)
Aspect Ratio	Low (< 12)	Low-Moderate (12 to 25)	Low-Moderate (12 to 25)	Moderate-High or High (> 40)
Aspect Ratio Variability	Stable	Intermediate	Intermediate	Diverse
Estimation of B/d_r $B/d_r = cB(X)^{0.40}$	$cB = 0.28$ to 0.71	$cB = 0.51$ to 0.70	$cB = 0.28$ to 1.34	$cB = 0.31$ to 1.00
Estimation of h/d_r $h/d_r = ch(X)^{0.38}$ $X = Q/(gId_r^5)^{0.5}$	$ch = 0.08$ to 0.11	$ch = 0.0602$ to 0.0741	$ch = 0.03$ to 0.09	$ch = 0.04$ to 0.09
Relationship Stream Power, Sediment Size, and Silt-Clay Percentage	Laterally immobile, no bar	Below ω_{sc} Meandering with scroll	Below ω_{sc} Meandering with scroll But also indicate below ω_{it} (laterally immobile, no bar)	Highly Braided
Target Rivers	Ciliwung, Sangkae	Cimanuk-L (Downstream of lower reach)	Cimanuk-U (Upstream of lower reach), Iruma, Oppe, Watarase (6-7)	Old Ara, Kano River, Serayu, Watarase(4), Kuji, Naka

4.10 Summary of Results and Discussion

Based on bed and bank material grain size distribution, four patterns (red, green, yellow and blue) are classified to explain to relationships among parameters. Grain size distribution of sand is same in any rivers because it is composed of suspended sand. Silt-clay percentages is clearly different between Japan and Southeast Asian rivers. U^*^2 under bankfull discharge is around $0.02(m/s)^2$ and that means τ_{bf} is around $20N/m$, and both values are almost constant. It follows the Yamamoto's line even if the material is fine. Aspect ratio is different among 4 marks color patterns and it can have the order from larger to smaller respectively: green, red, yellow, and blue. Low aspect ratio have constant and small wavelength and radius of curvature. These rivers are not affected by bar formation but intermediate aspect ratio (12-40) river's wavelength and radius of curvature maybe affected by bar formation. High aspect ratio rivers show the diverse value.

Impact of M value on cross-sectional shape is not clear in this study. But M value of 20 may classify cohesive and non-cohesive river. Higher stream power make some bedform except some Southeast Asian rivers that show low aspect ratio with small and constant wavelength and radius of curvature. Based on these findings, new classification is proposed based on bed-bank material condition, sinuosity and aspect ratio. Four classification the can be introduced as Type1, Type2a, Type2b and Type3. The numerical simulation is necessary to investigate the possible mechanism in intermediate condition of Type2a and Type2b.

Discussion on Forming Process of Aspect Ratios

5.1 Numerical Simulation of Cimanuk River (ICHARM Bank Erosion Model)

ICHARM Bank Erosion Model was developed based on iRIC Nays2DH Solver. Nays2DH is a computational model for simulating horizontal two-dimensional (2D) flow, sediment transport, morphological changes of bed and banks in rivers (Shimizu & Takebayashi, 2011).

Basic flow of continuity equation in the numerical simulation is using governing equations as follows

$$\frac{\partial h}{\partial t} + \frac{\partial uh}{\partial x} + \frac{\partial vh}{\partial y} = 0 \quad (27)$$

where, h is the flow depth, u and v are the x and y components of depth-averaged velocity.

Momentum Conservation of x and y components is as follows.

$$\frac{\partial uh}{\partial t} + \frac{\partial uuh}{\partial x} + \frac{\partial uvh}{\partial y} = -gh \frac{\partial (h + z_b)}{\partial x} - \frac{\tau_x}{\rho} + \frac{1}{\rho} \left(\frac{\partial h \tau_{xx}}{\partial x} + \frac{\partial h \tau_{yx}}{\partial y} \right) \quad (28)$$

$$\frac{\partial vh}{\partial t} + \frac{\partial vuh}{\partial x} + \frac{\partial vvh}{\partial y} = -gh \frac{\partial (h + z_b)}{\partial y} - \frac{\tau_y}{\rho} + \frac{1}{\rho} \left(\frac{\partial h \tau_{xy}}{\partial x} + \frac{\partial h \tau_{yy}}{\partial y} \right) \quad (29)$$

where z_b is the river bed elevation, t is the time, g is the acceleration due to gravity, and ρ is the mass density of water. τ_{xx} , τ_{yy} , τ_{xy} and τ_{yx} are the depth averaged Reynolds stresses. τ_x and τ_y are the x and y components of the bed shear stress. Bed shear stress can be express as follows.

$$\frac{\tau_b}{\rho} = \frac{n^2 g}{h^{\frac{1}{3}}} (u^2 + v^2) \quad (30)$$

where τ_b is the bed shear stress and n is the Manning's roughness coefficient. For bed load conditions, non-dimensional bed load transport rate is proposed by Egashira et al., (1991). This equation is based on the constitutive relation of the solid particle–water mixture. The equation is expressed as follows.

$$q_{b*} = \frac{4}{15} \frac{K_1^2 K_2}{\sqrt{f_d + f_f}} \tau_*^2 \quad (31)$$

where q_{b*} is dimensionless bedload transport rate, τ_* is non dimensional bed shear stress (Shields parameter) K_1, K_2, f_d and f_f are specified theoretically as follows (Okada et al., 2016).

$$K_1 = \frac{1}{\cos \theta} \frac{1}{\tan \phi - \tan \theta} \quad (32)$$

$$K_2 = \frac{1}{c_s} \sqrt{1 - \frac{h_s}{h_t}} \quad (33)$$

$$f_d = k_d (1 - e^2) \left(\frac{\sigma}{\rho} \right) c_s^{-\frac{1}{3}} \quad (34)$$

$$f_f = k_f (1 - c_s)^{\frac{5}{3}} c_s^{-\frac{2}{3}} \quad (35)$$

where, θ is local bed slope, ϕ is internal friction angle, h_s is total depth, h_s is thickness of sediment layer, c_s is the average sediment concentration of the bedload layer, σ is the density of sediment, ρ is the density of water, $e=0.85$, $k_d=0.0828$ and $k_f=0.16$.

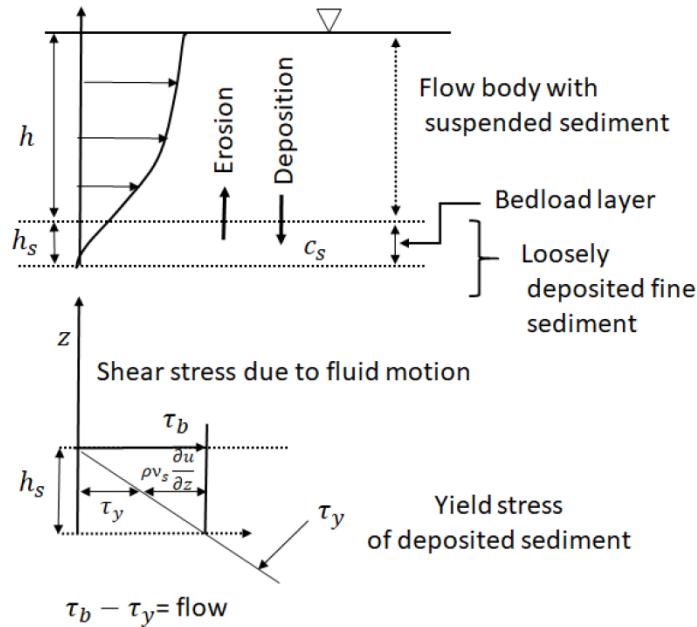


Figure 5.1 Schematic diagram of flow velocity at bed load layer and erosion velocity ((Egashira et al., 1997) (Ahmad, 2020))

In the case of suspended load, the particle entrainment from the bed layer occurs when the particle's upward velocity is greater than its fall velocity. The depth-integrated mass conservation equation of suspended sediment is defined as follows.

$$\frac{\partial \bar{c}h}{\partial t} + \frac{\partial r_2 \bar{c} \bar{u} h}{\partial x} + \frac{\partial r_1 \bar{c} \bar{v} h}{\partial y} = \frac{\partial}{\partial x} \left(h \epsilon_x \frac{\partial \bar{c}}{\partial x} \right) + \frac{\partial}{\partial y} \left(h \epsilon_y \frac{\partial \bar{c}}{\partial y} \right) + E - D \quad (36)$$

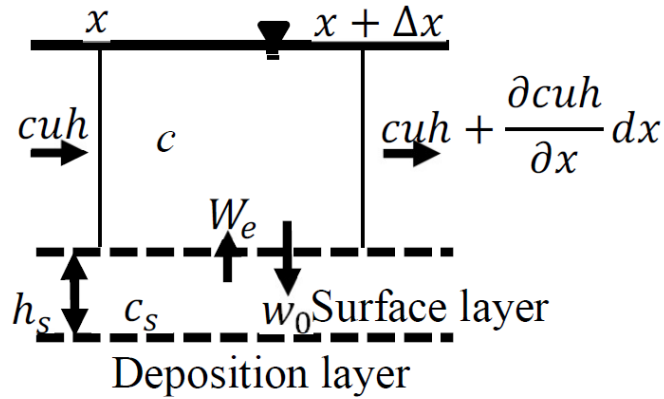


Figure 5.2 Particle Entrainment Model (Harada et al., 2019) (Modified by (Masbahul, 2020))

Where \bar{c} , \bar{u} and \bar{v} are the average values for sediment concentration, x-component of velocity, and y-component of velocity. ϵ_x and ϵ_y are the x and y-component of dispersion coefficient (similar to turbulent diffusion coefficient), h is the flow depth, E is the erosion rate of sediment, D is the deposition rate and r_1 and r_2 is the correction factor. Harada et al., (2019) proposed entrainment velocity equation for the computation of erosion term as follows

$$\frac{W_e}{V} = \frac{K}{R_{i*}}; R_{i*} = \frac{\Delta \rho g h}{\rho V^2}; K = 1.5 \times 10^{-3}; c_e = \frac{W_e}{w_0} c_s; V = \sqrt{u^2 + v^2} \quad (37)$$

Where $K = 1.5 \times 10^{-3}$, w_0 is the fall velocity, w_e is the entrainment velocity, c_s is the sediment concentration at the surface layer, c_e is the equivalent sediment concentration, h is the flow depth, and ρ is the mass density of water.

The differences from the original iRIC Nays2DH Solver and ICHARM Bank erosion model are bank line definition, flood plain inside computational domain, bank shifting stretchable grid and bank shifting based on erosion rate.

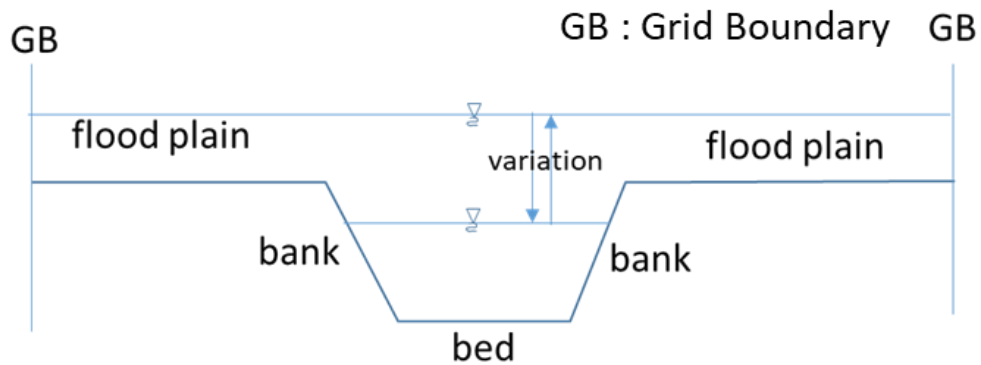


Figure 5.3 ICHARM Bank Erosion Model Computational Domain

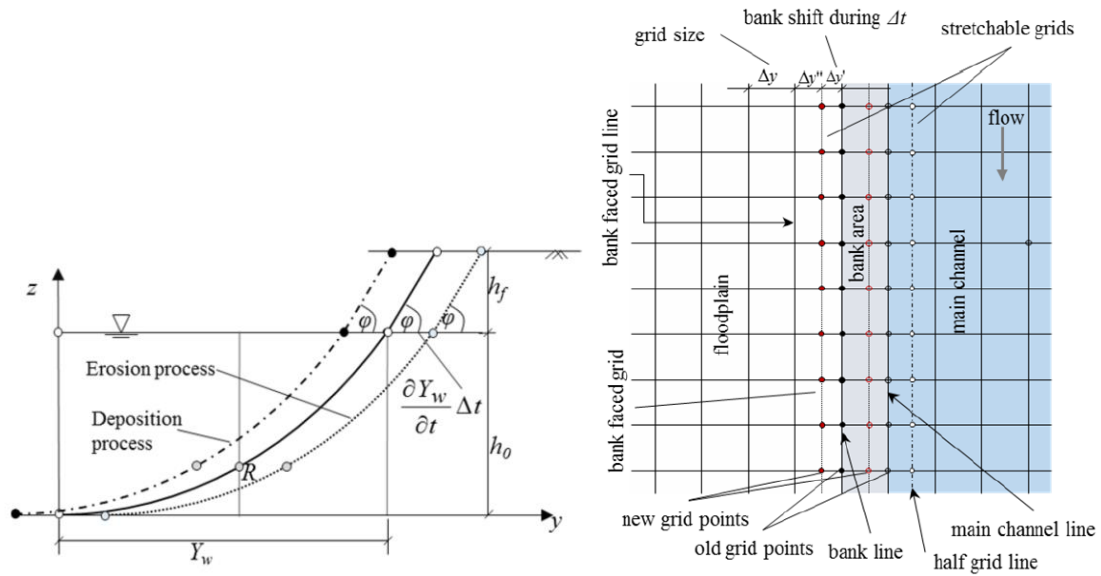


Figure 5.4 Schematic of Grid Updating by Stretchable Grid (Biswas et al., 2016)

Computational domain of ICHARM Bank Erosion Model is divided into bed, bank and flood plain (Figure 5.3). Results from calculation process on bed deformation will also lead the changing grid near bank and bank grid will be adjusted in stretchable grid process (Figure 5.4). The shape of the bank before and after the collapse of the bank maintains a slope that is equal to the angle of repose of the sediment particles (φ). Biswas et al., (2016) was developed this model for suspended material in Brahmaputra River where the riverbed and bank are composed of fine sand and silt). Bank slope was assumed to be constant during the calculation process because of uniform fine material condition in riverbed and bank.

However, there are still some limitations when the river bed-bank material condition is not uniform and contain cohesive material. In such condition, bank slope might be changed during the bank erosion process. In this model, bank slope in the model was assumed to be constant from the initial cross-sectional shape (from initial topography). In that case, it is

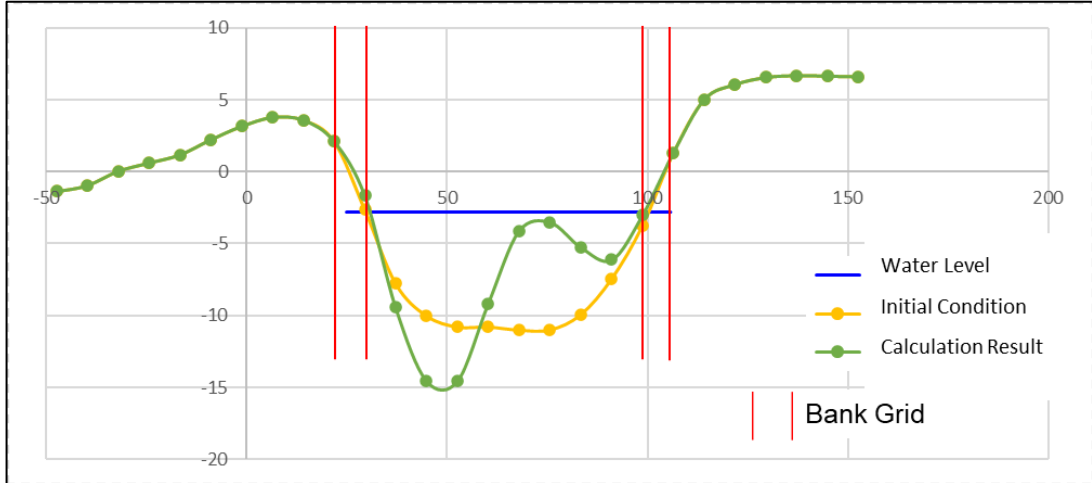


Figure 5.5 Bank Grid Treatment

necessary to prevent steep bank slope condition by preparing computational domain with sufficient number of grids. In real condition, riverbank might be narrow and bank grid in the model has to represent this condition. In order to solve this situation, trapezoidal channel was created by setting up grid domain with sufficient grid number. In the bank grid, steep bank slope treatment (Figure 5.5) was added to prevent steep slope which may lead to vertical bank grid and calculation failure. Checking calculation result periodically is also necessary to prevent steep slope condition.

In the numerical simulation for the Cimanuk River, bank grid was prepared as 7 m x 8.8 m (downstream of lower reach) and 7.5 m x 6 m (upstream of lower reach). These values were assumed to represent actual length of bank area in the Cimanuk River which is around 10 meter in cross-sectional direction.

In the case of uniform sediment particle size, the temporal change in river bed variation can be evaluated by applying continuity of mass condition of bed sediment as follows

$$\frac{\partial z_b}{\partial t} + \frac{1}{\lambda - 1} \left(\frac{\partial q_{bx}}{\partial x} + \frac{\partial q_{by}}{\partial y} + E_s - D_s \right) = 0 \quad (38)$$

z_b is the river bed elevation, q_{bx} and q_{by} are the components of bedload transport rate in the x and y directions. E_s is the erosion rate and D_s is the sediment deposition rate. Related to bank erosion process, temporal change of riverbed variation is evaluated by equation (38). If $\frac{\partial z_b}{\partial t}$ is less than zero 0, bank shifting is computed related to erosion rate as $\frac{\partial B}{\partial t}$, where B is the channel width.

In a suspended sediment-dominated river, the riverbed evolution and bank shifting are controlled by the erosion and deposition of the suspended sediment (Biswas et al., 2016). They also explained that the proposed model (Biswas et al., 2016) can be extended to evaluate the bank shifting process in case of curved channel.

Numerical simulation was conducted to understand bank erosion trend, bed-bank material interaction and how the channel centerline changes. Bank erosion rate will change based on SC percentage and this simulation also tried several cases of different SC percentage to evaluate bank erosion trend. In this simulation, the results will consist bank shifting value and centerline movement which will be validated with observation data.

The value of erosion rate was determined based on the cross-sectional data in the Cimanuk River (CS-52) which is located in 73 km from downstream. This location was selected because it is located in the middle of target area and could represent general condition of Cimanuk River. By assuming several values of SC% of river bank, excess shear stress and erosion rate was calculated by using (20) to(23). The result could be shown in Figure 5.6. The detail boundary condition of numerical simulation explained in table Table 5-1.

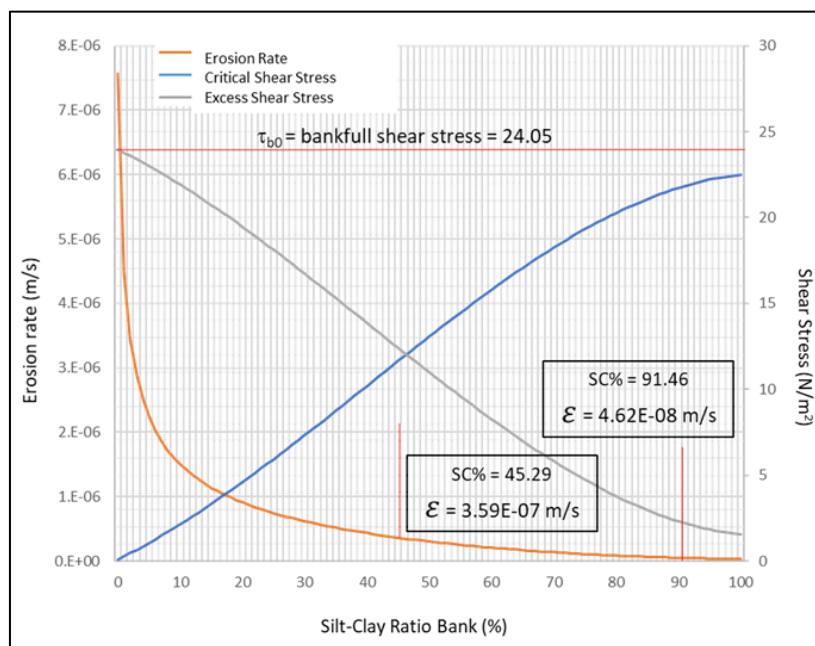


Figure 5.6 Erosion Rate Values for Numerical Simulation

Table 5-1. Boundary Condition of Cimanuk River Bank Erosion Simulation

	Case Type 2a Downstream of Lower Reach			Case Type 2b Upstream of Lower Reach		
Condition	Case-2a-1 (actual)	Case-2a-2	Case-2a-3	Case-2b-1	Case-2b-2	Case-2b-3 (actual)
Distance from Downstream (km)	55 km	55 km	55 km	75 km	75 km	75 km
Mesh Size	7 x 8.8 m	7 x 8.8 m	7 x 8.8 m	7.5 x 6 m	7.5 x 6 m	7.5 x 6 m

	Case Type 2a Downstream of Lower Reach			Case Type 2b Upstream of Lower Reach		
Condition	Case-2a-1 (actual)	Case-2a-2	Case-2a-3	Case-2b-1	Case-2b-2	Case-2b-3 (actual)
Discharge (m ³ /s)	600	600	600	600	600	600
Bed Material (mm)	0.05	0.25	0.05	0.25	0.05	0.25
SC Bank %	91.5%	91.5%	45.3%	91.5%	91.5%	45.3%
Erosion rate (m/s)	4.62E-08	4.62E-08	3.59E-07	4.62E-08	4.62E-08	3.59E-07
n manning coefficient	0.03	0.03	0.03	0.03	0.03	0.03

STANDAR DATA TMA MAKSIMUM SIAGA BANJIR
WILAYAH KERJA BALAI BESAR WILAYAH SUNGAI CIMANUK - CISANGGARUNG

LOKASI	WASPADA (mtr DPL)	SIAGA (mtr DPL)	AWAS (mtr DPL)	LOKASI	SIAPA (mtr DPL)	SIAGA (mtr DPL)	AWAS (mtr DPL)
1. S. CIPELES				7. S. KUMPUL KUISTA			
1. DU. Warung Peti	44.25	44.50	45.00	1. DU. Kaliwedi	3.85	4.10	4.60
2. S. CILUTUNG				2. BK. Kumpul Kuista	1.75	2.00	2.50
1. BD. Kamun	37.50	38.50	39.50	8. S. WINONG			
3. S. CIMANUK				1. BD. Gandasari	4.96	5.20	5.70
1. BD. Copong	-	3.125	4.100	2. BK. Winong	2.00	2.10	2.20
2. DU. Monjot	27.50	28.50	29.50	9. S. SIGRANALA			
3. BD. Rentang TMA	22.30	22.55	23.00	1. BD. Pegagan	1.80	1.90	2.00
4. BD. Rentang Debit m ³	600.00	900.00	1,200.00	2. BK. Sigranala	1.50	2.00	2.50
5. BD. Bangkir	5.70	5.95	6.45	10. S. JAMBLANG			
6. BK. Waledan	1.50	2.00	2.50	1. BK. Jambalang	2.80	3.10	3.50
7. BK. Brondong	1.50	1.70	2.00	11. S. CISANGGARUNG			
4. S. CIPANAS				1. BD. Cikeusik	3.00	3.50	4.00
1. BD. Sumur Watu	19.25	19.50	19.75	2. DU. Ciledug	8.30	8.60	9.10
2. BD. HBM Cipanas	4.48	4.68	5.18	3. BK. Tawang Sari	2.70	3.00	3.20
3. BK. Cipanas	1.90	2.00	2.10	12. S. CIJURAI			
5. S. PANGKALAN				1. BD. Seseupan	2.70	3.50	4.00
1. DU. Pangauban	2.75	3.00	3.50	13. S. BABAKAN			
2. BK. Pangkalan	1.50	1.70	2.00	1. BD. Cisadap	4.50	4.60	4.80
6. S. CIWARINGIN				14. S. KABUYUTAN			
1. DU. Gegesik	5.55	5.90	6.30	1. BD. Nambo	3.80	4.10	4.30
2. BD. Sigondang	3.00	3.50	4.00	15. S. CIJANGKELOK			
3. BK. Ciwaringin	2.00	2.50	3.00	1. BD. Cibendung	6.00	6.50	7.10

Figure 5.7. Flood Alert Level Cimanuk River at Rentang Weir (Ministry of Public Works and Housing, 2021)

Discharge of 600 m³/s has been selected to represent the bankfull and annual flood discharge based on the reasons as follows. Firstly, alert level in Rentang Weir had been decided as 3 level of discharge 600 m³/s, 900 m³/s and 1.200 m³/s. 600 m³/s can be assumed to be near to the bankfull discharge in some locations (see cross-sectional and discharge sample at Figure 3.27). If the discharge is 1200 m³/s, overflows occurs in some places. Therefore assuming 600 m³/s is suitable to represent bankfull discharge.

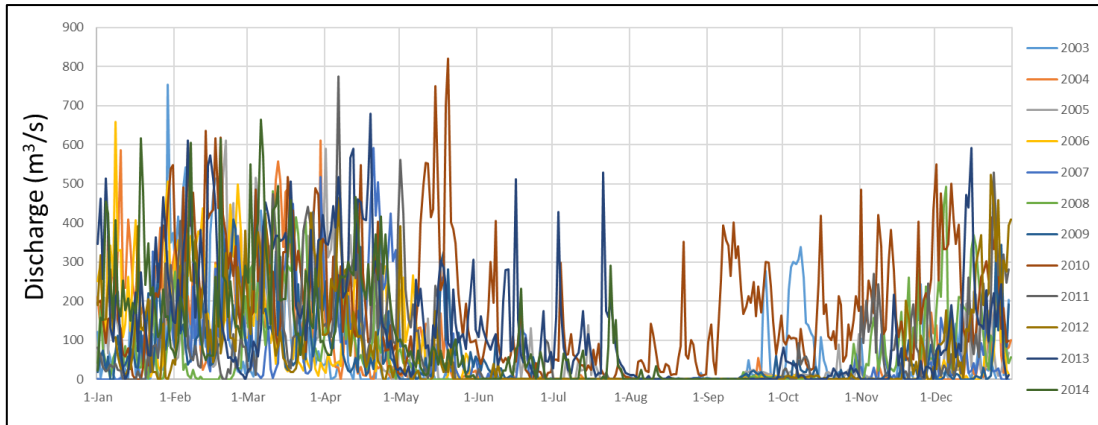


Figure 5.8. Daily Average Discharge at Rentang Weir (2003-2014)

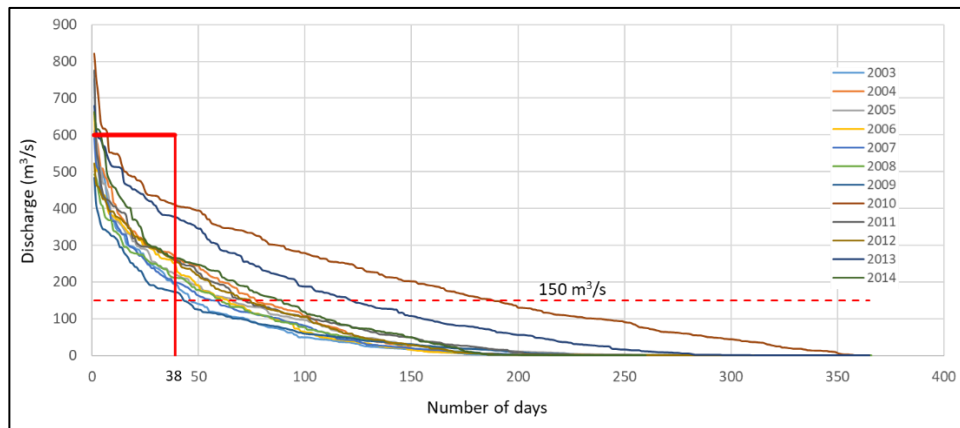


Figure 5.9. Flow Duration Curve at Rentang Weir (2003-2014)

Next explanation related to the annual flood discharge is as follows by observing yearly discharge at Rentang Weir. From Figure 5.8, it is necessary to analyze discharge that represents annual flood discharge and has capability to change bed morphology. Kallio (2010) explained that lower threshold might be established at water level that correspond to about 25% of the 2-year discharge. In this study, 25% threshold will be used based on 1st level alert discharge ($600 \text{ m}^3/\text{s}$). Then the discharge becomes $150 \text{ m}^3/\text{s}$. Flow duration curve can be shown in Figure 5.9.

Figure 5.9 shows flow duration curves from 2003 to 2014. 38 days of constant $600 \text{ m}^3/\text{s}$ discharge were selected based on the analyzed results of flow duration curve compared with total discharge and number of days summarized in Table 5-2. In this analysis, total water volume that flows when the discharge is more than $150 \text{ m}^3/\text{s}$ is calculated as (2) in Table 5-2. The total volume is divided by total days when discharge is more than $150 \text{ m}^3/\text{s}$. Finally, the unit is adjusted to be m^3/s ((1) in Table 5-2).

Table 5-2. Discharge Analysis for Cimanuk River Simulation

Year	Total Days Exceeded 150 m ³ /s (days) (1)	Total Annual Discharge that exceed 150 m ³ /s (Daily Mean Discharge (m ³ /s) x (1) days) (2)	Number of Days for 600 m ³ /s (days) (column (2) / 600 m ³ /s) (3)
2003	37	13,815.65	23.03
2004	60	22,076.47	36.79
2005	45	17,819.84	29.70
2006	48	17,803.13	29.67
2007	37	14,926.90	24.88
2008	44	15,621.28	26.04
2009	25	10,783.85	17.97
2010	152	58,753.97	97.92
2011	56	20,534.61	34.22
2012	55	20,217.39	33.70
2013	96	38,388.49	63.98
2014	67	25,512.38	42.52
Average	60.16	23,021.16	38.37

5.2 Results of Numerical Simulation

a) Case Cimanuk L Type 2a-1 SC Bank 91.5% Bed Material 0.05mm

Numerical simulation result for Case 2a-1 with SC Bank 91.5% and bed material 0.05mm is shown in Figure 5.10. Values of bank shifting are various in this reach with maximum value around 0.0712 m (Figure 5.10 (b)), while bank shifting in target cross-section is 0.018 m. Less changing of bed morphological trend (Figure 5.10 (c)) also can be detected and channel stability can be assumed with this condition.

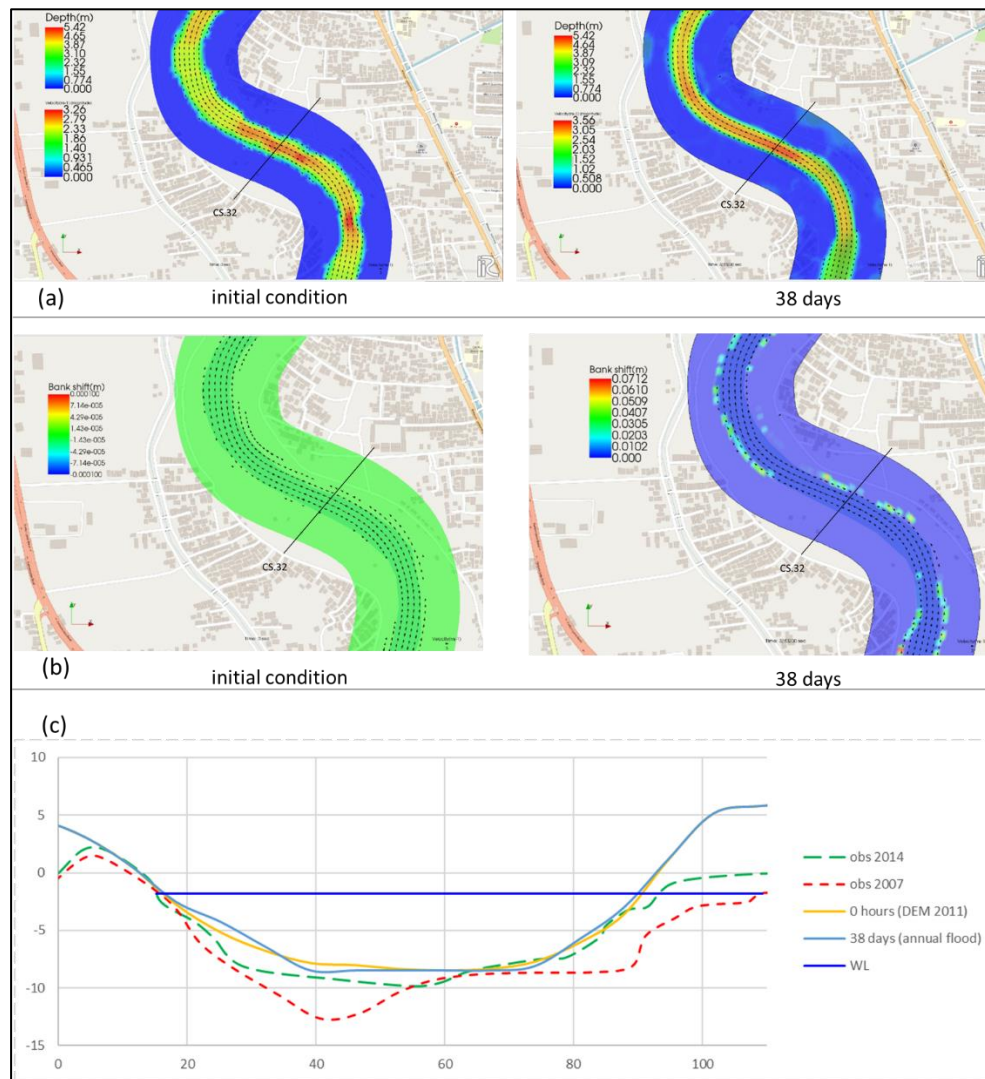


Figure 5.10. Numerical Simulation Result for Case 2a-1 SC Bank 91.46% Bed Material 0.05mm (a) Depth and Velocity Magnitude (b) Bank Shifting Distribution (c) Cross-Sectional Shape

b) Case Cimanuk L Type 2a-2 SC Bank 91.5% Bed Material 0.25mm

Numerical simulation result for Case 2a-2 with SC Bank 91.5% and bed material 0.25mm is shown in Figure 5.11. Values of bank shifting are various in this reach with maximum value around 0.0594 cm (Figure 5.11 (b)), while bank shifting in target cross-section is 0.018 m. Much less changing of bed morphological trend due to coarser bed material (Figure 5.11 (c)) also can be detected and channel stability can be assumed with this condition.

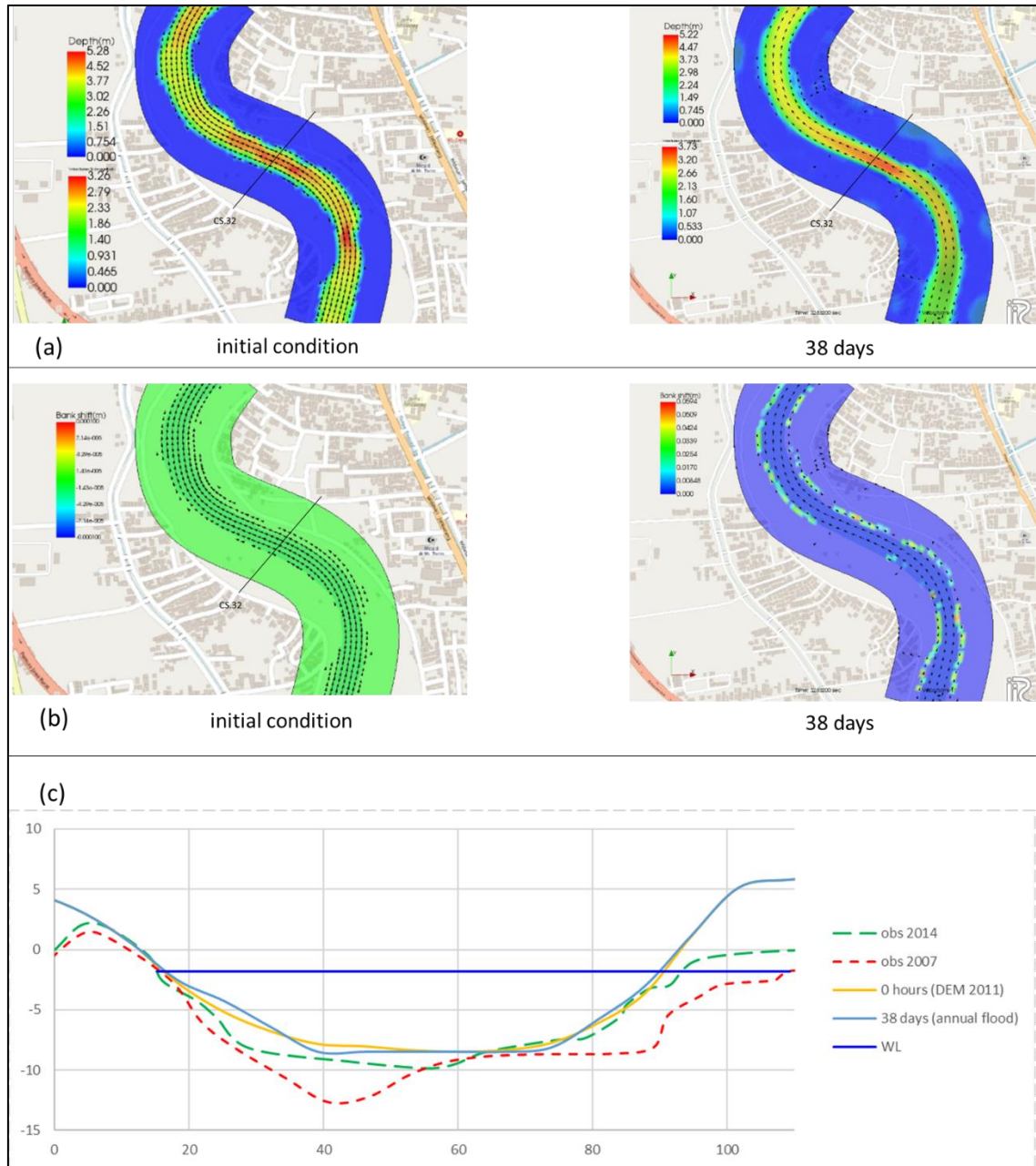


Figure 5.11. Numerical Simulation Result for Case 2a-2 SC Bank 91.46% Bed Material 0.25mm (a) Depth and Velocity Magnitude (b) Bank Shifting Distribution (c) Cross-Sectional Shape

c) Case Cimanuk L Type 2a-3 SC Bank 45.3% Bed Material 0.05mm

Numerical simulation result for Case 2a-3 with SC Bank 45.3% and bed material 0.05mm show in Figure 5.12. Values of bank shifting are various in this reach with maximum value around 0.790 m (Figure 5.12 (b)), while bank shifting in target cross-section is 0.219 m. Less changing of bed morphological trend (Figure 5.12 (c)) also can be detected and channel stability can be assumed with this condition.

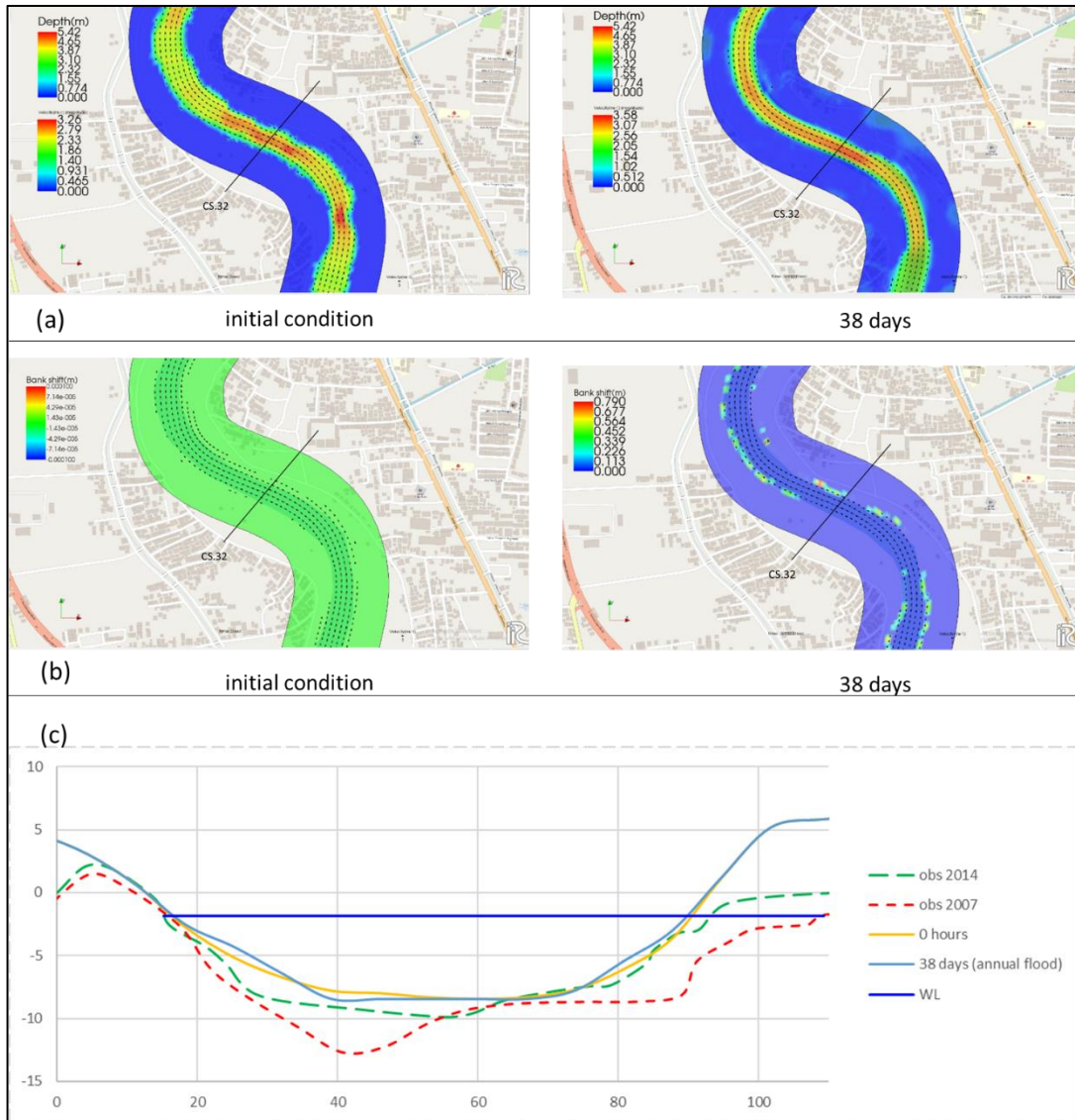


Figure 5.12. Numerical Simulation Result for Case 2a-3 SC Bank 45.29% Bed Material 0.25mm (a) Depth and Velocity Magnitude (b) Bank Shifting Distribution (c) Cross-Sectional Shape

d) Case Cimanuk U Type 2b-1 SC Bank 91.5% Bed Material 0.25mm

Numerical simulation result for Case 2b-1 with SC Bank 91.5% and bed material 0.25mm is shown in Figure 5.13. Channel shape change is more active compared to Case-2a (downstream of lower reach). Values of bank shifting are various in this reach with maximum value around 0.652 m (Figure 5.13 (b)), while bank shifting in target cross-section is 0.014 m. Active change of bed morphology trend (Figure 5.13(c)) also can be detected and channel instability can be assumed with this condition.

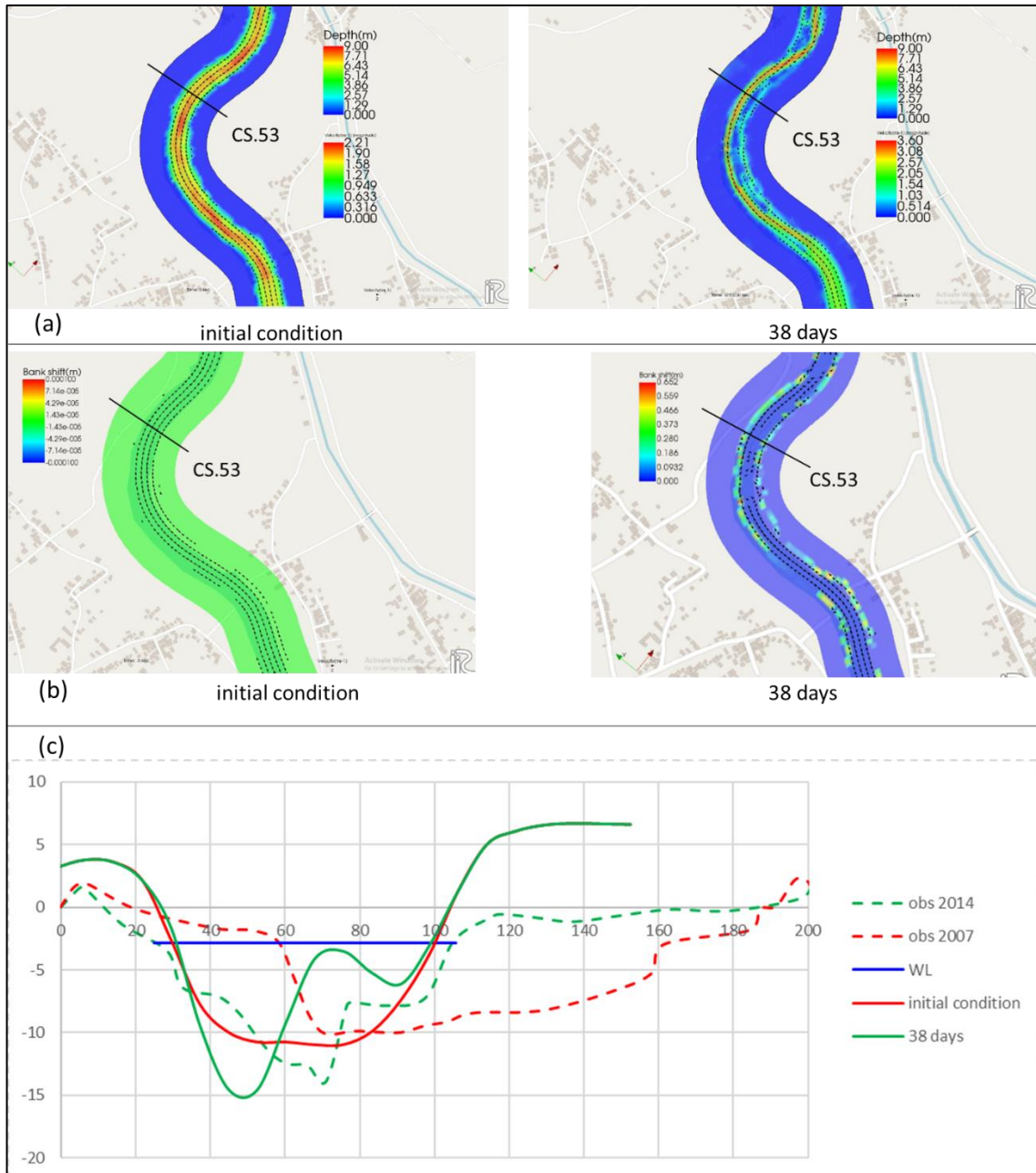


Figure 5.13. Numerical Simulation Result for Case 2b-1 SC Bank 91.46% Bed Material 0.25mm (a) Depth and Velocity Magnitude (b) Bank Shifting Distribution (c) Cross-Sectional Shape

e) Case Cimanuk U Type 2b-2 SC Bank 91.46% Bed Material 0.05mm

Numerical simulation result for Case 2b-2 with SC Bank 91.46% and bed material 0.05mm is shown in Figure 5.14. In this case also, channel shape change is more active compared to Case-2a (downstream of lower reach). Values of bank shifting are various in this reach with maximum value around 0.672 m (Figure 5.14 (b)), while bank shifting in target cross-section is 0.042 m. Active change of bed morphology (Figure 5.14 (c)) also can be detected and more active than case 2b-1 due to finer material.

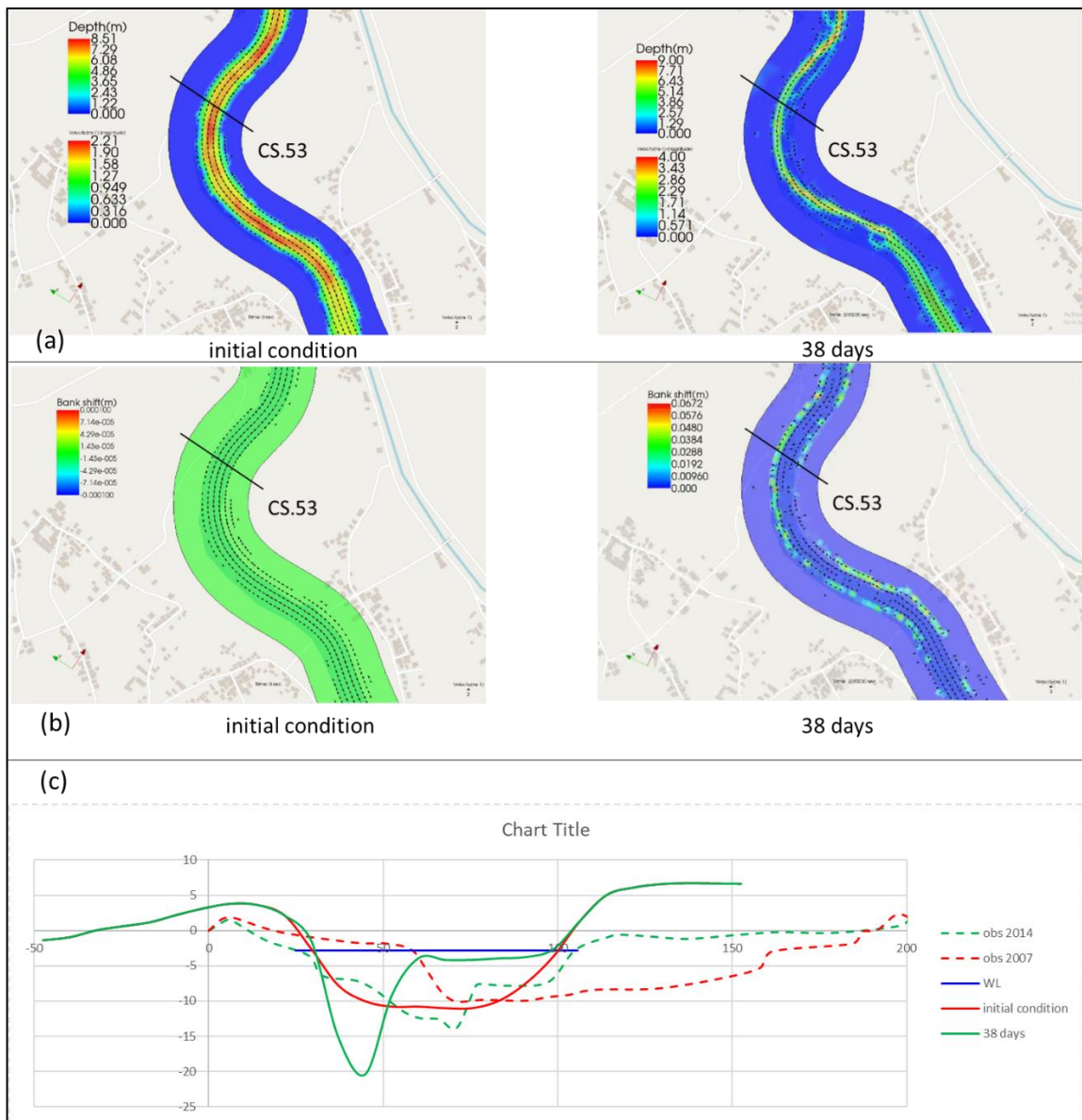


Figure 5.14. Numerical Simulation Result for Case 2b-2 SC Bank 91.46% Bed Material 0.05mm (a) Depth and Velocity Magnitude (b) Bank Shifting Distribution (c) Cross-Sectional Shape

f) Case Cimanuk U Type 2b-3 SC Bank 45.29% Bed Material 0.25mm

Numerical simulation result for Case 2b-3 with SC Bank 45.29% and bed material 0.25mm is show in Figure 5.15. Values of bank shifting are various in this reach with maximum value around 0.652 m (Figure 5.15 (b)), while bank shifting in target cross-section is 0.320 m. Instability condition in this case is the most active (Figure 5.15(c)) compared to all cases. Double channel was found and it might be caused by active bed deformation process and bank erosion process. Bar was formed, but due to active bed deformation stable clear bar difficult to be found.

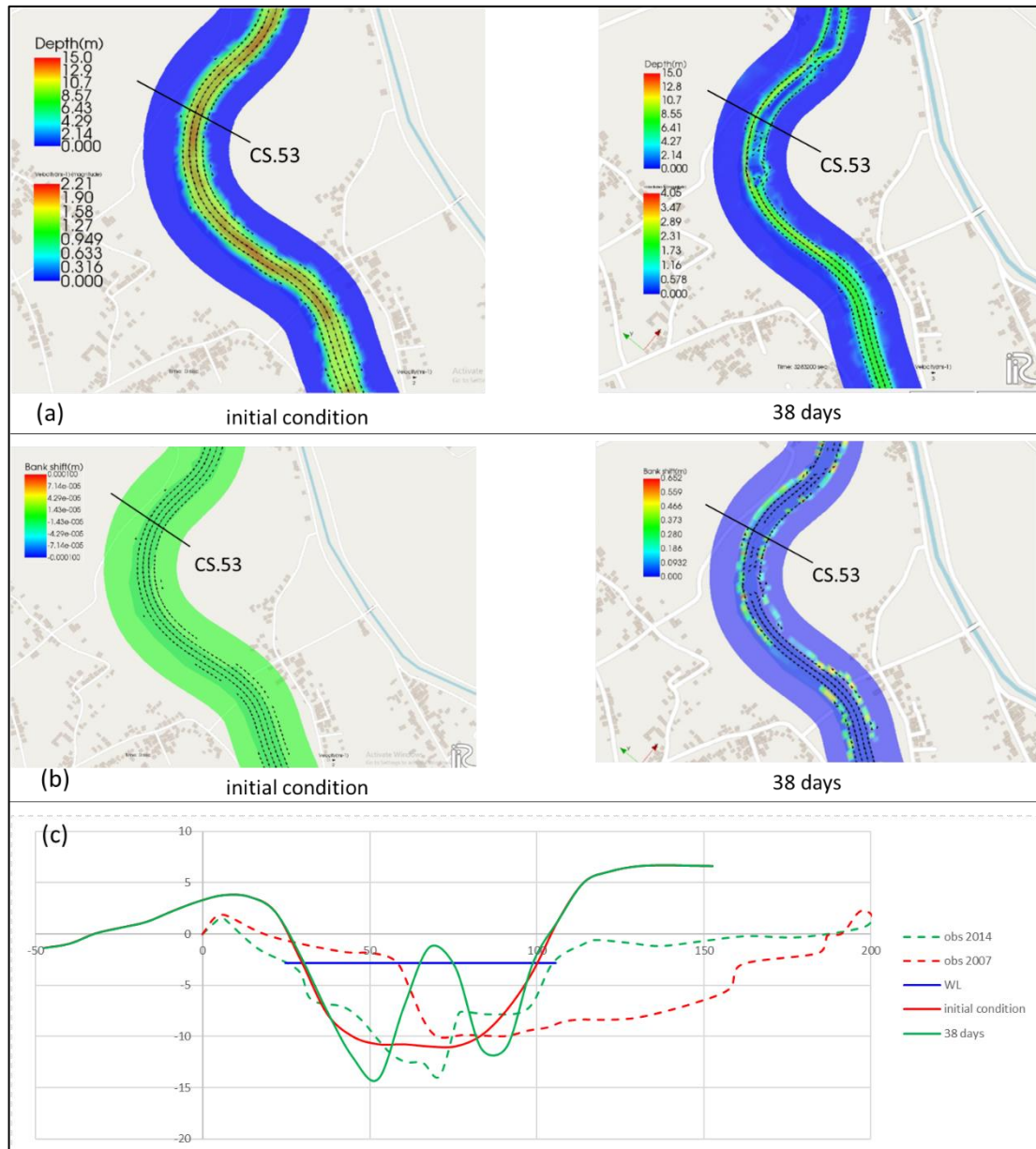


Figure 5.15. Numerical Simulation Result for Case 2b-3 SC Bank 45.29% Bed Material 0.25mm (a) Depth and Velocity Magnitude (b) Bank Shifting Distribution (c) Cross-Sectional Shape

5.3 Bank Shifting, Centerline Movement and Aspect Ratio

Numerical simulation results related to bank shifting and centerline movement could be summarized in Table 5-3. From this summary, it can be explained that Case-2b centerline movement is active compared to Case-2a, but bed deformation process shows overestimated result. Case 2a-1 shows reliable bed deformation process that have similar trend with observation data, even though bank shifting and centerline movement values are lower than observation value. However, Case 2b-3 shows remarkably underestimated result. This is the most active cross-sectional change and double channel was found. The reason is considered that centerline movement is not affected by bankfull discharge but maximum discharge especially in such steep channel.

Table 5-3. Bank Shifting and Centerline Movement Summary

	SC% Bank	Bed Material (mm)	Observation			Simulation		
			Centerline movement (m/year)	Bank shift (m/year)		Bank shift (m/year)		Centerline movement (m/year)
				Left	Right	Left	Right	
Case Type 2a								
Case 2a-1 (actual)	91.46	0.05	← 0.5	N/A	← 0.5	→ 5.52E-06	← 0.018	← 0.018
Case-2a-2	91.46	0.25				→ 2.8E-05	← 0.018	← 0.018
Case-2a-3	45.29	0.05				→ 7.01E-05	← 0.219	← 0.219
Case Type 2b								
Case 2b-1	91.46	0.25				← 0.005	← 0.009	← 0.014
Case-2b-2	91.46	0.05				← 0.037	← 0.005	← 0.042
Case-2b-3 (actual)	45.29	0.25	← 6.47	← 4.88	← 6.24	← 0.230	← 0.090	← 0.320

a) Type 2a Downstream of Lower Reach Segment II-2

Cross-sectional parameters and aspect ratio from simulation for each type also could be summarized in Table 5-4. From those results, several things can be explained. If Case 2a-1 and Case 2a-2 is compared, it can be identified that Case 2a-2 is deeper and slightly wider. In Case 2a-1 bed material and bank material is similar, hence the suspended 0.05mm (cohesive material) from the bed can form the bank. In this condition, width tend to be narrower. On

the other hand, bed material in Case 2a-2 cannot form the cohesive bank, and width tends to be wider. In the simulation, depth of Case2a-2 became deeper maybe because of the setting of boundary condition. As a result, aspect ratio in Case 2a-2 became smaller than Case 2a-1 but it is not significant difference.

Comparison between Case 2a-1 and Case 2a-3 shows that Case 2a-3 is shallower and slightly wider. In 2a-3 bank is eroded and width becomes wider due to low silt-clay percentage in the bank. Important point is that the sediment supply from the bank makes the channel shallower. Therefore, low silt-clay percentages in the bank may increase aspect ratio. If Type1 river and Type 2a river are compared, cohesive bed and bank (blue color plot) can be found in both types. However, as it was explained in previous chapter, silt-clay percentages in the Cimanuk River (Type2a) is smaller than the Ciliwung River (Type1). This condition implies that Type1 channel becomes Type2a when silt-clay percentages decreases. But the difference of sediment size distribution between the Ciliwung River (Type1) and Sangkae River (Type2a) or the Naka River (Type2a) is not clear. The reason should be examined in future including the check of measurement accuracy.

Table 5-4. Cross-Sectional Parameters and Aspect Ratio Summary for Case Type 2a

Case 2a-1	Obs 2007	Obs 2014	T = 0 hour	T = 1 hours	T = 1 day	T = 12 days	T = 23 days	T = 38 days
x-section area (m.sq.)	396.22	396.22	355.68	367.83	361.81	353.39	353.24	353.24
width (m)	76.75	76.75	73.73	73.01	72.93	72.65	72.65	72.65
mean depth (m)	5.16	5.16	4.82	5.04	4.96	4.86	4.86	4.86
Case 2a-2	Obs 2007	Obs 2014	T = 0 hour	T = 1 hours	T = 1 day	T = 12 days	T = 23 days	T = 38 days
x-section area (m.sq.)	396.22	396.22	355.68	364.16	367.27	362.56	361.73	361.12
width (m)	76.75	76.75	73.73	73.47	73.23	73.00	72.98	72.97
mean depth (m)	5.16	5.16	4.82	4.96	5.02	4.97	4.96	4.95
Case 2a-3	Obs 2007	Obs 2014	T = 0 hour	T = 1 hours	T = 1 day	T = 12 days	T = 23 days	T = 38 days
x-section area (m.sq.)	396.22	396.22	355.68	367.83	361.68	351.24	350.73	348.90
width (m)	76.75	76.75	73.73	73.01	72.94	72.67	72.67	72.66
mean depth (m)	5.16	5.16	4.82	5.04	4.96	4.83	4.83	4.80
Aspect Ratio	Obs 2007	Obs 2014	T = 0 hour	T = 1 hours	T = 1 day	T = 12 days	T = 23 days	T = 38 days
Case 2a-1	14.87	15.13	15.28	14.49	14.70	14.94	14.94	14.94
Case 2a-2	14.87	15.13	15.28	14.82	14.60	14.70	14.73	14.74
Case 2a-3	14.87	15.13	15.28	14.49	14.71	15.03	15.05	15.13

Table 5-5. Summary for Case Type 2a

	Case Type 2a Downstream of Lower Reach (Seg2-2)		
Condition	Case-2a-1 (actual)	Case-2a-2	Case-2a-3
Bed Material (mm)	0.05	0.25	0.05
SC Bank %	91.5%	91.5%	45.3%
Initial Width (m)	73.73	73.73	73.73
Final Width (m)	72.65	72.97	72.66
Initial Mean Depth (m)	4.82	4.82	4.82
Final Mean Depth (m)	4.86	4.95	4.80
Initial Aspect Ratio	15.28	15.28	15.28
Final Aspect Ratio	14.94	14.74	15.13

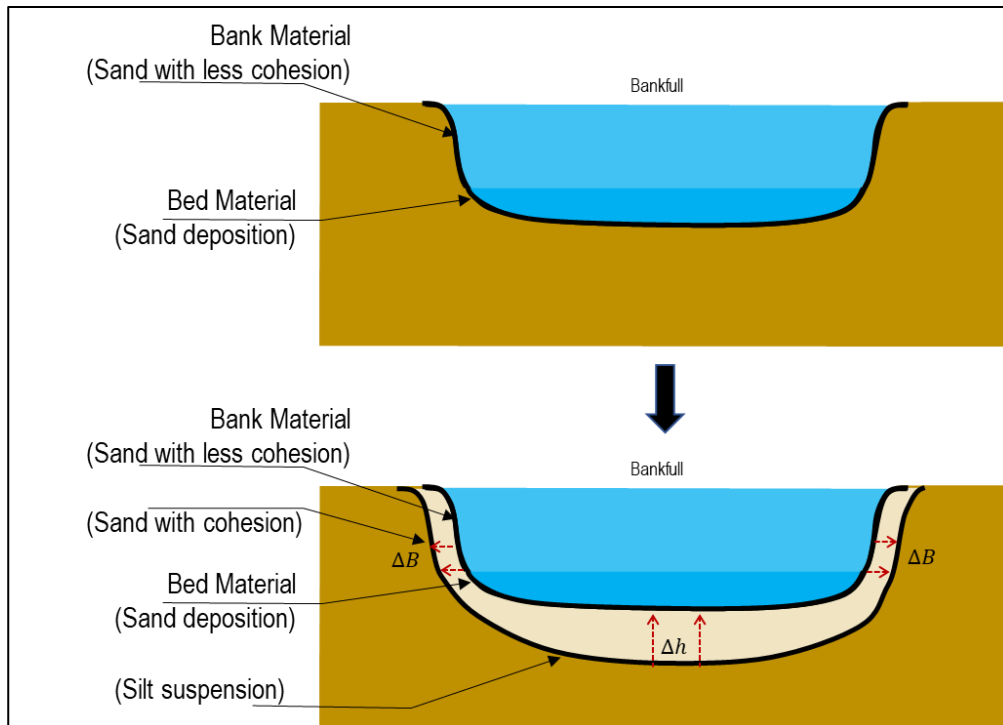


Figure 5.16. Forming Mechanism Type 2a Downstream of Lower Reach Segment II-2

As shown in Figure 5.16, if the bank cohesion becomes less (Case 2a-1 compared to Case2a-3), then aspect ratio become larger. It means that width becomes wider because it is

easily eroded and depth become shallower which formed by eroded material from the bank. Related to the proposed classification, Type1 may become Type 2a if bank is less cohesive.

b) Type 2b Upstream of Lower Reach Segment II-1

Cross-sectional parameters and aspect ratio from simulation for each type also could be summarized in Table 5-6 and Table 5-7. From those results, several things can be explained. If case2a and 2b is compared, aspect ratio in case 2b tends to be smaller than 2a because the channel in case 2b is narrower while depth is diverse. It is considered that aspect ratio in upper reach tends to be smaller than in lower reach, but the reason is considered to be scroll bar formation. As shown in Figure 5.13 to Figure 5.15, bar is formed in Case 2b due to high stream power and both width and depth are unstable temporally compared with 2a (see Table 5-6). Potential specific stream power of each numerical cases is plotted in Figure 5.17. As this figure shows case 2b has higher stream power compared to case 2a. Forming process of Type2b is also related to the imbalance of bed and bank material. The simulation could not represent aspect ratio well, but bank shifting and bed deformation of Type 2b were represented by simulation well.

Compared with Type3, braided and meandering scroll and chutes are formed in narrower channel of Case 2b and it may make case 2b more sinuous as is shown in Figure 4.28. Simulation result in type 2b-3 (actual condition) is not same with the observation result and stable clear bar is not found. This phenomenon which related to bar formation should be investigated in future.

Table 5-6. Cross-Sectional Parameters and Aspect Ratio Summary for Case Type 2b

Case 2b-1	Obs 2007	Obs 2014	T = 0 hour	T = 1 hours	T = 1 day	T = 12 days	T = 23 days	T = 38 days
x-section area (m.sq.)	532.54	532.54	431.57	402.91	384.80	317.99	328.93	333.43
width (m)	103.09	103.09	70.23	71.57	72.32	68.69	68.27	68.32
mean depth (m)	5.17	5.17	6.15	5.63	5.32	4.63	4.82	4.88
Case 2b-2	Obs 2007	Obs 2014	T = 0 hour	T = 1 hours	T = 1 day	T = 12 days	T = 23 days	T = 38 days
x-section area (m.sq.)	532.54	532.54	431.57	409.35	333.02	370.33	369.95	315.73
width (m)	103.09	103.09	70.23	70.06	69.67	68.04	69.64	67.33
mean depth (m)	5.17	5.17	6.15	5.84	4.78	5.44	5.31	4.69
Case 2b-2	Obs 2007	Obs 2014	T = 0 hour	T = 1 hours	T = 1 day	T = 12 days	T = 23 days	T = 38 days
x-section area (m.sq.)	532.54	532.54	431.57	404.24	378.92	308.09	333.84	345.78
width (m)	103.09	103.09	70.23	70.23	72.41	65.06	63.86	60.17
mean depth (m)	5.17	5.17	6.15	5.76	5.23	4.74	5.23	5.75
Aspect Ratio	Obs 2007	Obs 2014	T = 0 hour	T = 1 hours	T = 1 day	T = 12 days	T = 23 days	T = 38 days
Case 2b-1	<i>19.96</i>	<i>14.50</i>	<i>11.43</i>	<i>12.71</i>	<i>13.59</i>	<i>14.84</i>	<i>14.17</i>	<i>14.00</i>
Case 2b-2	<i>19.96</i>	<i>14.50</i>	<i>11.43</i>	<i>11.99</i>	<i>14.58</i>	<i>12.50</i>	<i>13.11</i>	<i>14.36</i>
Case 2b-3	<i>19.96</i>	<i>14.50</i>	<i>11.43</i>	<i>12.20</i>	<i>13.84</i>	<i>13.74</i>	<i>12.22</i>	<i>10.47</i>

Table 5-7. Summary for Case Type 2b

Condition	Case Type 2b Upstream of Lower Reach (Seg2-1)		
	Case-2b-1	Case-2b-2	Case-2b-3 (actual)
Bed Material (mm)	0.25	0.05	0.25
SC Bank %	91.5%	91.5%	45.3%
Initial Width (m)	70.23	70.23	70.23
Final Width (m)	68.32	67.33	60.17
Initial Mean Depth (m)	6.15	6.15	6.15
Final Mean Depth (m)	4.88	4.69	5.75
Initial Aspect Ratio	11.43	11.43	11.43
Final Aspect Ratio	14.00	14.36	10.47

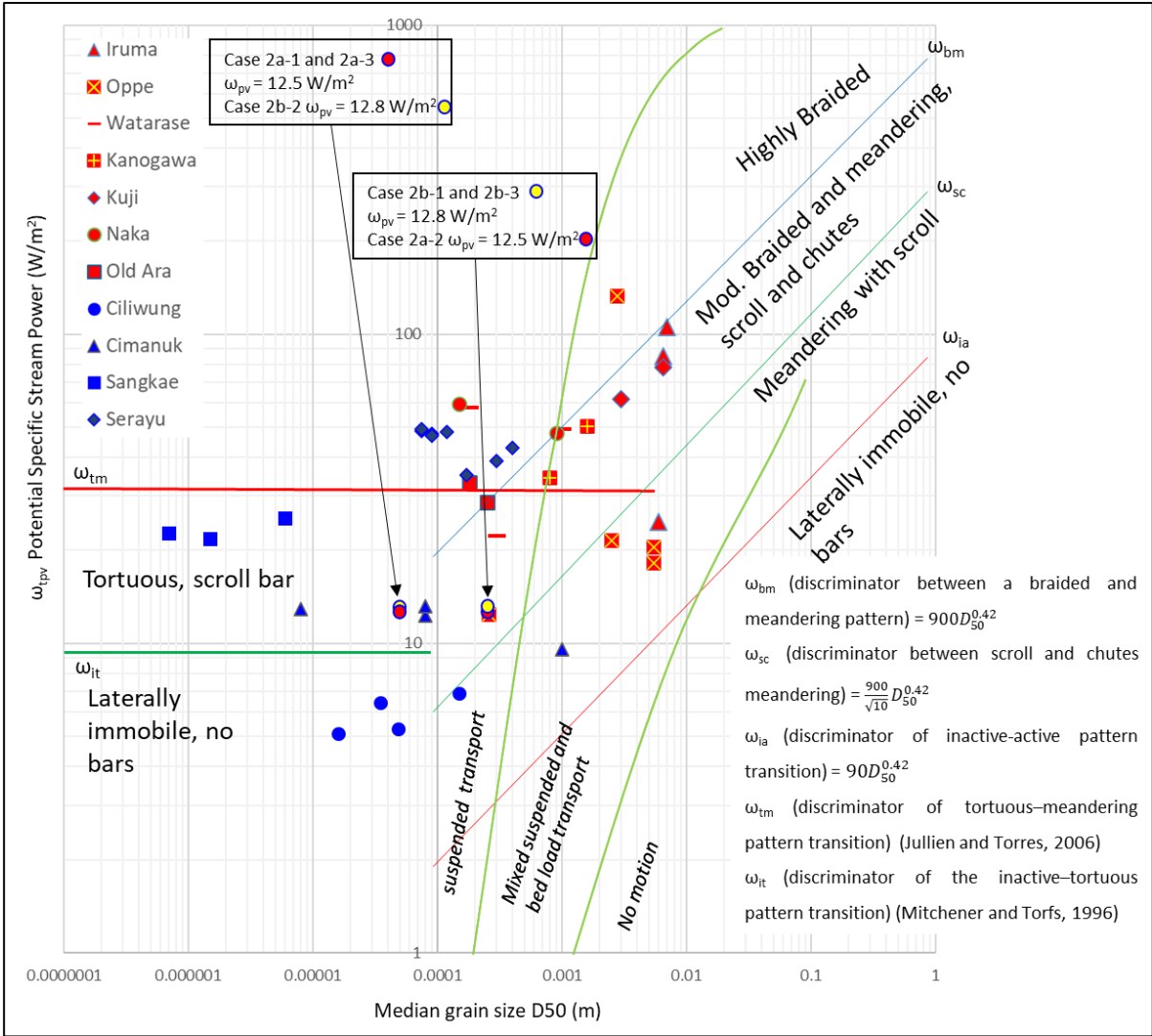


Figure 5.17. Potential Specific Stream Power of Numerical Simulation Cases

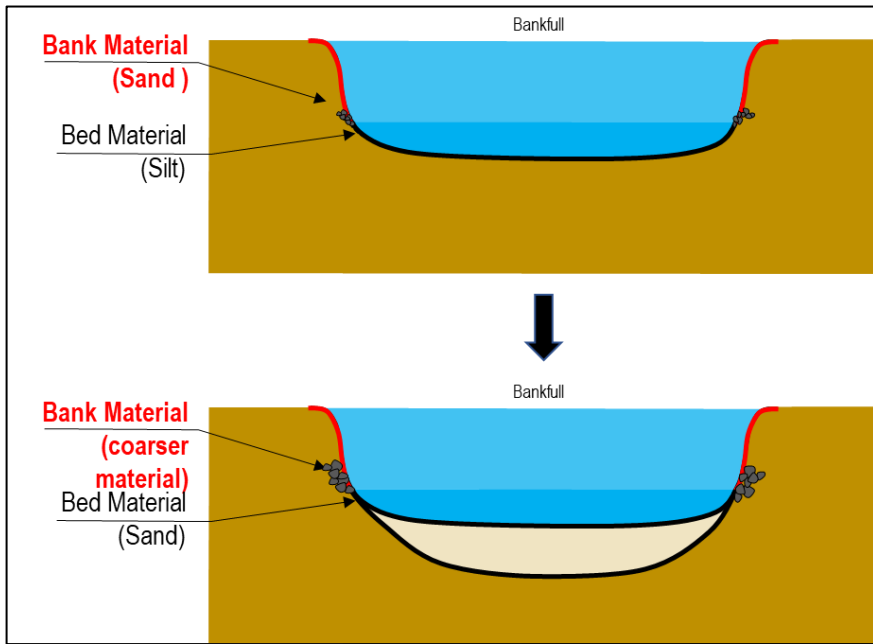


Figure 5.18. Forming Mechanism Type 2b Downstream of Lower Reach Segment II-1

As shown in Figure 5.18, Type 3 may become Type 2b by increasing depth when coarser material is contained in the river bed. It might be caused by coarser material at bank-toe stabilized the riverbank and suspended sand forms bank (Santoso, 2017). In the numerical simulation, cross-sectional shape in Case2b-3 which is close to actual condition was quite unstable due to bar formation. Actually, analysis on stream power implies scroll bar is formed in the channel. If the bank is more cohesive (Case 2b-1 compared to Case 2b-3), width is more stable, and depth become shallower. As a result, aspect ratio become larger. Similar condition also appears when bed material is finer (Case 2b-2 compared to Case 2b-3). It is similar with previous comparison, but this case can explain that finer material also easily deposited and depth is slightly shallower than Case 2b-1. Both cases were affected by deposition in the inner bank, as well as channel deepening in the outer bank. Channel deepening in both cases does not have significant effect on aspect ratio, because depth for aspect ratio calculation is mean depth (see Chapter 3.4.a). Related to proposed classification, Type 3 may become Type 2b in steeper case.

Similar like segment II-1 condition, Type 2b shows that upstream part of Cimanuk River shows active bed deformation and bank erosion process. It is also shown in observation data of the Cimanuk River as shown in Figure 5.19. CS-53 which simulated in this study located in 75 km from downstream. The active zone could be detected around 73 km to 81 km form downstream.

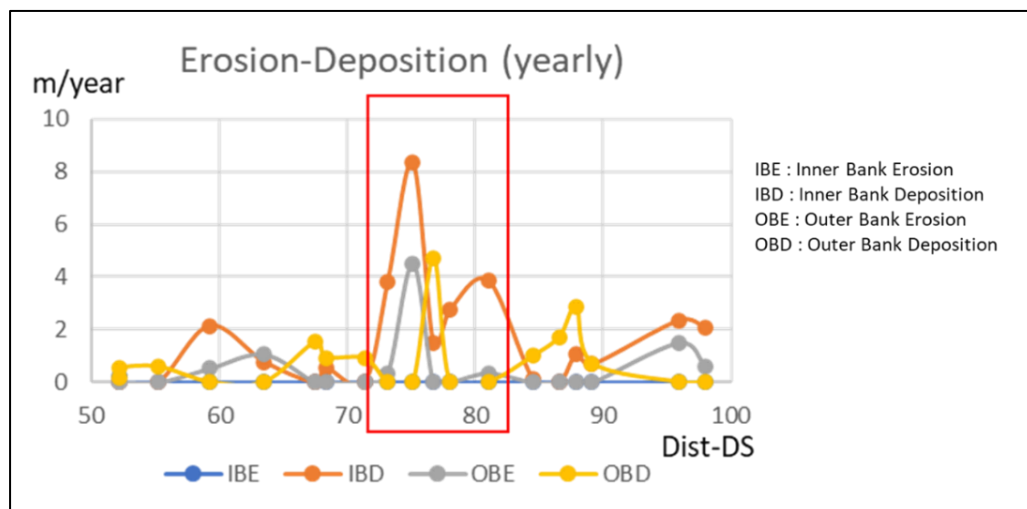


Figure 5.19. Active Erosion and Deposition of Cimanuk River

Summary, Limitation, and Conclusions

6.1 Summary

This study was conducted to explain about the interaction among sediment sizes, aspect ratio and planform dynamics. At the beginning part, sediment size variation was investigated and various conditions of bed-bank material were summarized into four types (blue, yellow, green and red marks). Based on this classification, aspect ratio variation is also related to this bed-bank condition type along with sinuosity variation. Aspect values 25 and 40 as well as sinuosity value 1.5 are important values to classify target rivers into four types of meandering channels. This classification is created by modifying the previous classification that has diverse characteristics in Type 2 which has low-moderate aspect ratio. This type 2 was divided into 2a that has lower sinuosity than 1.5 and 2b that has higher sinuosity than 1.5. Other meander parameters such as meander wavelength and radius of curvature also have individual characteristics in each type similar with aspect ratio and sinuosity comparison results. Weighted mean of silt-clay percentage (M value) of 20 was also important parameter to consider the bank stability, but M value in Type 2 was diverse.

Other parameters such as width, depth, slope and discharge are important to investigate stability condition of channel shape. Some past studies explained that empirical relationship among dimensionless width, depth, discharge and representative diameter are useful to predict channel width and depth even for fine material and cohesive bed. Related to channel pattern prediction, the existence of fine material, especially silt-clay are essential to improve channel pattern prediction by stream power.

Several parameters then were compared to propose new classification of meandering rivers. This proposed classification with some additional parameters expected to be helpful for understanding meandering rivers characteristics. This study also introduced numerical simulation to explain bank erosion trend, bed-bank material interaction and how it changes channel centerline movement. Then the difference between Type2a and 2b was examined.

Numerical simulation shows that type 2b has active bed deformation and bank erosion process compared to type 2a. Type 2a tend to be stable and less active. If the bank cohesion becomes less, then aspect ratio becomes larger. It means that width becomes wider because

it is easily eroded and depth become shallower due to the eroded material from the bank. Related to the proposed classification, Type1 may become Type 2a if bank is less cohesive. If the bed material changes into coarser sand, then width becomes wider because coarser sand cannot form the bank. In the simulation, depth became deeper but it may be caused by the boundary condition for sediment inflow.

On the other hand, sediment transport in Type 2b is active. Therefore, bar formation is confirmed in the simulation. If the bank is more cohesive, width is more stable.

6.2 Limitation

This study introduced detail characteristics and bank erosion simulation only for type 2a and 2b. Type 1 is considered to be stable based on the comparison with past studies. Moreover, the Sangkae River has the cohesive bank and bed material, but the channel is Type2a. The mechanism is still unknown. Type 3 has bar formation characteristics and the stability might be determined by bar movement. In this study, bar formation and movement for Type 3 was not investigated in detail. The number of simulation as well as field measurements are limited, therefore hypothesized mechanism in this study should be continuously examined. Bank erosion simulation also has limitation to conduct long-term simulation and it is necessary to cover long term simulation. Another point related to interaction among parameters, the impact of channel shape on sediment size was not clarified well and should be investigated in the future

6.3 Conclusions

The effect of sediment on aspect ratio could explain the change of planform dynamics. This effect could be investigated by several approaches and sediment size has important role to maintain channel stability. Active sediment movement detected in river with high sinuosity with low aspect ratio and fine sediment. Bank erosion is controlled by silt-clay percentage in river bank. Bed deformation found to be active when the stream power is large, but it is limited by river width when the silt-clay percentage in a river bank is high.

Proposed meandering characteristics is important to understand meandering rivers characteristics. Parameters of this classification could distinguish type of meandering rivers. Detail investigation of each parameter gives the comprehensive perspectives about each meandering types.

Each type could have different approaches related to maintaining stable cross-sectional shape in terms of river management. Type 1 and Type 2a have their shape stability. In that case river manager can spend less effort to maintain it compared to other types. Of course, some parts might have small scale characteristics such as local bank erosion due to human activities or impact of river crossing structures. For Type 3, river managers need to understand bar formation mechanism and give more attention to check the bar in every flood events.

Type 2b tend to be unstable, it might be the typical channel pattern located in upper part of lower reach.

Active erosion and deposition are necessary to be checked by periodical cross-sectional survey, and it should be compared to other types more often. Several actives zones can be identified by river managers and become focusing points to maintain the stable cross-sectional shape. Therefore, suitable river works plans could be selected based on design and budget optimization.

References

- ADB. (2007). *South Java Flood Control Sector Project*.
- Aerts, J. C. J. H., Botzen, W. J., Clarke, K. C., Cutter, S. L., Hall, J. W., Merz, B., Michel-Kerjan, E., Mysiak, J., Surminski, S., & Kunreuther, H. (2018). Integrating human behaviour dynamics into flood disaster risk assessment. *Nature Climate Change*, 8(3), 193–199. <https://doi.org/10.1038/s41558-018-0085-1>
- Ahmad, T. S. (2020). *NUMERICAL STUDY ON TIDAL CURRENTS AND BED MORPHOLOGY IN SITTAUNG RIVER ESTUARY, MYANMAR*. National Graduate Institute for Policy Studies (GRIPS) and International Centre for Water Hazard and Risk Management (ICHARM), Public Works Research Institute (PWRI).
- Arulanandan, K., Gillogley, E., & Tully, R. (1980). *Development of a quantitative method to predict critical shear stress and rate of erosion of natural undisturbed cohesive soils*.
- ASTM D-422-63. (2007). *Standard test method for particle-size analysis of soils*. Annual Book of ASTM Standards. ASTM International.
- Bagnold, R. A. (1966). *An approach to the sediment transport problem from general physics*.
- Biswas, R. K., Yorozya, A., Egashira, S., Disaster Management Program (DMP), National Graduate Institute for Policy Studies (GRIPS) 7-22-1 Roppongi, Minato-ku, Tokyo 106-8677, Japan, , & International Centre for Water Hazard and Risk Management (ICHARM), Public Works Research Institute (PWRI), Ibaraki, Japan. (2016). Numerical Model for Bank Erosion in the Brahmaputra River. *Journal of Disaster Research*, 11(6), 1073–1081. <https://doi.org/10.20965/jdr.2016.p1073>
- Brice, J. C. (1975). *Airphoto Interpretation of the Form and Behavior of Alluvial Rivers* (Report to the United States Army Research Office Durham No. ADA008108; p. 10). Washington University.
- Burmister, D. M. (1952). *Soil mechanics*: New York, Columbia Univ. Press,.
- Caksono. (2020, January 17). *Tren Bencana di Indonesia Sepanjang 2009-2019. (Trend of Disaster in Indonesia from 2009 to 2019)*. <https://mediaindonesia.com/infografis/283961/tren-bencana-di-indonesia-sepanjang-2009-2019>
- Candel, J., Kleinhans, M., Makaske, B., & Wallinga, J. (2021). Predicting river channel pattern based on stream power, bed material and bank strength. *Progress in Physical Geography: Earth and Environment*, 45(2), 253–278. <https://doi.org/10.1177/0309133320948831>
- Chitale, S. V. (1973). *Theories and Relationships of River Channel Patterns*.

- Church, M., & Rood, K. (1983). *Catalogue of Alluvial River Channel Regime Data*.
- D. E. Mecklenburg & A. Ward. (2004). STREAM MODULES: SPREADSHEET TOOLS FOR RIVER EVALUATION, ASSESSMENT AND MONITORING. *Self-Sustaining Solutions for Streams, Wetlands, and Watersheds, 12-15, September 2004*. Self-Sustaining Solutions for Streams, Wetlands, and Watersheds, 12-15, September 2004. <https://doi.org/10.13031/2013.17416>
- Diepart, J.-C. (2015). *Learning for resilience: Insights from Cambodia's rural communities*. Phnom Penh: The Learning Institute.
- Dunne, K. B. J. (2020). *A Sticky Pursuit Of The Threshold Channel: The Effect Of Cohesion On Alluvial River Channel Geometry*.
- Dunne, K. B. J., & Jerolmack, D. J. (2018). Evidence of, and a proposed explanation for, bimodal transport states in alluvial rivers. *Earth Surface Dynamics*, 6(3), 583–594. <https://doi.org/10.5194/esurf-6-583-2018>
- Dunne, K. B. J., & Jerolmack, D. J. (2020). What sets river width? *Science Advances*, 6(41), eabc1505. <https://doi.org/10.1126/sciadv.abc1505>
- Dutta, D., & Herath, S. (2004). Trend of floods in Asia and flood risk management with integrated river basin approach. *Proceedings of the 2nd International Conference of Asia-Pacific Hydrology and Water Resources Association, 1*, 55–63.
- Egashira, S., Ashida, K., Anonaka, S., & Takahashi, T. (1991). Bed-load formula derived from constitutive equations of solid particle–water mixture. *Bull Disas Prev Res Inst, Kyoto Univ, Japan*,.
- Egashira, S., MIYAMOTO, K., & ITOH, T. (1997). *Constitutive equations of debris flow and their applicability*. <https://doi.org/10.13140/2.1.4623.7122>
- Ercan, A., & Younis, B. A. (2009). Prediction of Bank Erosion in a Reach of the Sacramento River and its Mitigation with Groynes. *Water Resources Management*, 23(15), 3121–3147. <https://doi.org/10.1007/s11269-009-9426-1>
- Friend, P. F., & Sinha, R. (1993). Braiding and meandering parameters. *Geological Society, London, Special Publications*, 75(1), 105–111. <https://doi.org/10.1144/GSL.SP.1993.075.01.05>
- Fukuoka S. (2010). RIVER ENGINEERING ADAPTATIONS AGAINST THE GLOBAL WARMING–TOWARDS GENERALIZATION OF CLOSE-TO-NATURE RIVERS. *Doboku Gakkai Ronbunshuu F*, 66(4), 471–489. <https://doi.org/10.2208/jscejf.66.471>
- Fukuoka, S. (2012). Dimensionless width and depth and sediment transport rate in stable rivers. *3rd International Symposium on Shallow Flows (ISSF)*.
- Geospatial Information Authority of Japan. (2021). <http://maps.gsi.go.jp>
- Güneralp, İ., Abad, J. D., Zolezzi, G., & Hooke, J. (2012). Advances and challenges in meandering channels research. *Geomorphology*, 163–164, 1–9. <https://doi.org/10.1016/j.geomorph.2012.04.011>

- Harada D., Egashira S., Ahmad T. S., & Katayama N. (2019). EROSION RATE OF BED SEDIMENT BY MEANS OF ENTRAINMENT VELOCITY. *Journal of Japan Society of Civil Engineers, Ser. B1 (Hydraulic Engineering)*, 75(2), I_967-I_972. https://doi.org/10.2208/jscejhe.75.2_I_967
- Herdyasrastiti, A. (2015). *KAJIAN TRANSPOR SEDIMEN DAN BOD-DO DI SUNGAI SERAYU HILIR*.
- Hirabayashi, Y., Mahendran, R., Koirala, S., Konoshima, L., Yamazaki, D., Watanabe, S., Kim, H., & Kanae, S. (2013). Global flood risk under climate change. *Nature Climate Change*, 3(9), 816–821. <https://doi.org/10.1038/nclimate1911>
- Hu, P., Zhang, Q., Shi, P., Chen, B., & Fang, J. (2018). Flood-induced mortality across the globe: Spatiotemporal pattern and influencing factors. *Science of The Total Environment*, 643, 171–182. <https://doi.org/10.1016/j.scitotenv.2018.06.197>
- JICA. (2013). *PREPARATORY SURVEY ON THE PROJECT ON ADDITIONAL NEW WATER TREATMENT PLANTS FOR KAMPONG CHAM AND BATTAMBANG WATERWORKS IN THE KINGDOM OF CAMBODIA*.
- JICA. (2015). *Geo-Technical Investigation And Test for Rentang Irrigation Modernization Project Under PIRIMP*.
- Julian, J. P., & Torres, R. (2006). Hydraulic erosion of cohesive riverbanks. *Geomorphology*, 76(1–2), 193–206. <https://doi.org/10.1016/j.geomorph.2005.11.003>
- Julien, P. Y., & Wargadalam, J. (1995). Alluvial Channel Geometry: Theory and Applications. *Journal of Hydraulic Engineering*, 121(4), 312–325. [https://doi.org/10.1061/\(ASCE\)0733-9429\(1995\)121:4\(312\)](https://doi.org/10.1061/(ASCE)0733-9429(1995)121:4(312))
- Kallio, S. E. (2010). *The Graduate School of The Ohio State University*.
- Kleinhans, M. G., & van den Berg, J. H. (2011). River channel and bar patterns explained and predicted by an empirical and a physics-based method. *Earth Surface Processes and Landforms*, 36(6), 721–738. <https://doi.org/10.1002/esp.2090>
- Kundzewicz, Z. W., Pińskwar, I., & Brakenridge, G. R. (2018). Changes in river flood hazard in Europe: A review. *Hydrology Research*, 49(2), 294–302. <https://doi.org/10.2166/nh.2017.016>
- Kuroki, M., & Kishi, T. (1984). *Regime criteria on bars and braids in alluvial straight channels (in Japanese)*.
- Larsen, E. W., Premier, A. K., & Greco, S. E. (2006). CUMULATIVE EFFECTIVE STREAM POWER AND BANK EROSION ON THE SACRAMENTO RIVER, CALIFORNIA, USA. *Journal of the American Water Resources Association*, 42(4), 1077–1097. <https://doi.org/10.1111/j.1752-1688.2006.tb04515.x>
- Leopold, L. B., & Langbein, B. W. (1966). *River Meanders*.
- Luque R, F., & Van Beek, R. (1976). *Erosion and transport of bed-load sediment*.

- Masbahul, I. (2020). *A Numerical Study on Bank Erosion of a Braided Channel: Case study of the “Tangail and Manikganj Districts along the Brahmaputra River.”*
- Ministry of Public Works and Housing. (2008). *Ciliwung Flood Design Plan.*
- Ministry of Public Works and Housing. (2016). *Serayu Bogowonto Water Resources Management Masterplan.*
- Ministry of Public Works and Housing. (2017). *Cimanuk Cisanggarung Water Resource Management Masterplan.*
- Ministry of Public Works and Housing. (2021). *Cimanuk Cisanggarung Flood Management System.*
- Mitchener, H., & Torfs, H. (1996). Erosion of mud/sand mixtures. *Coastal Engineering*, 29(1–2), 1–25. [https://doi.org/10.1016/S0378-3839\(96\)00002-6](https://doi.org/10.1016/S0378-3839(96)00002-6)
- Montgomery, D. R., & Buffington, J. M. (1997). Channel-reach morphology in mountain drainage basins. *Geological Society of America Bulletin*, 16.
- Okada, S., Yorozuya, A., Koseki, H., Kudo, S., & Muraoka, K. (2016). Comprehensive measurement techniques of water flow, bedload and suspended sediment in large river using Acoustic Doppler Current Profiler. In S. Wieprecht, S. Haun, K. Weber, M. Noack, & K. Terheiden (Eds.), *River Sedimentation* (1st ed., pp. 1274–1280). CRC Press. <https://doi.org/10.1201/9781315623207-230>
- Osman, A. M., & Thorne, C. R. (1988). Riverbank Stability Analysis. I: Theory. *Journal of Hydraulic Engineering*, 114(2), 134–150. [https://doi.org/10.1061/\(ASCE\)0733-9429\(1988\)114:2\(134\)](https://doi.org/10.1061/(ASCE)0733-9429(1988)114:2(134))
- Parker, G. (1978). *Self-formed straight rivers with equilibrium banks and mobile bed.*
- Parker, G. (2004). *1D Sediment transport morphodynamics with applications to rivers and turbidity current, e-book,* http://hydrolab.illinois.edu/people/parkerg/morphodynamics_e-book.htm
- Partheniades, E. (1965). Erosion and deposition of cohesive soils. *J. Hydraulics Div. ASCE* 91(HY1): 105-139.
- Patsinghasanee, S., Kimura, I., & Shimizu, Y. (2015). Coupled Study of Fluvial Erosion and Overhanging Failure for Cohesive Riverbanks. *Journal of Japan Society of Civil Engineers, Ser. A2 (Applied Mechanics (AM))*, 71(2), I_533-I_544. https://doi.org/10.2208/jscejam.71.I_533
- Pfeifer, A. M., Finnegan, N. J., & Willenbring, J. K. (2017). Sediment supply controls equilibrium channel geometry in gravel bed rivers. *PNAS*.
- Purwono, N. A. S. (2018). *STUDI PERUBAHAN MORFOLOGI SUNGAI SERAYU HILIR AKIBAT DEBIT BANJIR*. 19(1), 8.
- Ramdhani, H., Chibana, T., & Santoso, A. (2020). *MEANDERING CHARACTERISTICS OF CIMANUK RIVER FOCUSING ON ASPECT RATIO VARIATIONS AND GEOLOGICAL CONDITION.*

- Ramdhani, H., & Setiawan, F. (2015). *DETERMINATION OF RIPARIAN ZONE BORDER OF CILIWUNG RIVER BY CONSIDERING MEANDERING CHARACTERISTICS*. 8.
- Rosgen, D. (1996). *Field Survey Procedures for Characterization of River Morphology*.
- Rosgen, D. L. (1994). A classification of natural rivers. *CATENA*, 22(3), 169–199. [https://doi.org/10.1016/0341-8162\(94\)90001-9](https://doi.org/10.1016/0341-8162(94)90001-9)
- Santoso, A. (2017). *Aspect ratio variation in lower reach rivers focusing on sediment size distribution*.
- Schumm, S. A. (1960). *The effects of sediment type on the shape and stratification of some modern fluvial deposits*.
- Schumm, S. A. (1963). Sinuosity of Alluvial Rivers on the Great Plains. *Geological Society of America Bulletin*, 74(9), 1089. [https://doi.org/10.1130/0016-7606\(1963\)74\[1089:SOAROT\]2.0.CO;2](https://doi.org/10.1130/0016-7606(1963)74[1089:SOAROT]2.0.CO;2)
- Seminara, G. (2006). Meanders. *Journal of Fluid Mechanics*, 554(1), 271. <https://doi.org/10.1017/S0022112006008925>
- Shimizu, Y., & Takebayashi, H. (2011). *Nays2DH Solver Manual*.
- Soar, P. J., & Thorne, C. R. (2001). *Channel Restoration Design for Meandering Rivers*: Defense Technical Information Center. <https://doi.org/10.21236/ADA397049>
- Time Series Topographic Map*. (2021). <http://ktgis.net/kjmapw/index.html>
- van den Berg, J. H. (1995). Prediction of alluvial channel pattern of perennial rivers. *Geomorphology*, 12(4), 259–279. [https://doi.org/10.1016/0169-555X\(95\)00014-V](https://doi.org/10.1016/0169-555X(95)00014-V)
- Van Rijn, L. (2020). *LITERATURE REVIEW OF CRITICAL BED-SHEAR STRESSES FOR MUD-SAND MIXTURES*.
- Williams, G. P. (1986). River meanders and channel size. *Journal of Hydrology*, 88(1–2), 147–164. [https://doi.org/10.1016/0022-1694\(86\)90202-7](https://doi.org/10.1016/0022-1694(86)90202-7)
- Yamamoto, K. (2004). Structural Alluvial Potamology. *Sannkaido*.